Winter 12-15-2021

Short-term memory and olfactory signal processing

Lijun Zhang
Washington University in St. Louis

WASHINGTON UNIVERSITY IN ST. LOUIS

McKelvey School of Engineering

Department of Electrical & Systems Engineering

Dissertation Examination Committee:
Baranidharan Raman, Chair
Mark Anastasio
Dennis Barbour
Shantanu Chakrabartty
ShiNung Ching

Short-term Memory and Olfactory Signal Processing

by
Lijun Zhang

A dissertation presented to
The Graduate School
of Washington University in
partial fulfillment of the
requirements for the degree
of Doctor of Philosophy

May 2022
St. Louis, Missouri

Table of Contents

List of Figures v
Acknowledgments ix
Abstract xi
Chapter 1: Introduction 1
1.1 Biological Olfaction 1
1.2 The Anatomy of Olfactory System 1
1.2.1 The Locust Olfactory System 6
1.2.2 The Fly Olfactory System 7
1.3 Olfactory Coding: The Information Representation 8
1.3.1 The 'Spatial' Code and 'Temporal' Code 8
1.3.2 The 'Spatiotemporal' Code 10
1.4 Short-term Memory in Sensory System 12
1.4.1 Desensitization at The Level of Sensory Neurons 13
1.4.2 Neural Adaptation in Higher Order Processing Centers 14
1.5 Thesis Outline 17
Chapter 2: Methods 18
2.1 Spiking data analysis 18
2.2 Dimension reduction methods 20
2.3 Calcium imaging analysis 22
2.4 Neural decoding methods 26
Chapter 3: Sensory Memory for Repetition Suppression and Novelty Enhancement in an Olfactory Circuit 31
3.1 Introduction 31
3.2 Results 32
3.2.1 Spontaneous activity is negatively correlated with stimulus-evoked responses of a recurring stimulus 32
3.2.2 Spontaneous activity carries information about stimulus identity and intensity 37
3.2.3 PN firing patterns change reliably across trials 40
3.2.4 Adaptation-invariant encoding of odor intensity 42

3.2.5 Contrast-enhanced response to an unexpected stimulus 47
3.2.6 Activity-dependent plasticity in single projection neurons 52
3.2.7 A simple linear model for adaptation and contrast enhancement 55
3.3 Discussion 57
3.4 Author Contributions 63
Chapter 4: Temporal Organization of Odor-evoked Responses in a Fly Olfactory Circuit: Inputs, Outputs, and Idiosyncrasies 64
4.1 Introduction 64
4.2 Results 66
4.2.1 Light-sheeting imaging of odor-evoked neural activity 66
4.2.2 Temporal patterning of odor-evoked responses 73
4.2.3 Idiosyncratic processing underlies how odorants are segregated over time 77
4.2.4 Idiosyncratic processing under short-term memory 85
4.2.5 Stimulus evoked ON and OFF responses 90
4.3 Discussion 93
4.4 Author Contributions 96
Chapter 5: Invariant Odor Recognition with ON-OFF Neural Ensembles 98
5.1 Introduction 98
5.2 Results 99
5.2.1 Robust odor recognition under short-term memory 99
5.2.2 Robust odor recognition in a behavioral assay 104
5.2.3 Stimulus dynamics, history, and competing cues induce variations in PN responses 111
5.2.4 Variations due to changes in ambient conditions 115
5.2.5 A decoding scheme for robust odor recognition 117
5.2.6 Discrete classifier with ternary weights allows robust recognition 122
5.2.7 A generic binary neural network inspired by the insect olfactory system 127
5.3 Discussion 129
5.4 Author Contributions 144
Chapter 6: Conclusions 145
6.1 Short-term memory in locust antennal lobe 146
6.2 Short-term memory in fruit fly olfactory system 147

6.3 Robust odor recognition with ‘ON’ and ‘OFF’ features 149
6.4 Future work 151
References 153

List of Figures

Figure 1.1: The anatomy of the vertebrate olfactory system. 4

Figure 1.2: The anatomy of the insect olfactory system.....5

Figure 1.3: The anatomy of the locust olfactory system.....7

Figure 1.4: The anatomy of the fruit fly olfactory system.....8

Figure 1.5: Typical response dynamics of the olfactory systems 10

Figure 1.6: Visualization of Trajectories Representing PN responses over time 11

Figure 1.7: Coherence and spike time precision increase over stimulus repetition 16

Figure 2.1 ROI masks extracted for each plane and each region.....26

Figure 2.2 Discrete weights neural network 28

Figure 3.1: Repetitively encountered stimulus generates persistent sensory memory 35

Figure 3.2: Spontaneous activity carries information about stimulus identity and intensity network 38

Figure 3.3: Stimulus identity and intensity information can be identified using spontaneous activities.....39

Figure 3.4: Inter-trial neural dynamics are diverse in individual projection neurons.....41

Figure 3.5: Ensemble neural activity change systematically over repeated trials 44

Figure 3.6: Projection neurons response profiles robustly encode odor identity and intensity information.....46

Figure. 3.7: Contrast enhancement of ensemble responses to the deviant stimulus 49

Figure. 3.8: Neural responses to the deviant stimulus can be robustly decoded 51

Figure 3.9: Activity-dependent plasticity in individual projection neurons 53

Figure 3.10: Persistent changes in PN spontaneous activity following current injections 55

Figure 3.11: A linear model for repetition suppression and novelty contrast enhancement 56

Figure. 3.12: Schematic representation of the main ideas of the chapter 62

Figure 4.1: Light-sheet imaging for volumetric in vivo characterization of odor-evoked responses at the input and outputs of the antennal circuitry.....68

Figure 4.2: Extraction of spatial and temporal patterns of odor-evoked neural activity 70

Figure 4.3: Temporal responses in higher concentrations 72

Figure 4.4: Odor-evoked responses decorrelate over time 75

Figure 4.5: Odor-evoked responses decorrelate over time 76

Figure 4.6: Pairwise odor similarities vary across flies 80

Figure 4.7: Identified glomeruli examples.....82

Figure 4.8: Identified glomeruli across all flies 83

Figure 4.9: Comparing temporal responses of the same glomerulus across flies.....84

Figure 4.10: Short-term memory across different microcircuits 87

Figure 4.11: Within-fly vs. across-flies comparison.....88

Figure 4.12: Mean pair-wise cosine similarity comparison across trials.....89

Figure 4.13: Odor evoked ON vs. OFF responses 92

Figure 5.1 Robust odor recognition under short-term memory 102

Figure 5.2 Comparison of weights and PNs' responsiveness 103
Figure 5.3: Invariant odor recognition in an appetitive conditioning assay 108
Figure 5.4: Summary of odor recognition performance in the behavioral assay.....110
Figure 5.5: Individual projection neuron responses are highly variable.....112
Figure 5.6: Projection neuron responses are highly variable under different encounters of stimuli 114
Figure 5.7: Changing humidity conditions alters both individual and ensemble level PN activity 116
Figure 5.8: Support Vector Machine classification for robust hexanol recognition.....119
Figure 5.9: SVM classification for robust isoamyl acetate recognition.....121
Figure 5.10: Performance comparison between discrete SVM vs. ternary vs. Boolean classifiers 123
Figure 5.11: Performance comparison for isoamyl acetate recognition 125
Figure 5.12: Performance of a classifier with randomized weight assignment 126
Figure 5.13: Weights assigned to each PN in different classification schemes are shown 127
Figure 5.14: Boolean neural network for non-olfactory pattern recognition.....131
Figure 5.15: Performance of ternary classifiers in humid condition 135
Figure 5.16: Similarity analysis between analog and discrete high-dimensional weight vectors 136
Figure 5.17: Generalization performance of the Hex-trained classifier 137
Figure 5.18: Characterization of PN responses recorded from unstarved locusts 139
Figure 5.19: Characterization of PN responses recorded from starved locusts 141
Figure 5.20: Characterization of PN responses recorded from starved and then trained locusts 142

Figure 5.21: Performance of SVM classifiers for PNs pooled across from unstarved locusts, starved locusts, and starved then trained locusts 143

Acknowledgments

I want to express my deepest thanks and appreciation to my advisor, Dr. Barani Raman, for his mentorship. I started my program as an electrical engineer. Dr. Raman introduces me to the amazing field of neuroscience and the study of the brain with system and computational methods. His encouragement and guidance have helped me get through every difficulty I encountered. Ph.D. is a journey. I am truly grateful I can finish this journey with the company of Dr. Raman.

I also want to sincerely thank the rest of my committee members: Dr. Dennis Barbour, Dr. Shantanu Chakrabartty, Dr. Shinung Ching, and Dr. Mark Anastasio, for their thoughtful feedback and comments.

It has been a great experience working with the amazing scientists in Raman lab. I sincerely thank all the lab members for their active collaboration and support. I want to thank Dr. Debajit Saha for his help and guidance in my early years joining the lab and Dr. Srinath Nizampatnam for all the projects we collaborated on. I would like to thank Dr. Haoyang Rong for working with the flies imaging project. It's hard to name all, but I am truly blessed to work with every single of you.

I will be forever grateful to my parents for all the understanding, encouragement, and support through this journey.

Lijun Zhang

Washington University in St. Louis

May 2022

Dedicated to my parents.

ABSTRACT OF THE DISSERTATION

Short-term Memory and Olfactory Signal Processing

by

Lijun Zhang

Doctor of Philosophy in Electrical Engineering

Washington University in St. Louis, 2022

Professor Barani Raman, Chair

Modern neural recording methodologies, including multi-electrode and optical recordings, allow us to monitor the large population of neurons with high temporal resolution. Such recordings provide rich datasets that are expected to understand better how information about the external world is internally represented and how these representations are altered over time. Achieving this goal requires the development of novel pattern recognition methods and/or the application of existing statistical methods in novel ways to gain insights into basic neural computational principles. In this dissertation, I will take this data-driven approach to dissect the role of short-term memory in olfactory signal processing in two relatively simple models of the olfactory system: fruit fly (*Drosophila melanogaster*) and locust (*Schistocerca americana*).

First, I will focus on understanding how odor representations within a single stimulus exposure are refined across different populations of neurons (faster dynamics; on the order seconds) in the early olfactory circuits. Using light-sheet imaging datasets from transgenic flies expressing calcium indicators in select populations of neurons, I will reveal how odor representations are decorrelated over time in different neural populations. Further, I will examine how this computation is altered by short-term memory in this neural circuitry.

Next, I will examine how neural representations for odorants at an ensemble level are altered across different exposures (slower dynamics; on the order of tens of seconds to minutes). I will examine the role of this short-term adaptation in altering neural representations for odor identity and intensity.

Lastly, I will present approaches to help achieve robustness against both extrinsic and intrinsic perturbations of odor-evoked neural responses. I will conclude with a Boolean neural network inspired by the insect olfactory system and compare its performance against other state-of-the-art methods on standard machine learning benchmark datasets. In sum, this work will provide deeper insights into how short-term plasticity alters sensory neural representations and their computational significance.

Chapter 1: Introduction

Modern large-scale multi-neuronal recording methodologies, including multielectrode recordings [1] and calcium imaging [2], allow us to monitor a large population of neurons with finer spatial and temporal resolution. These advances in recording technologies have increased the number of simultaneously recorded neurons by orders of magnitude [3, 4] and enabled us to examine neural coding problems that cannot be answered on a single-neuron basis [5, 6].

The data produced by these large-scale recording techniques are intrinsically high-dimensional. Multi-electrode arrays allow the activity of hundreds of neurons to be recorded simultaneously, with covariates across multiple experimental trials, various stimuli, and behavioral tasks conditions [7, 8]. Optical recordings, on the other hand, record brain images over time, generating large volumes of data with neural information embedded [9, 10]. Processing and understanding these large-scale neural signals with high spatiotemporal resolution poses a fundamental challenge and requires the use of advanced pattern recognition and machine learning methods [5, 6]. In this dissertation, I will focus on developing novel or adapting standard statistical methods for understanding how odorants are processed in relatively simpler insect olfactory circuits.

1.1 Biological Olfaction

Olfaction is a primary sensory modality for many organisms and serves a vital role in their survival and procreation [11]. Many organisms rely on olfaction foraging for food [12], detecting predators [13], and for communication through social cues [14, 15]. Odors are also critical for learning and memory about events and places, and constitute efficient retrieval cues for the recall

of episodic memories [16]. Intriguingly, the olfactory system across species and phyla appears to have striking similarities [17]. This suggests that a generic solution to the problem of odor detection and subsequent signal processing may exist and examining them using simpler olfactory neuronal networks, such as those used in insects, may provide us with insights necessary for understanding more complex vertebrate systems.

The principles of detection and recognition in olfaction are still not fully understood. Unlike vision and audition, where the stimulus can be fully characterized, which molecular features are detected by olfactory receptors and the overall dimensionality of the chemical space are only poorly understood [18]. Transduction of even a single odorant molecule, such as coffee, will require the activations of complex combinations of receptor neurons expressing different olfactory receptor proteins rather than by the activity of a specific receptor [19]. Additionally, sensory stimuli encountered in the natural environment are often highly dynamical in temporal encounters, constantly varying in duration of encounters, and received in the presence of interference arising from other competing or distracting stimuli, and/or variations in intensity and changes in ambient conditions. Therefore, understanding the design and computing principles of olfaction and maintaining robustness that overcomes extrinsic and internal perturbation poses a very complex and challenging problem. In this work, I will investigate this problem using the relatively simple insect olfactory systems of grasshoppers and fruit flies.

1.2 The Anatomy of Olfactory System

In mammals, the primary olfactory pathway starts from the olfactory receptor neurons (ORNs) in the olfactory epithelium within the nasal cavity at the roof of the nose [20]. ORNs transduce chemical cues into neural signals and project their axons onto spherical structures of

neuropil called glomeruli in the olfactory bulb (**Figure 1.1**). Single olfactory neurons typically express a single receptor gene [21] that encodes for a specific olfactory receptor G-coupled protein [22]. ORNs expressing the same odorant receptors send their axons to either a single or a pair ofspherical structure of neuropil called glomeruli [17]. In the glomerular layer, the glutamatergic mitral and tufted (M/T) cells form synaptic connections with inhibitory periglomerular cells that release GABA [23]. In the same layer, GABAergic short axon cells, as well as juxtaglomerular cells, have also been identified to form inter-glomerular connections with M/T cells [24]. At the output of the olfactory bulb, M/T cells form dendrodendritic interactions with GABAergic granule cells, which are the dominant cell type of the olfactory bulb inhibiting M/T cells. Granule cells also receive massive feedback from piriform cortex. M/T cells in the OB send their output through the olfactory tract to several different cortical targets in the vertebrate brain, such as the anterior olfactory nucleus, piriform cortex, cortical amygdala, etc.[25]. These areas integrate olfactory information with other sensory modalities through reciprocal connections with different cortical regions[26] (**Figure 1.1**).

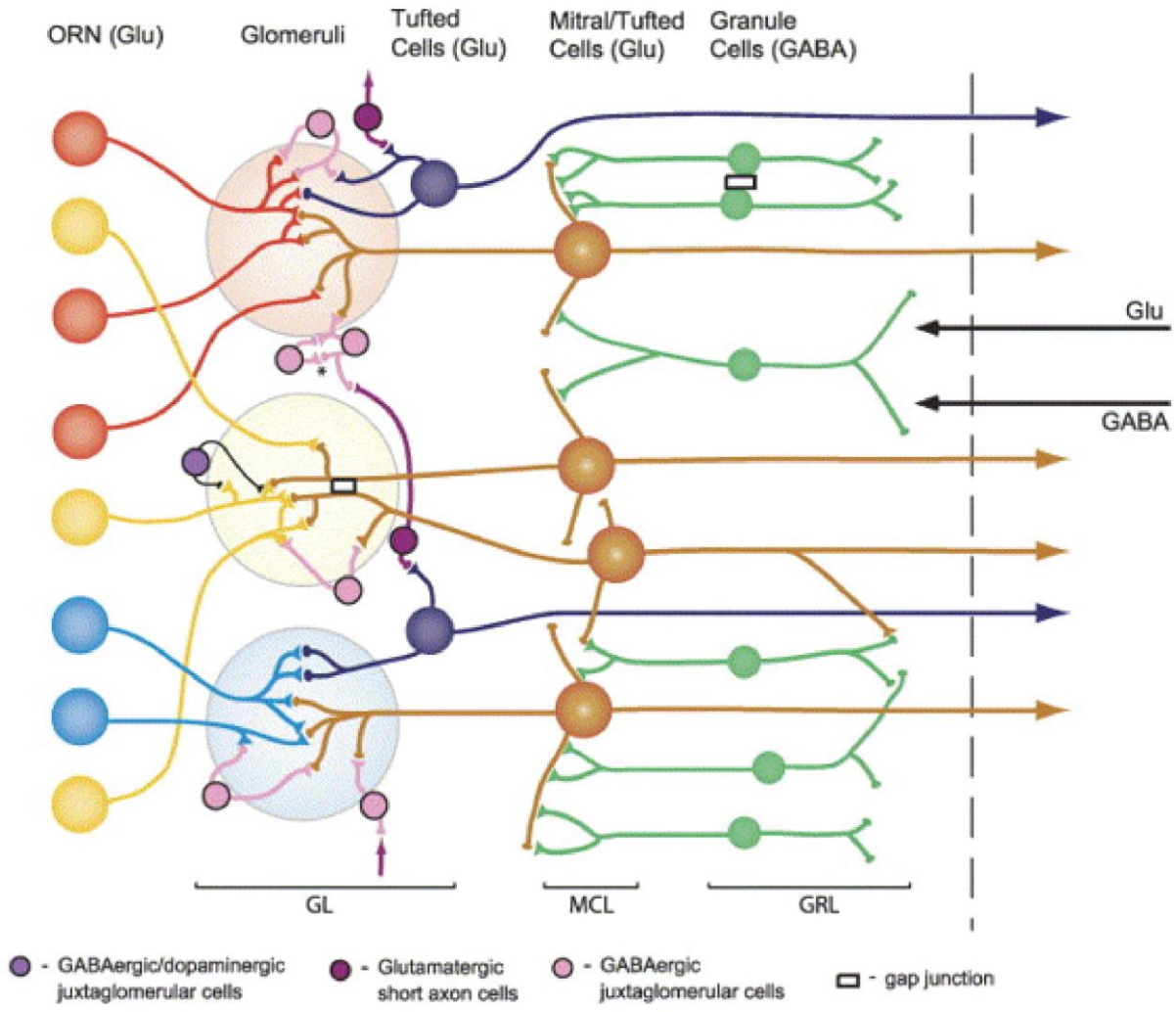

Figure 1.1: The anatomy of the vertebrate olfactory system. For vertebrates, glutamatergic ORNs expressing the same receptors (indicated by the same color) send their excitatory axons to their postsynaptic target in the olfactory bulb (OB), where different types of cells, including glutamatergic mitral and tufted (M/T) cells, GABAergic short axon cells, periglomerular cells, and granule cells, form synaptic interaction. M/T cells provide the output of the OB to the higher olfactory center. GL: glomerular layer. MCL: mitral cell layer. GRL: granule cell layer. The dashed line indicates the boundary of OB (reproduced from [17]).

The insect olfactory system shares several similar circuit motifs as those reported in the vertebrate olfactory system (**Figure 1.2**). Odorants are sensed by olfactory receptor neurons (ORNs) in the antenna. The ORN transduces chemical stimuli into electrical signals and relays the information downstream to the glomeruli in the antennal lobe (AL; analogous to the OB). The

ORN signals are processed through interactions between cholinergic projection neurons (PNs, excitatory; analogous to M/T cells in mammal olfactory system) and GABAergic local neurons (LNs, inhibitory). The PNs then relay their signals to two downstream centers, mushroom body and lateral horn, associated with olfactory learning [27-29] and mediate innate behaviors [30, 31], respectively. This generic description of the initial circuitry in the insect olfactory system is true for the two model organisms used in this dissertation work: locust (*Schistocerca americana*) and fruit fly (*Drosophila melanogaster*). Notably, the layout of the locust and fly olfactory systems also differ in important ways as discussed below.

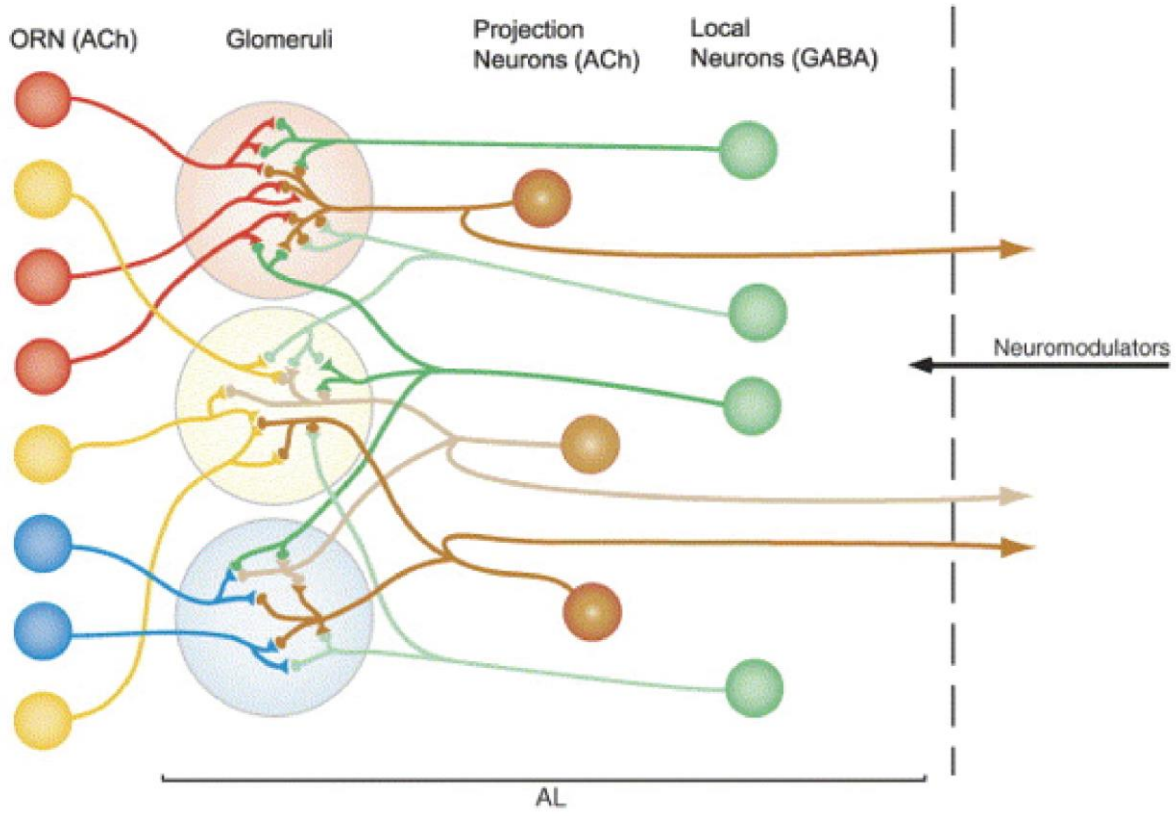

Figure 1.2: The anatomy of the insect olfactory system. The cholinergic olfactory receptor neurons (ORNs) send their axons to the downstream structure in the antennal lobe (AL). Within glomeruli, excitatory projection neurons (PNs) and inhibitory local neurons (LNs) form recurrent interactions. Only PNs send their outputs onto the higher brain centers (Reproduced from [17]).

1.2.1 The Locust Olfactory System

The locust antenna is composed of several flagellar segments called annuli. On these segments are hundreds of small cone-like structures called sensilla, which house the ORNs. There are four main types of sensilla present on locust antenna: basiconica, trichodea, coeloconica, and chaetica. They each have a different function, distributions, and house different numbers of ORNs[32]. Each odor activates a combinatorial response across the array of ORNs [33]. The current dogma is that every ORN selectively expresses a specific olfactory receptor (OR) gene, along with a broadly expressed co-receptor (Or83b) [34, 35], and can detect a variety of odorants [17].

The locust antennal lobe has a circuitry layout more similar to the mice accessory olfactory bulb. Here, inputs from the sensory neurons, ORNs, are integrated and processed by excitatory cholinergic PNs and inhibitory GABAergic LNs [36, 37]. There are 830 PNs in a locust antennal lobe, receiving inputs from roughly 50,000 ORNs [36, 37]. PN cell dendrites are all located on the surface of the antennal lobe, which is mainly made up of thousands of small bundles of neuropils called glomeruli [37]. Several PNs innervate a single glomerulus and each PN arborizes 10-20 microglomeruli [36, 37]. Approximately 300 axon-less LNs are projecting broadly within the antennal lobe and forming inhibitory synapses with a large number of PNs and ORNs. In locusts, LNs do not have full-blown sodium action potentials but show small calcium spikelets [38] during spontaneous and stimulus presentation periods.

The PN outputs project onto downstream circuits in the mushroom body and lateral horns, the higher-order circuits that are thought to underlie associative learning and innate behaviors [39, 40]. There are approximately 50,000 Kenyon cells (KCs) in the locust mushroom body, and each

KC receives input from approximately half the PNs [41, 42]. KCs respond sparsely and selectively to very few odorants in a specific concentration range [43].

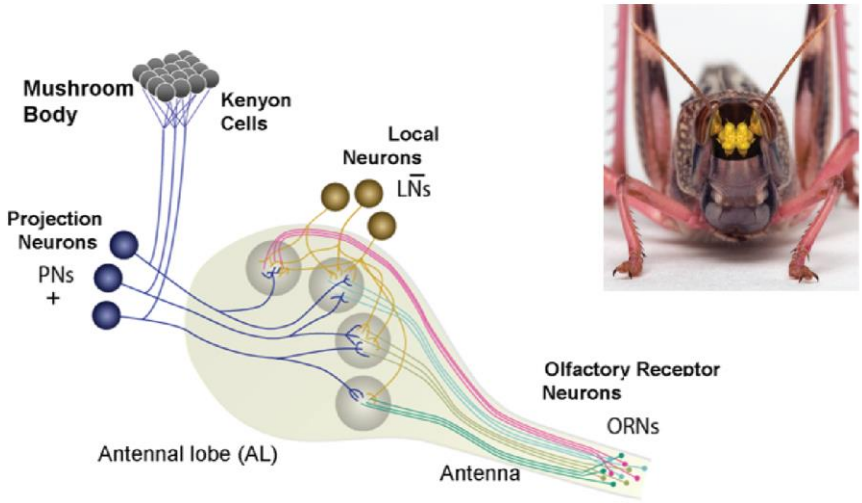

Figure 1.3: The anatomy of the locust olfactory system.

1.2.2 The Fly Olfactory System

In Drosophila, there are only 1200 ORNs in the Drosophila antenna, housed in three morphologically distinct sensillum classes: basiconic, trichoid, and coeloconic, with the basiconic being the primary type [44]. Like locusts, an ORN type can be defined by the unique olfactory receptor it expresses. The OR and a universal co-receptor Or83b (Orco) give the ORN unique response characteristics [45, 46].

Unlike locust sensory neurons, ORNs in flies project their axons bilaterally to the same glomerulus in both ALs. Post-synaptic to the ORNs are the 2nd order PNs of the AL. In Drosophila, excitatory PNs (ePNs) are uni-glomerular and multi-glomerular [47], and a glomerulus may be innervated by ~ two to six ePNs per glomerulus. Another lesser-known group of multi-glomerular inhibitory PNs (iPNs), which release GABA, and form a parallel pathway in addition to the ePNs.

The ePNs convey signals to MB and LH, whereas iPNs only project to the LH, bypassing MB [48]. Unlike locusts, in *Drosophila*, the local interneurons (LNs) also have two major functional categories, the inhibitory LNs (iLNs) and excitatory LNs (eLNs). Specifically, eLNs can both depolarize and hyperpolarize PNs. Meanwhile, eLNs and iLNs are interconnected via mixed synapses [49].

The MB has around 2000 intrinsic KCs in each hemisphere. Each KC extends several 'claws' to connect with boutons of distinct PNs, with one 'claw' only sampling from one PN. However, a PN bouton can synapse with 'claws' from several KCs, forming micro neuropil. Similar to the locust olfactory system, the representation of odor stimulus in the MB is sparse [50]. Relatively less is known about odor processing in the lateral horn.

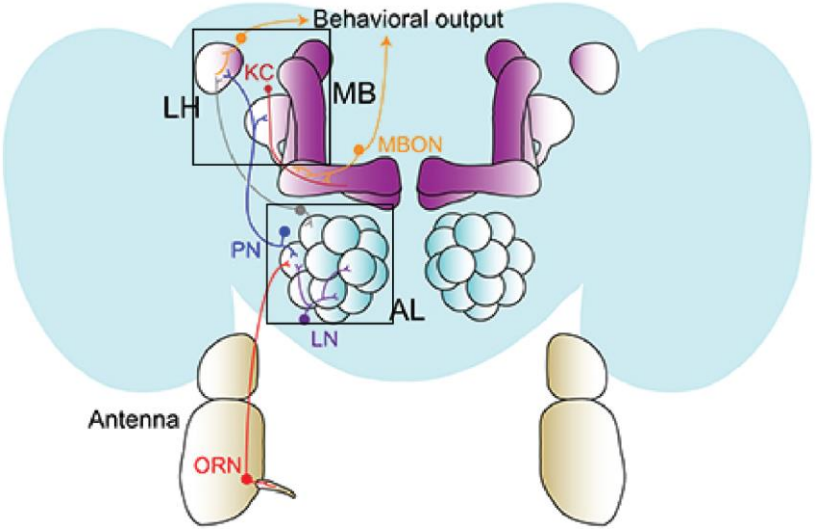

Figure 1.4: The anatomy of the fruit fly olfactory system. Prominent neuron types and circuits are identified: olfactory receptor neurons (ORNs) in the antenna, projection neurons (PNs) and local neurons (LNs) in the antennal lobe, Kenyon cells in the mushroom body, dopaminergic mushroom body output neurons (MBONs), and Lateral Horn (Reproduced from [51]).

1.3 Olfactory Coding: The Information Representation

1.3.1 The 'Spatial' Code and 'Temporal' Code

Neural coding describes the study of information representation and processing by individual or ensembles of neurons [52]. Starting from a sequence of action potentials ('spikes'), sensory stimulus evokes spiking activities patterned over space and time. What features of a sensory stimulus are encoded by the active set of neurons ('spatial code') and what aspects are represented in their temporal structure ('temporal code') is a fundamental problem in systems neuroscience [53]. In the spatial dimension, the stimulus-specific information can be represented by spiking activities distributed across a unique combination of neurons activated[54-56]. In some cases, particularly for ecologically relevant cues such as pheromones, the spatial code has been shown to be limited to a single neuron or a small group of neurons. This strategy has been referred to as the 'labelled-line' scheme[57, 58].

On the other hand, temporal codes focus on the timing of spikes. First-spike latency has been proposed as the neural code that is important for odorant identification and initiating a behavior response[59]. Neurons that receive stronger input have shorter response latency, allowing rapid odorant identification[60, 61]. Temporal dynamics in the olfactory system are more complex and typically go beyond the first spike latency [56]. The coding scheme based solely on early odor-evoked neural activity for odor identification, referred to as the primacy coding scheme has recently been proposed to link neural responses to behavioral outcomes in mice [62].

The odor-evoked neural responses in the AL or OB generated by an odor stimulus slowly evolve over time [63, 64]. Typically, the population neural responses change more dramatically after the odor onset and offset, which are referred to as on- and off-transient periods (**Figure 1.5**).

For a prolonged odor puff, between these two transient periods, the population neural activity becomes less intense and converges onto a stable spiking pattern, referred to as a steady state. This steady state is typically reached within 1 to 1.5 s of odor onset [65, 66].

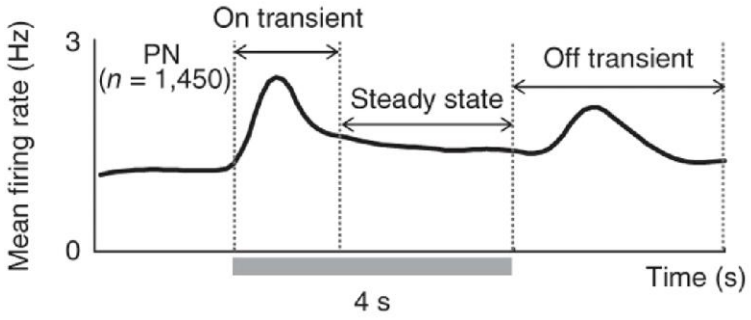

Figure 1.5: Typical response dynamics of the olfactory systems. Mean firing rates across projection neurons (PNs) as a function of time are shown. The 4-s odor stimulation period is shown as a gray bar along the x-axis. In all three neural populations, three dynamical states can be clearly identified: an on-transient response after odor onset, an off-transient response after stimulus termination and a steady-state between the two transient activity phases (Reproduced from [67]).

In addition to spiking activities, various types of neural oscillations have been proposed to be closely associated with neural coding functions. Oscillatory local field potential (LFP) signals that arise from transient synchronization of neurons in the AL and OB exhibits unique frequency and amplitude to represent odor's identity and intensity[68, 69]. For example, beta oscillations (15-30 Hz) in the rat OB can only be evoked by some organic solvents (e.g., xylene) but not strong odors (like ammonia)[70]. M/T cells in the zebrafish OB can exhibit phase-locked response patterns to some odorants but not for others [71]. In the locust AL, the synchronization of PN activities results in field potential activity with power in the gamma range (~ 20 Hz)[72]. Additionally, the honeybees AL has been shown to produce LFP oscillations during olfactory learning that correlate with spiking activity[73].

1.3.2 The ‘Spatiotemporal’ Code

Different coding algorithms have been implemented in various stages of insect olfactory systems. At the level of first-order olfactory receptor neurons, both firing rates and firing patterns of the odor-evoked responses were shown to be odor-specific and temporally distinct [33]. At the level of second-order projection neurons in the antennal lobe, a more elaborate spatiotemporally patterned activities, which combines both the population and temporal aspect of the ensemble neural responses, is utilized for encoding the information about different odorants [66, 74, 75]. The representations of high-dimensional neural responses were found to be organized into odor-specific manifolds and with the intensity-specific trajectories lying within the odor-specific manifold, (**Figure 1.6**) [76]. In other words, the variability with respect to intensity changes of a stimulus was relatively less when compared to those observed when different odorants are presented.

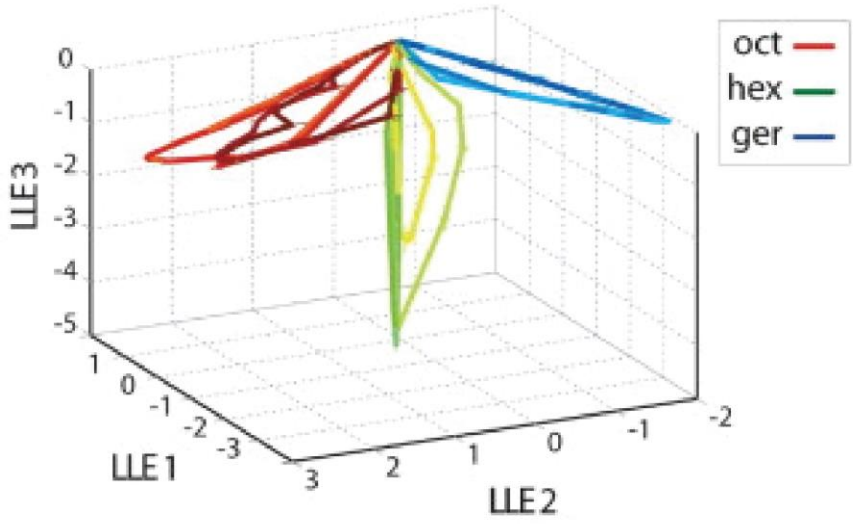

Figure 1.6: Visualization of Trajectories Representing PN responses over time.
Spatiotemporal neural responses (110 PNs) are plotted as trajectories for four concentrations of three odors (octanol – red, hex – green, geraniol – blue; Lighter color indicates lower intensities). Note that the trajectories in response to different concentrations of the same odor remain on the same odor-specific subspace (reproduced from [76]).

While the encoding approach using spatiotemporal response patterns organized in odor-specific manifolds presents an elegant way to decouple odor identity from intensity information, it also raises several interesting questions regarding robustness. Most stimuli are encountered in a multitude of ways in natural environments. Previous studies have shown that single neuron response patterns can vary when the same odorant is encountered in a temporally overlapping sequence with other stimuli[67, 77], or in a pulsatile fashion [78, 79]. While the activity of individual projection neurons varied, the spatiotemporal patterns based on the ensemble of neurons were found to be odor-specific and reliable [8, 80]. Whether this holds when other perturbations such as changes in environment conditions (humidity), and particularly internal short-term memory, are included remains unclear and needs further examination.

1.4 Short-term Memory in Sensory System

Neural systems have shown a strong capacity to represent the world using neural codes, such as rate codes, temporal codes, and spatiotemporal codes. However, the neural responses can be disturbed by various types of perturbations. Among them, the memory stands as one of the most challenging factors to confound the neural representations. In this dissertation, I will examine the stability of neural codes when perturbed by short-term memory.

The sensory system adjusts to changes in the environment. For example, in the visual system, prolonged viewing of a high contrast stimulus reduces both perceptual and neural sensitivity to subsequent stimuli of the similar pattern [81, 82]. In the auditory system, adaptation

occurs as early as in the auditory nerve fibers and becomes more diverse with numerous types of adaptation processes along the auditory pathway [83]. In this dissertation, I will seek to understand how the sensory system, particularly the olfactory system, stores sensory information about recurring cues (typically repeated over the range of tens to hundreds of seconds). More importantly, how short-term memory about a recurring cue alters the neural processing of the familiar or novel stimuli will be examined. To illustrate this idea, let's consider this scenario where a dog sitting in a garden exposed to the smell of flowers. Upon continuous exposure, the dog sense of smell will habituate and filter out the smell of the flowers. Any change in the environment, for example, a coyote appearing in the distance, would more likely be detected by the dog, despite the fact that the coyote's smell represents only a small component of the raw odor cocktail entering the dog's nose. Here, habituation, as a form of implicit short-term memory [84], decreases the responsiveness to repeated stimulus and allows sensory systems to filter out background or currently nonsignificant stimuli (i.e. the smell of flower) while maintaining responsiveness to novel stimuli (i.e. the smell of coyote). In which stage of the olfactory sensory system does the neural adaptation to the smell of the persisting or recurring cue start and what neurons or neuronal populations play crucial roles in the process of adaptation? I will examine these issues in this dissertation.

1.4.1 Desensitization at The Level of Sensory Neurons

Desensitization to an odorant starts right from the olfactory receptor neurons. In response to a prolonged and steady odor stimulus, ORN responses peak rapidly, then decay[85]. A prolonged stimulus also reduces responses to subsequent exposures to the same stimulus with a recovery time over a range of 4 – 5 s [86, 87]. Prior studies [85] have suggested that the adaptation

in ORNs is mediated by a diffusible factor, Ca^{2+}, that accumulates in the cell as a result of feedback regulation of odor transduction. In rodents, individual receptors respond to long odor pulses by accumulating intracellular calcium, which eventually inhibits the receptor and renders it in an inactive state [88, 89]. In *Drosophila,* mutants for either the TRP channel or the IP3 receptor have normal olfactory responsivity but show defective adaptation [90, 91]. Ca^{2+} transients in the olfactory cilia also play an essential role in the recovery from short-term adaptation with its recovery time course after stimuli presentation sufficiently close to the recovery of short-term adaptation [89]. The similar observation regarding desensitization at the level of peripheral sensory neurons has also been reported in other sensory systems such as vision [92, 93] and audition [94, 95].

1.4.2 Neural Adaptation in Higher Order Processing Centers

In the second stage of processing (invertebrate antennal lobe or vertebrate olfactory bulb), the depression of responses to familiar stimuli is generally explained by the potentiation of inhibition onto active neurons. In honeybees, habituation is achieved by potentiating synaptic strength between local inhibitory neurons and project neurons [96]. Similar mechanisms have also been reported in other insects such as fruit flies[97]. In the locust's antennal lobe, the feedback inhibition provided by LNs has been hypothesized to change with repeated exposures of the same stimulus [72, 98]. Repeated stimulus presentations have been shown to entrain local field potential oscillations, and the integrated power in the 20 Hz range was found to be significantly higher during later trials (**Figure 1.7**). Both the LN activity and PN spike time were found to be increasingly coherent with the LFP waveform during stimulus presentation. The number of PN spikes evoked decreased as the stimulus became more familiar. This change was found to be

stimulus-specific and intrinsic to the antennal lobe circuit as a form of short-term memory and lasted typically around 15 minutes [72]. Further, a model in which inhibitory synaptic weights were scaled according to the activity of postsynaptic excitatory neurons was proposed. This model, termed 'negative image' model, was also used to explain defining features of habituation as well as several related forms of implicit or perceptual memory [99].

Response in the higher-order sensory centers was also adapted to recurring olfactory cues. In *Drosophila*, inactivation of the mushroom bodies resulted in decreased olfactory habituation [100]. In vertebrates, although olfactory bulb mitral cells have been shown to adapt to odorant stimulation under certain conditions [101, 102], piriform cortical neurons adapt much more rapidly and strongly following either prolonged or repeated odor stimulation [102]. Cerebral blood volume (CMV) fMRI studies also show neural responses to repeated stimulations adapt more in higher olfactory regions than in OB [103]. More importantly, the interactions between multiple regions also play a key role in the habituation. In piriform cortex, rapid adaptation has been arguably associated with mGluR II/III-mediated depression of the glutamatergic mitral-pyramidal cell synapse [104, 105]. Similarly, in mice models, habituation has been implemented via short-term depression of synaptic strength between mitral cells in the OB and principal cells in the cortex [106] (analogous to Kenyon cells in the insect mushroom body). In *Drosophila*, the adaptation was also mediated by interactions between inhibitory PNs, excitatory PNs, and their targets in the lateral horn (LH). To better understand how adaptation changes across multiple regions, I will use the *Drosophila* olfactory system to thoroughly study and compare neural responses after stimulus repetition from peripheral sensory neurons axonal input to AL, ePNs dendrites in AL to ePNs/iPNs axonal output into LH/Calyx.

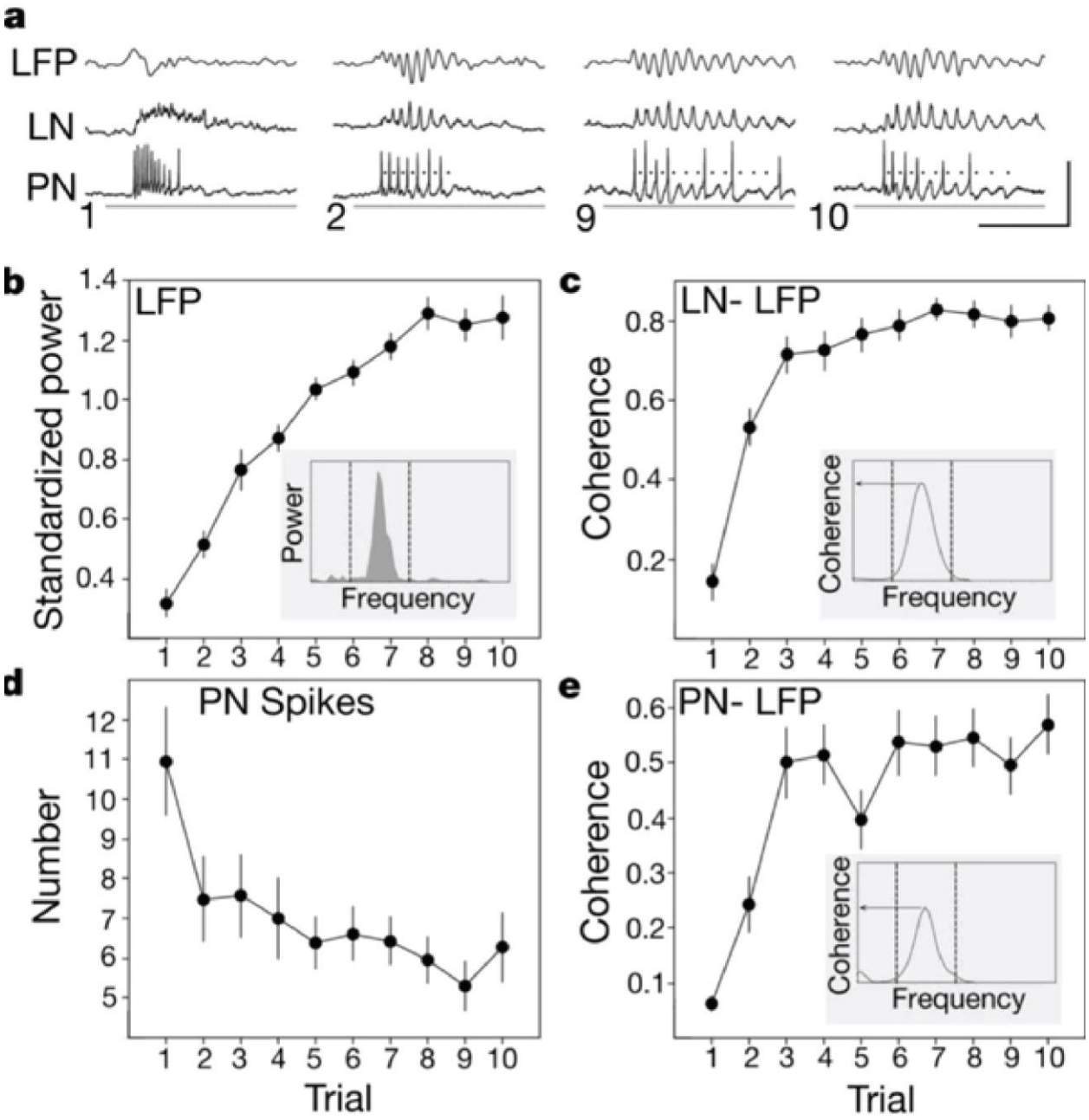

Figure 1.7: Coherence and spike time precision increase over stimulus repetition.
(a) Comparison between the initial (trials 1-2) and later trials (trials 9-10) of the same stimulation is shown for local field potential (LFP), local neuron (LN), and projection neuron (PN).
(b) LFP power spectrum increased during the first 7 or 8 trials before reaching asymptote.
(c) Coherence between LN and LFP increased rapidly in the first two trials.
(d) Number of odor-elicited PN spikes is plotted as a function of the trial number.
(e) Coherence between PN spike time and LFP increased over trials (reproduced from [72])

1.5 Thesis Outline

This dissertation focuses on using state-of-the-art analytic methods to study the role of short-term memory in altering odor-evoked neural responses in both locust and fruit fly olfactory systems. The overall organization of the dissertation is as follows. All computational methods will be developed and described in Chapter 2, including all statistical analyses for interpreting both electrophysiological and imaging datasets. This includes dimensionality reduction methods, region-of-interests extraction methods for imaging data, and various classification methods to quantify the robustness of odor recognition. In Chapter 3, I will study the influence of repetitive stimuli on the antennal lobe neural circuit and how the spontaneous activity is altered to carry stimulus-specific information. The influence of short-term memory on neural responses to both repetitive stimuli and novel stimuli will be studied. In Chapter 4, I will focus on neural responses in the fruit fly olfactory systems. For this, I will analyze light-sheet calcium imaging datasets. Particularly, the responses across multiple trials will be studied to compare the short-term memory effects and identify loci for short-term memory. Comparison within and across different flies will also be made to identify generic and idiosyncratic features of olfactory information organization and processing. Lastly, in Chapter 5, I will study whether odor identity could still be robustly recognized and the statistical structure of these decoding algorithms necessary to achieve this result. I will correlate results from decoding neural responses with behavioral recognition responses recorded to constrain the statistical models. Chapter 6 summarizes the contributions made and concludes the dissertation. Future work in the study of olfactory signal processing will also be proposed.

Chapter 2: Methods

In this chapter, I will introduce the analytical methods used to understand high-dimensional neural datasets from multielectrode recordings and light-sheet calcium imaging. Firstly, the statistical analysis methods will be presented for the analysis of single and population neurons responses. Then I will summarize the dimensionality reduction methods to understand high-dimensional population data with a focus on the trial-by-trial tensor decomposition method. The following section will introduce imaging analysis and regions of interest extraction methods for calcium imaging data. Lastly, the decoding methods are described, and a discrete weights network for classification is developed.

2.1 Spiking data analysis

Peri-stimulus Time Histogram (PSTH): Spike trains of each PN were separated into 50 ms time bins and summed. Then spike trains were averaged across trails or cells to obtain population-level PSTHs.

PN response characterization: We classified projection neurons as ON-responsive if the spike counts in any time bin during the stimulus presentation exceeded mean + 6.5 s.d. of pre-stimulus activity (2 s window just before the onset of any stimulus). Similarly, a PN was regarded OFF responsive if it met the same criterion in a 4 s window after the termination of the stimulus (0.5 s to 4.5 s after stimulus termination. Note that a 500 ms window immediately after the termination of the odorant pulse was ignored as it confounded both ON and OFF responses. All PNs that did not meet either of these criteria set for ON or OFF responders were regarded as ‘non-responders'. PNs that met both these criteria were included in the sets of both ON and OFF responders.

Correlation analysis of PN response: The PN spikes were binned in 200 ms non-overlapping time bins, and spike counts of different PNs concatenated to obtain a population spike count vector. Pearson correlation coefficients between two PN ensemble spike count vectors were calculated using equation 1 (here x_i represents population PN response vector in the ith time bin). Each pixel in the correlation plot (**Figure 3.1c, d; ith row – jth column**) indicates the correlation value between projection neuron spike count vectors observed in the ith and jth time bins.

To compute correlation values across trials (as shown in **Figure 3.1e, f**), we used mean PN spike counts in different periods of a single trial: during 15 s pre-stimulus period, during 4 s stimulus presentation window (stimulus-evoked response vector), 4 s window after stimulus termination (Off response vector), and over a 16s period after Off response period (starts 4 s after stimulus termination; post-Off response vector).

$$Correlation = \frac{\sum_k (x_i^k - \bar{x}_i)(x_{avg}^k - \overline{x_{avg}})}{\sigma_i \sigma_{avg}} \quad (1)$$

Prediction analysis and confusion matrix: We considered ensemble projection neuron spike counts in a non-overlapping time bin as a high-dimensional response vector for this analysis. To estimate prediction probabilities, we followed the leave-one-trial-out validation approach. Twenty-four trials were regarded as training trials, and the remaining one trial was left out as the test trial. This was repeated 25 times so that all trials were made a test trial once. Five trial-averaged reference templates were generated for each odorant at each dilution level. These reference templates represented the mean responses during the following five temporal windows: -15 to -12 s, -12 to -9 s, -9 to -6 s, -6 to -3 s, and -3 to 0 s (all before the stimulus was delivered).

An angular distance metric was used to find the nearest reference template:

$$\text{Angular distance} = \cos^{-1}\left(\frac{V_t \cdot V_r}{|V_t| \cdot |V_r|}\right) \quad (2)$$

Then test vector in each time-bin was assigned to the same odor category as its best matching reference template. Those vectors that are not within a certain angular distance of any reference templates were categorized as unclassifiable responses (a 60 degrees angular distance threshold was used for all classification analyses). The classification analysis was repeated using four different time bin sizes to calculate PN spike counts: 100 ms, 250 ms, 500 ms, 1 s (**Figure 3.3d**).

Vector analysis: For this analysis, we averaged the 15 s pre-stimulus spiking activities and 4 s odor-evoked spiking activities separately for each projection neuron in a given trial. This resulted in an n-dimensional pre-stimulus activity vector and an n-dimensional response vector for each trial (n = number of projection neurons recorded). To compare baseline and odor-evoked projection neuron activities during different trials, we concatenated projection neuron firing count vectors during both these epochs and performed a linear principal component analysis. The high-dimensional PN activity vectors in each trial were projected along the leading three eigenvectors of the data covariance matrix to obtain the low-dimensional vector shown in **Figure 3.11**. All dashed vectors were obtained by applying vector addition of baseline activity vector and odor-evoked response vector.

2.2 Dimensionality Reduction Methods

Principal component analysis: We used linear principal component analysis (PCA) as a basic method to visualize high-dimensional PN spike counts. The spike counts observed for each PN in 50 ms non-overlapping time bins were binned to generate an n-dimensional vector of neural activity for each time bin (n = 89 PNs). The high-dimensional PN spike count vector was projected onto the top three eigenvectors of the data covariance matrix for visualization purposes. These

low-dimensional representations of PN activity were color-coded depending on whether the target odorant was presented during that time bin. Linear PCA has been used in various places in this dissertation.

Dimensionality reduction analysis for baseline activities: We averaged the spike counts observed for each PN during the 15 s pre-stimulus window and concatenated spike counts across PNs to generate an *n*-dimensional vector for each trial (*n* = number of projection neurons). The high-dimensional PN spike count vector for each trial was projected onto the top three eigenvectors of the data covariance matrix (**Figure. 3.2b)**.

Tensor-based data decomposition: We first organized neural response data as a three-way array (Neuron × Time × Trials; the stimulus information was also blended into trial dimension), then employed a direct 3-way tensor decomposition approach [107]. Here, the 3-d data cube was approximated using three loading matrices, A, B, and C with elements a_{if}(neuron dimension), b_{jf} (time dimension), and c_{kf} (trial dimension). e_{ijk} was the residual element (see the equation 2). The tri-linear model was found using alternating least squares.

$$x_{ijk} = \sum_{f=1}^{F} a_{if} b_{jf} c_{kf} + e_{ijk} \quad (3)$$

where i, j, k denotes the three different dimensions, and F indicates the total number of factors used for the analysis that was determined by the core consistency diagnostics[108]. In our case, when $F = 3$, the core consistency was above 50 %, while it dropped to below 40% when $F = 4$. Therefore, we used three factors for our data decomposition. The basis vectors c_k across trials in the trial dimension are shown in trial mode plots (**Figure 3.5e, f**).

Trial-to-trial odor trajectory: For this analysis, we first reconstructed the dataset by computing the outer product of the loading matrices obtained by the tensor decomposition. The reconstructed

3-d tensor was then unfolded into a concatenated matrix (i.e., along the trial dimension). After unfolding, the ensemble projection neuron responses were arranged as time series data of *n* dimensions (where *n* is the number of neurons) and *m* steps (the number of 50 ms time bins × the number of trials). Note that only the projection neuron activities during the four-second stimulus presentation window in each trial were used for this analysis. The ensemble projection neuron response vectors (in a given 50 ms time bin) were projected onto the three eigenvectors of the response covariance matrix that accounted for the most variance in the dataset, using principal component analysis. Finally, the low-dimensional points were connected in a temporal order to visualize neural response trajectories to different stimuli on a trial-to-trial basis. All trajectory plots shown in **Figure 3.5a-d** were generated after smoothing with a 3-point running average low-pass filter.

2.3 Calcium Imaging Analyses

Motion correction using histogram matching: Extracting functional information from a series of images requires that the location of a given voxel within the brain does not change over time. However, there is usually some degree of subject motion within the scanner. Therefore, to render the data fit for statistical analysis, this motion must be preprocessed and corrected. We will normalize the statistics of images within the series accounting for flashing activities of neural response by histogram matching. Then we will select the time frame with minimum standard deviation as the template and use a rigid-body transformation to align all frames to the template frame.

Constrained Nonnegative Matrix Factorization for image segmentation: We will identify the region of interest by applying constraint nonnegative matrix factorization. The spatiotemporal calcium activity can be expressed as a product of a spatial basis matrix *A* and a temporal matrix *C*.

$$Y = AC + E \tag{4}$$

Y represents spatiotemporal calcium response, where each column represents a vectorized calcium image in a time frame. Each row represents a pixel value across time frames, and *E* indicates the observation noise. The factorization procedure is similar to regular nonnegative matrix factorization, requiring spatial matrix *A* and temporal matrix *C* being nonnegative. Moreover, the spatial component matrix is endowed with additional sparsity constraints to promote more compact and regularized spatial response regions identified. The problem can be summarized as following optimization problem:

$$\min_{A,C} \|Y - AC\| \tag{5}$$

$$\text{s.t.} \quad \mathrm{A}, \mathrm{C} \geq 0$$

$$\|A\|_1 \leq \epsilon$$

We will optimize the spatial component and temporal component in an alternative way such that a new estimate of *A* is obtained by use of the last estimate of *C* and vice versa. And similar to [109], at the end of each iteration, we will merge overlapping components with high temporal correlation and remove components with a low signal-to-noise ratio. I will introduce the spatial subproblem and temporal subproblem separately in the following part.

Estimating spatial components: The spatial problem can be described as equation:

$$\min_{A} \|Y - AC^{k-1}\| \tag{6}$$

$$\text{s.t.} \quad \text{A} \geq 0, \|A\|_1 \leq \epsilon$$

Each column of spatial matrix A expresses the location and shape of a neuron. The number of columns is the number of spatial regions to be identified. Again, we want A to be sparse to promote the localized spatial regions. It is done by imposing a sparsity constraint on l_1 norm of spatial components A. To speed up the optimization process further, we restricted the candidate spatial support of regions j at iteration k to a dilated version of the support of region j at iteration k-1. When estimating the i-th row of A^{k}, we can restrict our search to the regions whose spatial support includes pixel i. As this subproblem is convex, there exists a variety of methods to solve it. I will solve this optimization problem by a nonnegative least-angle regression (LARS) algorithm row-wisely.

Estimating temporal components: After each iteration of updating spatial components, the optimization of temporal components can be described as:

$$\min_{\text{C}} \|Y - A^{k-1}C\| \tag{7}$$

$$s.t. \quad C \geq 0$$

As we don't want to impose any additional structure into temporal traces, we won't explicitly model temporal calcium dynamics. Such a problem can be simply solved by a nonnegative least-squares procedure.

Flexible Initialization using Local Correlation Map: Due to the non-convexity of optimization problem, the quality of the solution is highly sensitive to the initialization. Many initialization methods need to pre-run a matrix factorization. But such method is time-consuming and requires

presetting a specific number of spatial components identified. In this study, I will use a local correlation map to initialize the response regions. The correlation value in each pixel is obtained by computing correlation coefficients between the temporal trace of that pixel and the mean temporal trace of surrounding pixels. After obtaining the local correlation map, we apply the median filter and morphological closing to obtain the initial response regions. Compared to initialization using factorization, it is computationally more efficient and does not require predetermining the number of spatial components.

With the initialization using local correlation map and constraint nonnegative matrix factorization, we were able to identify spatial response regions accurately and efficiently. The response regions of the antennal lobe are shown in **Figure 2.1** (top two rows). Also, the response regions obtained from the lateral horn and mushroom body are shown in **Figure 2.1** (bottom three tows). Although the shape and size are different across different layers, the pipeline developed can still accurately detect the regions of interest.

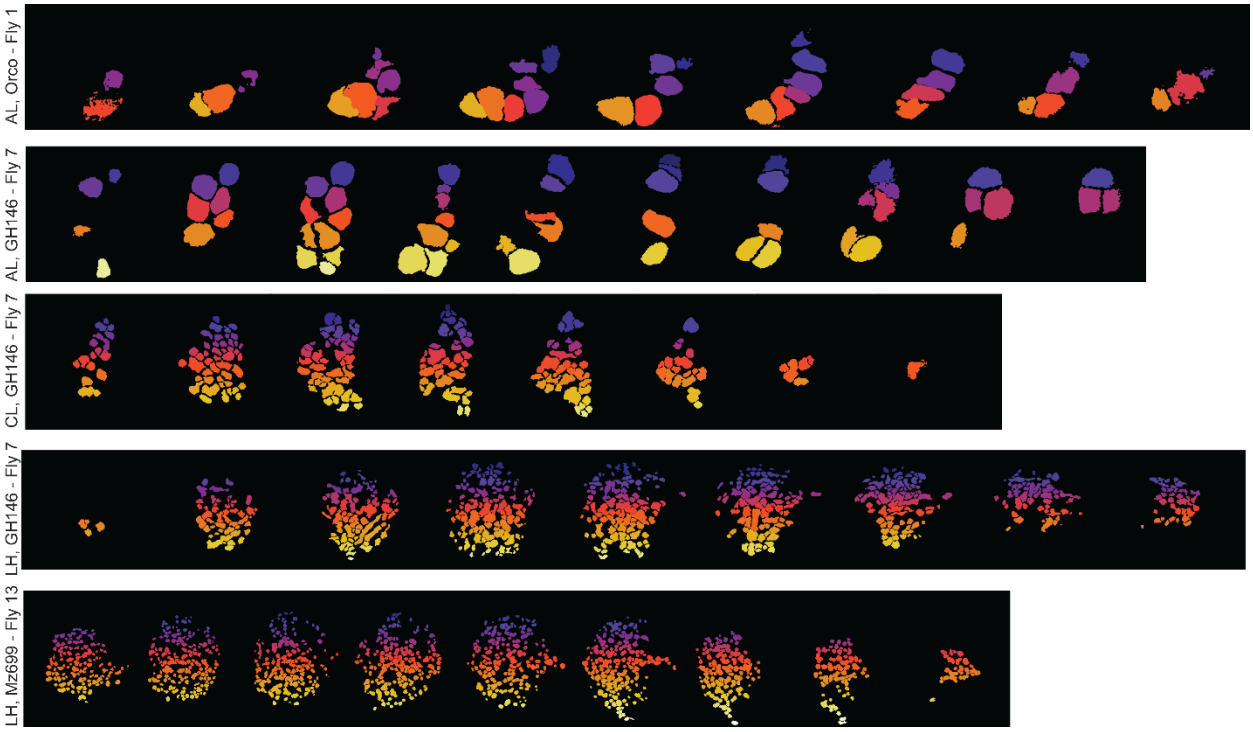

Figure 2.1 ROI masks extracted for each plane and each region are shown. In each row, the left-most panel shows ROI masks in the dorsal areas, and the rightmost panel shows ROIs in more ventral regions. In each plane, different ROIs are labeled using different colors. Each row shows ROIs across different regions and neuronal subtypes (from top to bottom: AL, Orco; AL, GH146; Calyx, GH146; LH, GH146; LH, Mz699).

2.4 Decoding methods

Linear SVM Decoder: The support vector machine classifier was used to classifier PN responses under different encounters of target stimulus. In the SVM classifier, the separating hyperplane was found to maximize the perpendicular distance between the hyperplane and the closest of the data points (support vector): $\gamma = y(v_{svm}^{T}x + b)$, where γ is the distance between the hyperplane and the data point x (89-dimensional PN responses vector). The algorithm was implemented using fitcsvm function in the MATLAB toolbox. During the training phase, only the neural responses to the solitary presentation of hex (or iaa) were used to determine the optimal SVM weight vector. For the hex-SVM classifier, neural responses during hex exposures were used as the positive class,

whereas baseline activities and neural responses to iaa were used as the negative class. The iaa-SVM classifier was trained similarly. After the SVM classifier was fit, it was used to classify trials when the trained or an untrained target stimulus was presented with variations in pulse dynamics, stimulus history, and background, as shown in **Figures 5.6 and 5.7**.

The discretization of the linear SVM classifier is done by comparing the linear weights learned with two different thresholds. If the weight is larger than the positive threshold, the corresponding weight is set to 1. If the weight is less than the negative threshold, the corresponding weight is set to -1. If the weight falls between two thresholds, the weight is set to 0. After discretization, the classifier was used to test the neural responses again. A statistical method to train the discrete weights is provided in the next section.

A Bayesian approach to train the binary weights neural network: A neural network is constructed with a collection of connected units or nodes called artificial neurons. A signal gets transferred from one unit to the other depending on the weight of the connection between the two units. This weight is similar to the synaptic strength between two neurons. As shown in **Figure 2.2a**, most artificial neural networks use real-valued weights for the connection between different neurons, and the output of each artificial neuron is computed by a non-linear transformation ($g(.)$) of the weighted sum of its inputs. Similarly, the Binary weights neural network uses only two values for weights in the computation and, therefore, simplifies regular neural networks (**Figure 2.2b**). As such, BNN implementation permits us a much simpler computation using hardware. In addition, this implementation also allows us to understand if there are two types of competing features (with two opposing weights) that we need to understand from the data.

A well-studied training method of a neural network involves performing a backpropagation step, which is based on gradient descent. To obtain the gradient information, firstly, the output of

the previous layer (or the network's input) will forward propagate through the network (**Figure 2.2c**) to find the activations of all the hidden and output units. Next, the gradient information can be efficiently sent backward (**Figure 2.2d**) to each node layer by layer. While training the BNNs, however, the backpropagation step with regular gradient descent step encounters a non-differentiable term as the weights are constrained to be binary. Here, we will focus on binary weights neural network (BNN) and seek to find an efficient way to obtain the weights. We proposed to relax the binary weights and learn them in a Bayesian framework.

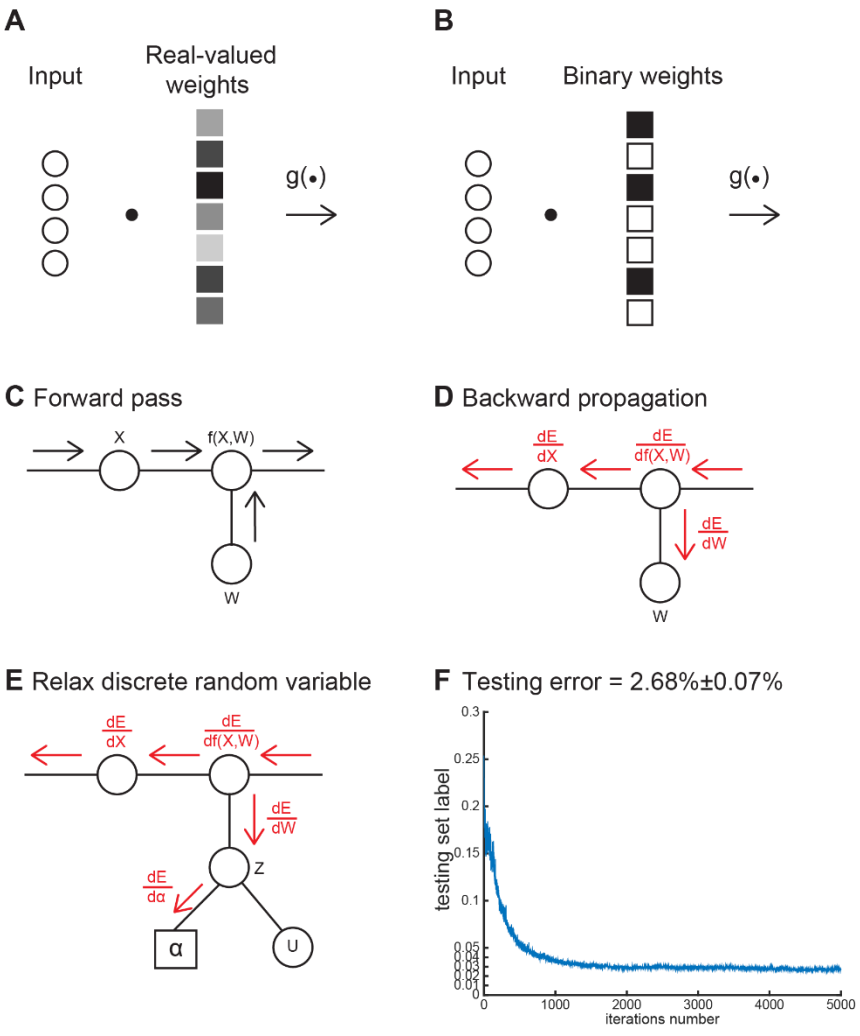

Figure 2.2 Discrete weights neural network.

(a) Diagram of a regular feed-forward network model. Here shows one layer of network computation. Network input or output from the previous layer is weighted by real-valued weights, and then the sum is sent to a non-linear activation function to downstream nodes. **(b)** Diagram of a binary weights network model. The network structure is the same as before, but all the weights are constrained to 1 or -1. **(c)** The forward pass of neural network. All inputs traverse through all neurons layer-by-layer to the neural network's output. **(d)** After the output and loss function is calculated. The gradient information is sent backward layer-by-layer to the first layer of the neural network. Note that if one node is discrete, e.g., discrete weights, the gradient cannot be used to update the weights. **(e)** Relax and reparameterize the discrete weights using fixed random variables and a parameterized function. The gradient information can now be used to update the parameters. **(f)** The learning curve of the training algorithm. The testing error converged after around 2000 iterations to 2.68%±0.07%.

Let us consider a classification problem with the samples $\{\boldsymbol{x}_n, y_n\}$, where $\boldsymbol{x}_n$ denote input patterns in R^n, and y_n represents class labels. Our formulation of Binary neural network will build on a Bayesian treatment of the neural network. The joint distribution of the model is:

$$p(\boldsymbol{x}_n, y_n, \theta) = p_o(\theta \prod_{n=1}^{N} p(y_n | f(\boldsymbol{x}_n), \theta)) \tag{6}$$

θ represents the weights, $p_o(\theta)$ is the prior distribution of the weights, $f(\boldsymbol{x}_n)$ represents the computation of neural network. We constrained the weights (equivalent to connections in a neural network) to be binary (or discrete), $\theta \in \{-1,1\}$. Readout function $p(\cdot)$ is either softmax function for multiple-classes problem or sigmoid function for two class problem. After framing the network as a probabilistic model, we can now find the posterior distribution of the network weights $p(\theta|\boldsymbol{x}_n, y_n)$ and use the uncertainty information encoded in it for future predictions. The direct inference of weights from this posterior distribution is intractable. We approximated the intractable posterior distribution with a tractable distribution $q_\phi(\theta)$ parameterized by the variational parameters ϕ and train the variational parameters by maximizing the evidence lower bound $L(q)$. To obtain an unbiased Monte Carlo gradient estimator of lower bound with respect to variational

parameters, we sought to relax and reparameterize the weights θ using the Gumbel-Softmax variable[110, 111]:

$$\theta_k = \frac{\exp\left(\log \alpha_k - \log\left(-\log U_k\right)/\lambda\right)}{\sum_{i=1}^{n} \exp\left(\log \alpha_i - \log\left(-\log U_i\right)/\lambda\right)}, \qquad U_i \sim Uniform(0,1) \tag{7}$$

Then the gradient can be approximated unbiasedly by:

$$\nabla E_{q_\phi(\theta)}\left[\log \frac{p(y,\theta)}{q_\phi(\theta)}\right] \approx \nabla_\phi \frac{1}{K} \sum_{k=1}^{K} \log \frac{p\left(y, g_\phi(\epsilon_k)\right)}{q\left(g_\phi(\epsilon_k)\right)}, \qquad \epsilon \sim p(\epsilon) \tag{8}$$

During the training phase, we can utilize the gradient information obtained by regular backpropagation to update the binary weights (**Figure 2.2e**). We also follow standard stochastic gradient descent to update the parameters of approximation distribution and adaptively choose the step size using ADAM[112]. As the size of mini-batch for stochastic gradient descent was large enough, the sample drawn per point can be set to 1, which makes the computation complexity of proposed method to be almost identical to training a regular neural network with gradient back-propagation. We verified our technique using the MNIST dataset and achieved a testing error rate of 0.0268 (Figure 2.2f), close to the benchmark result of 0.018 (standard neural network with same network structure).

Chapter 3: Sensory Memory for Repetition Suppression and Novelty Enhancement in an Olfactory Circuit

3.1 Introduction

The ability to adapt is key to the survival of many living organisms [99]. While this computational task appears relatively straightforward, any solution should satisfy at least a few important constraints or requirements. First, attenuation of stimulus-evoked responses upon recurrence should not corrode information regarding its identity. Second, behavioral preferences for many stimuli may vary with intensity [113-115]. Therefore, at least in such cases where behavior diverges with stimulus intensity, the information about the intensity of the recurring stimulus should be encoded in an adaptation invariant manner. Finally, only the response evoked by the familiar stimulus should be selectively impeded, and sensitivity to novel or unexpected cues should be ideally retained. In this study, we explored whether and how the locust olfactory system deals with these challenges.

In the olfactory system, adaptation to a persisting cue begins right at the level of olfactory receptor neurons. Usually, sensory neuron responses to prolonged chemical exposures reduce throughout that exposure [87, 116-119]. However, a lengthy time-window of non-exposure to the stimulus, typically on the order of tens of seconds, can allow full recovery of the sensory neuron response strength [89, 114, 118, 120]. Interestingly, such temporal discontinuity in stimulus encounters does not prevent the stimulus-evoked responses in downstream centers from diminishing upon subsequent encounters of the familiar stimulus [76, 121-123]. This suggests that

information about the temporally discontinuous but repetitive stimuli continues to persist even in the absence of olfactory sensory neuron input.

If sensory memory persists in the early olfactory circuits, how does it interfere with subsequent responses evoked by the familiar cue that caused this short-term memory? Stimulus-specific sensory adaptation can be achieved relatively easily in sensory systems with labeled-line coding schemes. However, it becomes particularly challenging in a modality such as olfaction, where most chemosensory cues are encoded by spatiotemporal patterns of neural activities distributed across an ensemble of overlapping sets of neurons [56, 124-127]. In the vertebrate and the invertebrate olfactory systems, each olfactory receptor neuron and their downstream targets (projection neurons in the invertebrate antennal lobe or mitral/tufted cells in the vertebrate olfactory bulb) respond to multiple stimuli [76, 127-131]. Conversely, most odors activate an overlapping set of neurons in these early processing stages. To add further complexity, the set of neurons activated is not static but has been shown to evolve over time [132]. How are neural responses to a repetitive olfactory stimulus altered in this dynamic and combinatorial nature of odor-evoked neural representations? Do alterations in neural response strength upon repetition confound information regarding stimulus intensity? More importantly, how does adaptation to a stimulus alter the processing of other cues? We explored these issues in this study using a model of the invertebrate olfactory system.

3.2 Results

3.2.1 Spontaneous activity is negatively correlated with stimulus-evoked responses of a recurring stimulus

We sought to understand how projection neuron (PN) activities change after the very first stimulus exposure. The first set of experiments included multiple blocks, with twenty-five trials

each, when one odorant at one intensity was repeatedly presented (**Figure 3.1a**). Each trial in the block included a four-second stimulus presentation window. The inter-stimulus interval was sixty seconds. The inter-trial interval was twenty seconds. Different odorants at different intensities were repeatedly presented in different blocks. A 15-minute window, when no stimulus was presented, separated two consecutive blocks of trials. This window was included to reset any short-term memory that may have formed due to repeated presentation of the same stimulus[72]. **Figure 3.1b** shows the spike counts as a function of time (in 50 ms time bins) in all 81 neurons recorded as a heat map (dark colors indicate higher firing rates). Note that the responses were sorted based on the overall change in the spontaneous activity (i.e., mean pre-stimulus – mean post-stimulus). Interestingly, PNs that responded during odor presentation (ON response) had the most reduction in their post-stimulus spiking activity and therefore appeared at the top of the heat map. On the other hand, PNs that were inhibited during odor presentation but were released from this inhibition after the stimulus termination had elevated and sustained spiking activities in the post-stimulus period. Therefore, these neurons appear at the bottom of the heat map. Note that the changes in spiking responses immediately following the termination of the stimulus persisted for tens of seconds after its termination.

How do these observed changes in spontaneous activities relate to the stimulus-evoked responses? To understand this, we computed correlations between the ensemble neural activities in different time bins recorded during a single trial (pre-, during- and post-stimulus windows included **Figure 3.1c-e**). As expected, we found that the ensemble responses during the odor presentation window were highly correlated only amongst themselves. We observed no noticeable correlation between the pre-stimulus activities and the odor-evoked responses in the first trial. Because the ON and OFF responses involved nearly non-overlapping sets of PNs, there was a

negative correlation between observed neural activities during these epochs. Interestingly, these negative correlations persisted well after the termination of the odor pulse (15 s post-stimulus shown in the plot; indicated using white arrows). As a result, the ensemble activities in the pre-stimulus time window gained a negative correlation during later trials of the same odorant (the prominent blue '†' pattern observable in the later trials and not in the first trial; indicated using white arrows; as the pre-stimulus activities in the later trials are merely a continuation of post-stimulus activity from the previous trial).

This systematic reduction in correlation between the pre-stimulus and stimulus-evoked ensemble responses was observed for all four odorants used in this study (**Figure 3.1f**; left-most panels). The effect was stronger at higher concentrations and became weaker when we lowered the odorant concentrations (**Figure 3.1g**; left-most panels). Also, note that the PN responses immediately after the termination of the stimulus were the least correlated with the odor-evoked neural activities (**Figure 3.1f, g**; middle panels), whereas the PN spiking responses during OFF response period and post-OFF epochs in every trial remained highly correlated with one another across trials (**Figure 3.1f, g**; rightmost panels). In sum, our results reveal that sensory memory about a repetitively encountered stimulus persists in the antennal lobe and generates a persistent negatively correlated spontaneous response. Further, the duration of persistence of this sensory memory increased with the intensity of the odorant.

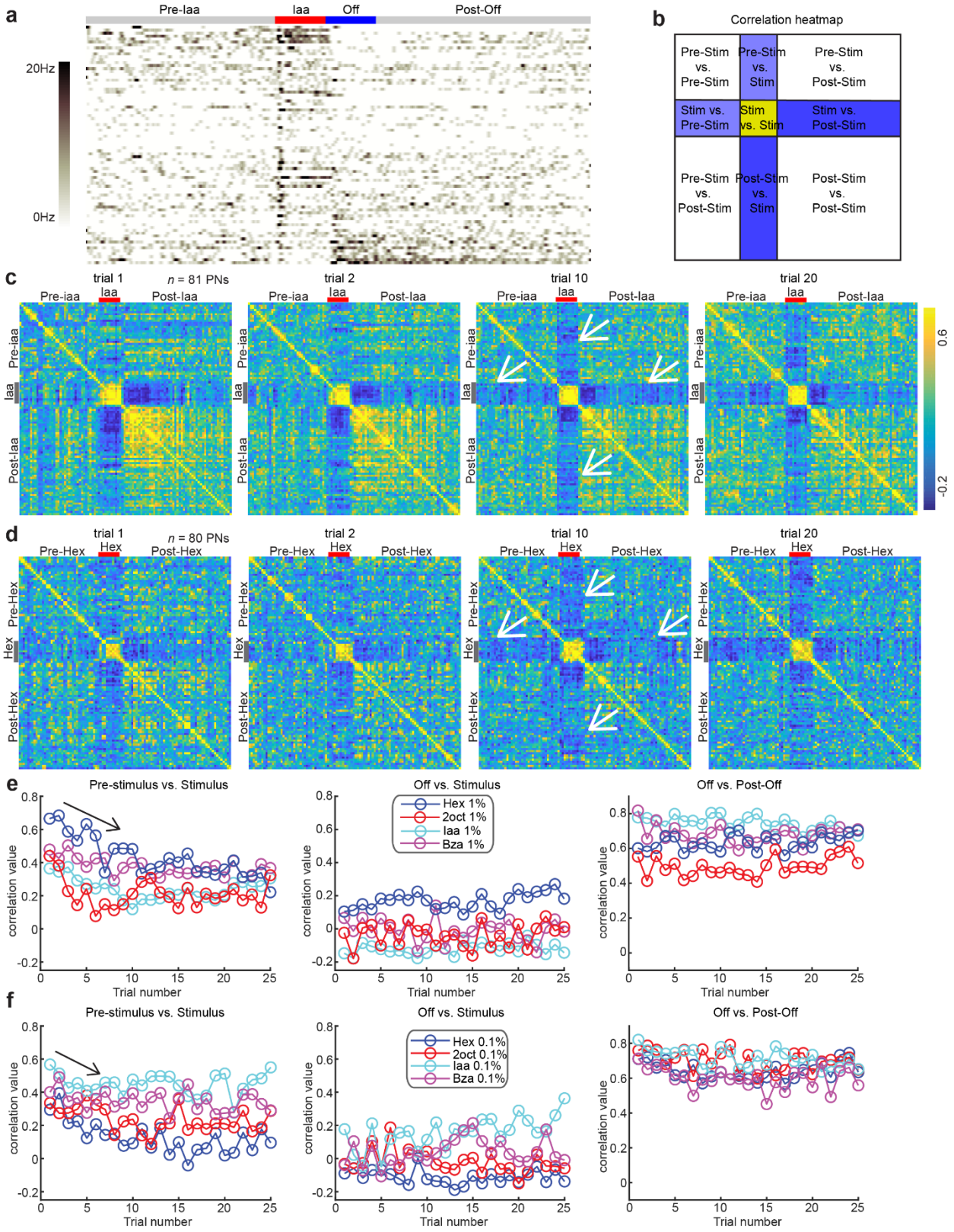
a
Pre-Iaa
Iaa
Off
Post-Off
20Hz
0Hz
b
Correlation heatmap
Pre-Stim vs. Pre-Stim
Pre-Stim vs. Stim
Pre-Stim vs. Post-Stim
Stim vs. Pre-Stim
Stim vs. Stim
Stim vs. Post-Stim
Pre-Stim vs. Post-Stim
Post-Stim vs. Stim
Post-Stim vs. Post-Stim
c
trial 1
n = 81 PNs
trial 2
trial 10
trial 20
Pre-iaa
Iaa
Post-Iaa
0.6
-0.2
d
trial 1
n = 80 PNs
trial 2
trial 10
trial 20
Pre-Hex
Hex
Post-Hex
e
Pre-stimulus vs. Stimulus
Off vs. Stimulus
Off vs. Post-Off
Hex 1%
2oct 1%
Iaa 1%
Bza 1%
correlation value
Trial number
f
Pre-stimulus vs. Stimulus
Off vs. Stimulus
Off vs. Post-Off
Hex 0.1%
2oct 0.1%
Iaa 0.1%
Bza 0.1%
correlation value
Trial number

Figure 3.1: Repetitively encountered stimulus generates persistent sensory memory.
(a) A schematic of the odor stimulation protocol used. Each block included twenty-five trials. A 4-second odor puff was presented in each of the trials. The inter-stimulus interval was set to a minute. Within a single block of trials, the same stimulus was repeatedly presented. Two blocks of trials were separated by a 15-minute no-odor window to reset any adaptation/memory induced by the previous odorant**.**
(b) Firing rates of 81 projection neurons (in 50 ms time bins; 81 rows) are shown as a function of time (columns; 40 s in total). The odor-evoked responses during the very first exposure to isoamyl acetate (iaa) are identified using color bars (red – 4 s odor ON and blue – 4s after odor OFF) at the top of the plot. Spiking activities across PNs during a 15 s pre-stimulus stimulus window and a 17 s post-Off response period are also included in the plot. Note that the PNs were sorted based on the difference between mean firing rates of the pre-stimulus period and post-stimulus period (includes both off and post-off epochs). Below the image plot, the mean firing rate across projection neurons (PNs) is shown as a function of time. The 4-s odor stimulation period is shown as a gray bar along the *x* axis. We define the period before odor stimulus as the pre-stimulus period, the odor-stimulus period as the ON period, and 4 s after odor termination when the PSTH is still above the baseline levels as the OFF period. Finally, the period after the OFF period was defined as the post-OFF period.
(c) A schematic overview of the correlation analysis is shown in panels **(d)** and **(e)**. Regions in the correlation heat maps comparing ensemble neural responses observed during stimulus presentation with pre- and post-stimulus are identified.
(d) Correlation maps for different trials are shown. The 4 s stimulus presentation period is identified using a red bar. Note that each non-diagonal pixel represents the similarity between ensemble PN spike counts in one time bin and those in another. Cooler colors indicate lower correlation, and hotter colors indicate higher similarity/correlations. Four representative trials are shown. Note that the correlation values between pre-stimulus PN spiking activities and odor-evoked spiking responses decrease across trials.
(e) Similar plots as **(d)** but for a different odorant.
(f) Left, correlations between mean pre-stimulus ensemble PN responses and stimulus-evoked population PN responses are shown when the same stimulus is repeated 25 times with a 60 s inter-stimulus interval. Different colors are used to show results for different odors and concentrations. Middle, similar correlation plots but now showing the comparison between stimulus-evoked responses and off responses. Right, similar plots showing correlation changes over trials between off and post-off neural responses.
(g) Similar plots as in **(f)** for a lower intensity of the same four odorants.

3.2.2 Spontaneous activity carries information about stimulus identity and intensity

Are these changes in the PN spontaneous activity odor-specific? We found that at the individual PN level, the pre-stimulus spiking activities tended to vary in an odor-specific manner (**Figure 3.2a**). To understand how odor-specific changes were in the ensemble firing rates in the pre-stimulus window, we calculated the mean spontaneous firing rate across PNs in a given trial (one ~80-dimensional vector per trial). The mean, pre-stimulus ensemble firing across PNs in each trial was visualized using principal component analysis. We found that each odorant at a given intensity formed a distinct cluster of baseline activities (**Figure 3.2b**). Also, while the ensemble-level spontaneous activity during the first trial was random (origin of the arrows shown in the plot), the pre-stimulus activity in subsequent trials evolved consistently and formed a tighter cluster. Furthermore, when the same stimulus was repeated after a reset period, the directions in which the pre-stimulus activity changed (direction of the arrows shown in the plot) were aligned (**Figure 3.2c**), resulting in them both acquiring a net negative correlation with the response evoked by the same stimulus. This result suggests the hypothesis that, during the later trials, it would be possible to predict the identity of the repeatedly occurring stimulus given the spontaneous activity in the antennal lobe network.

To test this hypothesis, we performed a classification analysis. Consistent with the PCA results, we found that the identity and intensity of a stimulus can be reliably predicted, well above chance level, on most trials. The prediction performance was greater when a larger time window was used for determining the PN spike counts during the pre-stimulus window (**Figure 3.3a, b**; see **Methods** for additional information).

Taken together, these results indicate non-random, odor-specific changes in spontaneous PN activities occur when an odorant is repeatedly encountered.

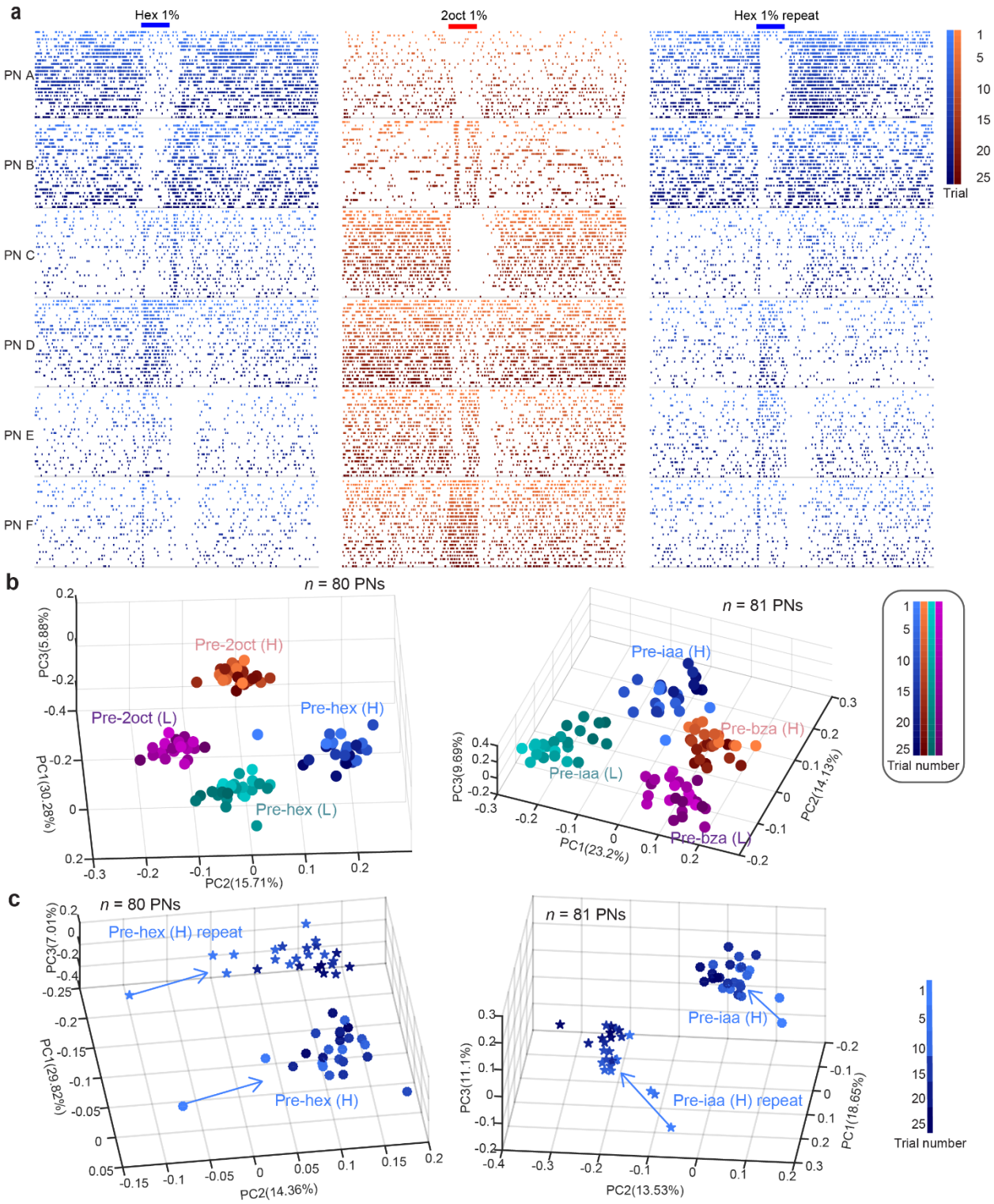

Figure 3.2: Spontaneous activity carries information about stimulus identity and intensity.
(a) Raster plots of six representative projection neurons are shown. Each trial is 40 s in duration: 15 s pre-stimulus period, 4 s odor presentation window (colored bar on the top), and 21 s post-stimulus period. The interval between odor presentations in consecutive trials is 60 seconds. For each neuron, spiking activities during twenty-five trials are shown (top-row – trial 1, bottom-row – trial 25). Note that the rasters are color-coded based on the trial number. The three columns correspond to three blocks of trials. In each block, one odorant was repeatedly presented. A 15-minute no-odor window separated consecutive blocks. Hexanol was presented in two different blocks of trials to evaluate reproducibility.
(b) Pre-stimulus ensemble projection neuron activities in a trial were averaged and visualized using principal component analysis (i.e., one high dimensional vector per trial). Lighter colors indicate earlier trials, and darker colors are used to distinguish later repetitions of the same odorant.
(c) Similar plot as **(b)**, but pre-stimulus ensemble projection neuron activities when the same stimulus is repeated during two different epochs are visualized. The direction in which the baseline activities change between stimulus exposures is highly reproducible when the same stimulus is repeated in different time segments.

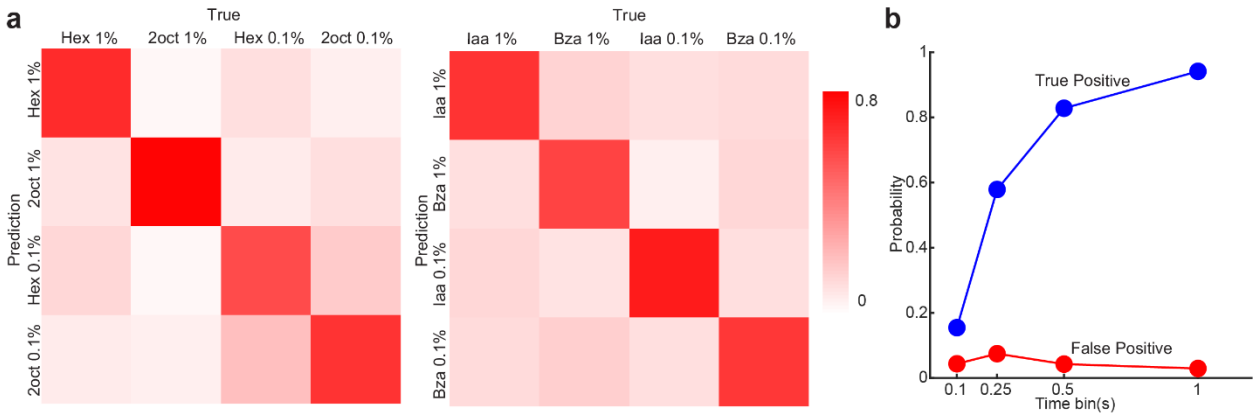

Figure 3.3: Stimulus identity and intensity information can be identified using spontaneous activities.
(a) Confusion matrices summarizing results from a classification analysis are shown. Templates of pre-stimulus activities in all but one trial were used to predict the identity of the odorant that is expected to be presented in the left-out trial (see **Materials and Methods**). Each column in the matrix shows the probabilities of assigning the identity of the odorant to one of the four possible stimuli. Chance level is 25% assignment to each of the four stimuli. High diagonal values indicate that the predicted and the actual odor identity matched on most trials.
(b) The classification accuracy with varying time-bin length. The pre-stimulus PN responses were binned using time bins of various sizes before classification using template matching. Recognition performance is plotted as a function of time-bin size. Larger the time-bins, more likely was the correct recognition of the stimulus to be encountered in the left-out trial.

3.2.3 PN firing patterns change reliably across trials

In addition to the spontaneous activity changes, we also noticed systematic changes in the odor-evoked firing patterns. Response features such as response latency and duration of inhibition changed substantially over trials across many projection neurons (**Figure 3.4a**). Furthermore, when the same stimulus is presented repeatedly after a desensitization period (> 15 min of no odor stimulation), these changes in firing patterns are repeatable (**Figure 3.4b**). Our results indicated that the total number of odor-evoked spikes across all recorded neurons reduced over trials. Consistent with prior results [72], the spiking activity reduction was greater during the first few encounters and was intensity dependent. For the two alcohols examined, the difference in spike counts between responses elicited at high and low stimulus intensities were maintained even after adaptation (**Figure 3.4c**; two left-most panels). On the other hand, spike count differences between two different stimulus intensities diminished over trials for the other two odorants used (iaa and bzald; **Figure 3.4c;** two right-most panels). More importantly, the earlier trials of odor exposures at low intensities elicited a response comparable to those evoked during the later trials of the same stimulus but at a higher intensity. These results suggest that adaptation may potentially confound the representation of stimulus intensity.

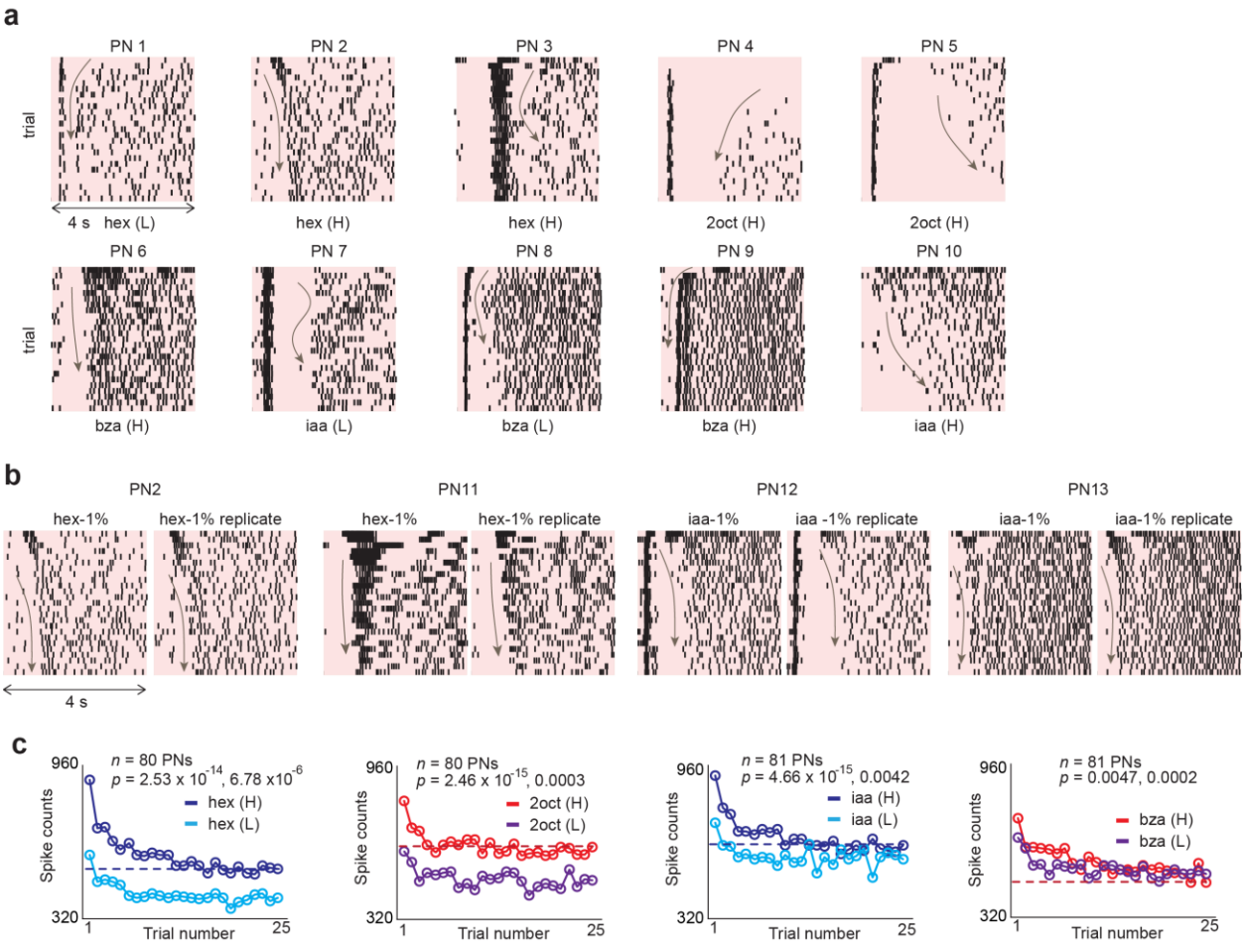

Figure 3.4: Inter-trial neural dynamics are diverse in individual projection neurons.
(a) Responses of ten representative projection neurons (PNs) to various odorants are shown as raster plots (25 trials each). Arrows highlight the systematic changes in stimulus-evoked response features such as inhibition duration and response latency across trials. Note that the spiking activity is shown during the entire four seconds of stimulus exposure.
(b) Raster plots of four representative PNs responses to two blocks of trials when the same stimulus was presented repeatedly in all 25 trials. A no-odor reset period greater than 15 minutes preceded each block of trials. The color box represents 4-s stimulus duration, and the arrows in the box indicate the systematic change in individual PN responses observed across trials.
(c) Total spike counts across all PNs during the entire four seconds of stimulus exposure were calculated and plotted as a function of trial number. Each panel reveals the total odor-evoked response generated across all recorded PNs to two different intensities of the same stimulus (H = 1% by volume, L = 0.1% v/v). The dotted line indicates the spike count observed during the 25th trial of higher intensity odor presentations. Two-way ANOVA was used to compare the spike counts between different trials and different odorant concentrations (see **Methods**).

3.2.4 Adaptation-invariant encoding of odor intensity

Could the information regarding stimulus intensity be robustly encoded in the population neural responses? Previous studies have indeed shown the ensemble neural activities cluster based on odor identity and intensity [72, 76]. However, this representation of stimulus-specific information stabilized only when the first trial responses were not considered. Given that major changes in spike counts due to adaptation occurred between the first and second encounters of a stimulus, we sought to examine how encoding of stimulus intensity varied before and after adaptation (i.e., across all trials).

To qualitatively understand this, we visualized the high-dimensional neural activities using a dimensionality reduction approach. The ensemble responses across multiple trials were concatenated to create a 3-D data cube (neuron x time x trial dimensions). Then, we directly performed a 3-D tensor decomposition and approximated the data cube as a sum of three rank-one tensors (for a rank 3 approximation to facilitate visualization). This pre-processing step, to approximate the original tensor by a rank-3 tensor, followed by regular unfolding the data cube for linear dimensionality reduction, resulted in neural response trajectories that captured the trial-to-trial variations in the dataset better than the direct unfold-then-PCA approach[133].

We plotted the ensemble responses in each 50 ms time bin during the odor presentation time window (4 s) and linked them based on the order of their occurrence to generate trial-by-trial odor response trajectories (**Figure 3.5a-d)**. Note that each trial generated a single loop response trajectory after dimensionality reduction. Six such trajectories (shown in blue) correspond to the responses evoked by *hex* (1% dilution) in representative trials: 1, 5, 10, 15, 20, and 25. Similarly, for comparison, six hex (0.1% dilution) trajectories (cyan) for corresponding trials are also shown.

The response trajectories showed a systematic change from light colors (early trials) to darker colors (late trials). Notably, the population responses changed such that the trajectories evolved in similar directions, but the length of the trajectory monotonically reduced over repeated trials. Similar results were also observed for the other three odorants used in the study (**Figure 3.5a-d**). Hence, these results suggest that even though the total number of spikes reduced with adaptation (correlated with the length of the trajectory), the combination of neurons activated (direction of the vector) can still robustly encode information about both odor intensity and identity. Further examination of factors extracted along the trial dimension (**Figure 3.5e, f**) revealed that different odorants presented at different concentrations robustly clustered, indicating the availability of odor identity and intensity information in the high-dimensional neural responses. The same was retained after dimensionality reduction.

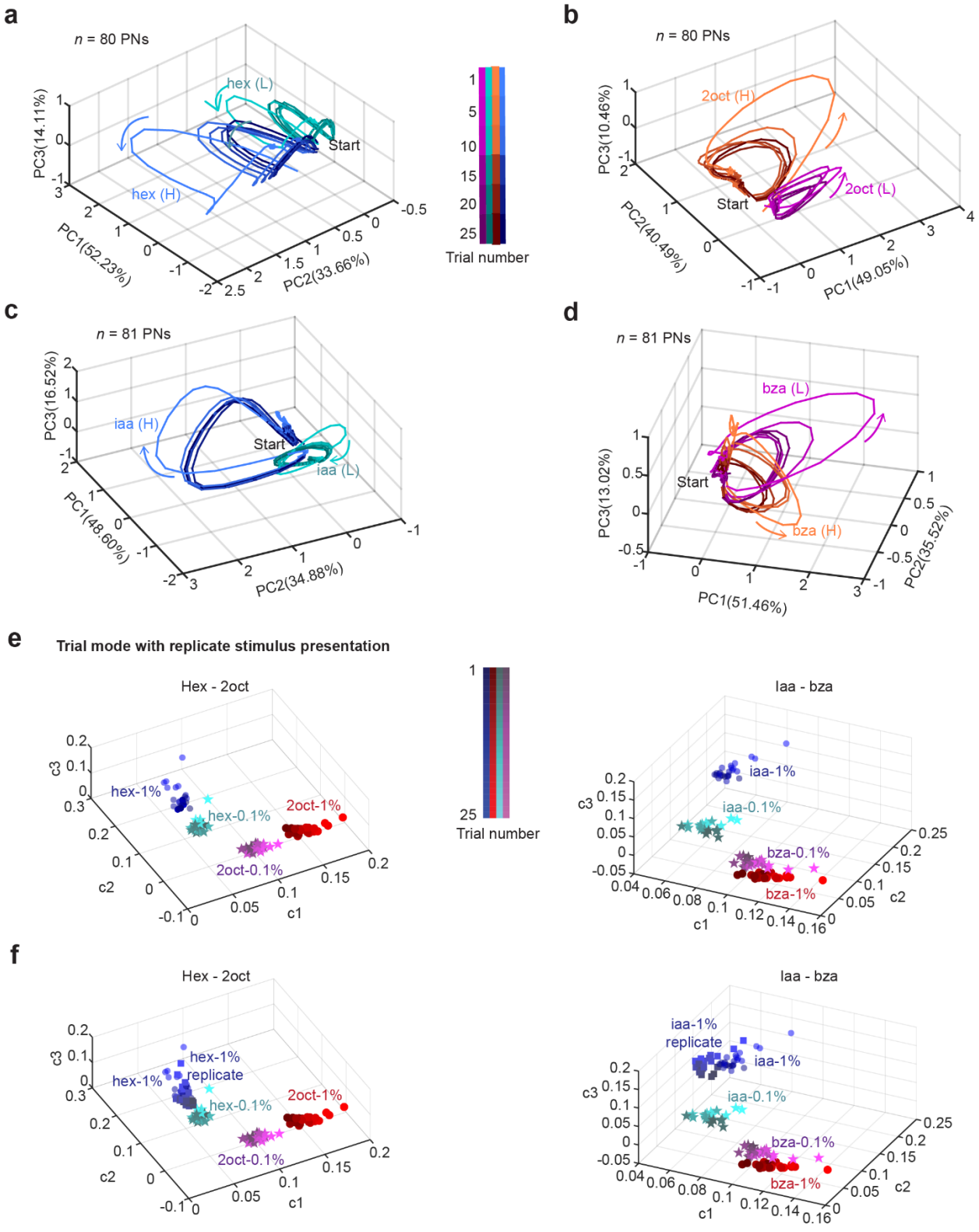

Figure 3.5: Ensemble neural activity change systematically over repeated trials.

(a-d) Odor-evoked ensemble projection neuron response trajectories are shown after dimensionality reduction using a tensor decomposition method (see **Methods**). The '*Start'* label indicates where the trajectories begin following odor onset, and the direction of response evolution over time is indicated (colored arrows). The response trajectories of representative trials 1, 5, 10, 15, 20, and 25 are shown. A color gradient from light (early trials) to dark (later trials) distinguishes responses observed in different trials.
(e) Information retained (loading elements) in the trial dimension following a 3-rank tensor decomposition (see **Methods**) is plotted as a 3-D plot. Each trial is represented as a symbol in this plot (a total of 25 trials are shown for each odor). The solid circle and star symbols represent higher (1%) and lower (0.1%) odorant concentrations.
(f) Similar plot as panel **e**, but the repeated block of twenty-five trials (*hex* 1% or *iaa* 1%) used in this study are also shown as squares for comparison.

To further corroborate our conclusions, we calculated the correlation between responses evoked by the same stimulus in different trials and between neural ensemble responses elicited at two different concentrations (**Figure 3.6)**. As can be noted, the correlation between neural responses evoked in different trials (diagonal blocks) was high, whereas the correlation between ensemble neural responses evoked by different concentrations was lower (off-diagonal blocks). Similar results were observed for all the four odorants used in the study (**Figure 3.6a-d**). We also performed a trial-by-trial, bin-by-bin classification analysis to quantify whether the concentration information was confounded by adaptation (**Figure 3.6e-h**). We used a leave-one-trial-out approach to validate the results. Our results indicate that a nearest-reference template classifier could correctly classify time bins in each trial as elicited during exposures to high or low concentrations of the odorant.

In sum, our results show that a combinatorial code could encode information regarding odor identity and intensity in an adaptation-invariant fashion. Since the same information about a stimulus is represented with fewer spikes in the later trials, we conclude that adaptation refines the odor codes by making them more efficient.

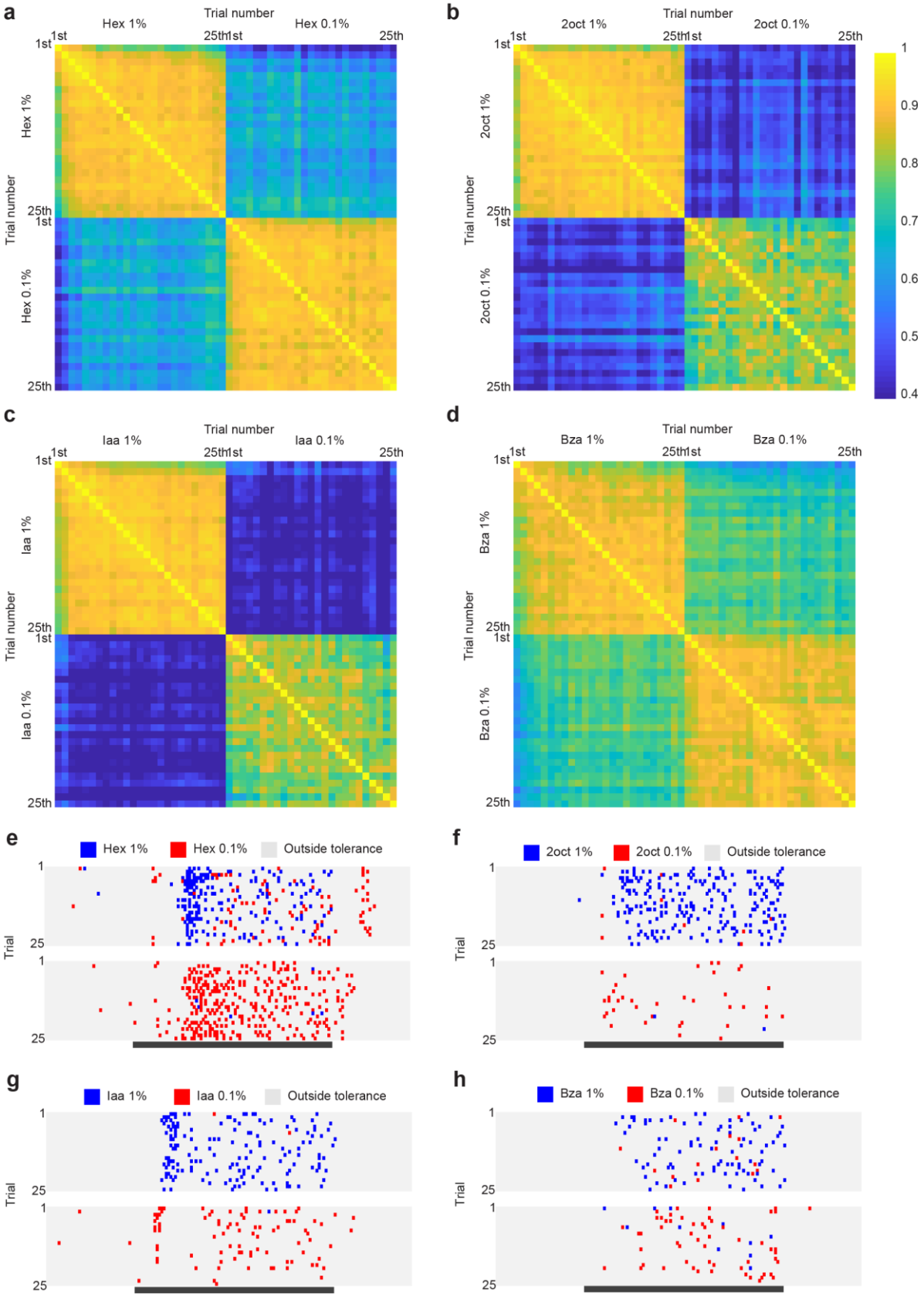
a
Hex 1%
Trial number
Hex 0.1%
1st
25th
Trial number
b
2oct 1%
2oct 0.1%
1
0.9
0.8
0.7
0.6
0.5
0.4
c
Iaa 1%
Iaa 0.1%
d
Bza 1%
Bza 0.1%
e
Hex 1%
Hex 0.1%
Outside tolerance
Trial
f
2oct 1%
2oct 0.1%
g
Iaa 1%
Iaa 0.1%
h
Bza 1%
Bza 0.1%

Figure 3.6: **Projection neurons response profiles robustly encode odor identity and intensity information.**
(a) Correlations between neural responses observed in different trials are shown. Each pixel represents the similarity between mean neural responses in one trial versus those in another trial. Diagonal blocks are correlations between trials when the same odorant at a specific intensity was repeatedly presented.
(b) Classification results are shown in a trial-by-trial and bin-by-bin fashion. Each row corresponds to a trial, and each pixel corresponds to a 50 ms time bin. A nearest template matching scheme with leave-one-trial-out validation was followed to generate these results (see **Methods**). The 4 s odor presentation period is indicated with a black bar along the x-axis. Blue pixels indicate pattern match with ensemble responses during high-concentration exposures of an odorant, and red pixels indicate pattern match with low-concentration odor responses. Neural responses in any time bin outside an angular tolerance threshold (i.e., did not pattern match with the reference neural response templates) were labeled as gray pixels. Note that each block of 25 trials mostly pattern matches with either the high-intensity or low-intensity templates of that odorant.

3.2.5 Contrast-enhanced response to an unexpected stimulus

We next wondered whether the network-level adaptation allowed differential processing of repetitive vs. deviant stimuli. To understand this, we repeatedly presented an odorant (*hex*) for twenty-five trials, but in the twenty-sixth trial (a 'catch trial'), we switched and presented a different stimulus (i.e., a 'deviant' stimulus) (**Figure 3.7a)**. Two different odorants were used as the deviant stimulus in two different blocks of trials. Note that isoamyl acetate (*iaa*) is similar to hexanol (locusts trained with *hex* in an appetitive-conditioning assay also respond to *iaa*, whereas apple is less similar to *hex* (no cross-learning for these two odorants in the behavioral assay [80]).

We examined the ensemble PN responses to the repetitive and the deviant stimulus. We observed four main PN response motifs (**Figure 3.7b**). Responses of PNs activated by repetitive and deviant stimuli were diminished during the catch trial (i.e., overlap reduction; ~31% PN responses belonged to this category). At the same time, PNs that were activated by the deviant stimulus alone responded without significant reduction during the catch trial (**Figure 3.7c**; ~12%

of PN responses belonged to this category; A paired-sample t-test was used to compare maximum spike rates of two trials (catch trial and the first trial in block 2) across projection neurons in this category, p=0.1588).

To understand how the neural activities were altered at an ensemble level, we again visualized the ensemble activities elicited during each trial (**Figure 3.7d, e**). Notably, while the response to the repetitive stimuli systematically diminished across trials (i.e., trajectory length shortened), the responses to the deviant stimuli during the catch trial were stronger than responses observed during all other encounters of the same odorant (the lone exception being the first trial in block 2). Furthermore, consistent with ensemble PN responses (**Figure 3.7b**), the neural response trajectory during the catch trial moved further away from the repetitive stimuli indicating a population-level contrast enhancement of neural representation (**Figure 3.7d, e**). Responses to the repeating stimulus, post catch trial, increased modestly in response magnitude but still pattern-matched well the ensemble activity evoked by that stimulus **Figure 3.7f, g**).

To quantify our results, we compared the similarity between ensemble neural activity elicited by the repetitive stimulus and the deviant stimulus (**Figure 3.8a, b**). Consistent with the dimensionality reduction results, we found that the ensemble neural responses in the catch trials were consistently more distinct from the repetitive hex-evoked responses. In fact, the response dissimilarities were lower than those observed when the catch (*iaa* or *app*) and recurring (*hex*) stimulus were presented in a separate block of trials. Notably, a simple nearest reference template based classification approach still revealed that the contrast-enhanced responses could be correctly pattern-matched with the responses evoked by *iaa* or *app* (**Figure 3.8c, d;** see **Methods**).

Taken together, these results indicate that repetitive and deviant stimuli are differentially processed in this neural network. While the response to the repetitive stimuli is selectively

suppressed, the ensemble neural activities are altered to emphasize the unique features of the deviant stimuli while still preserving information about their identity.

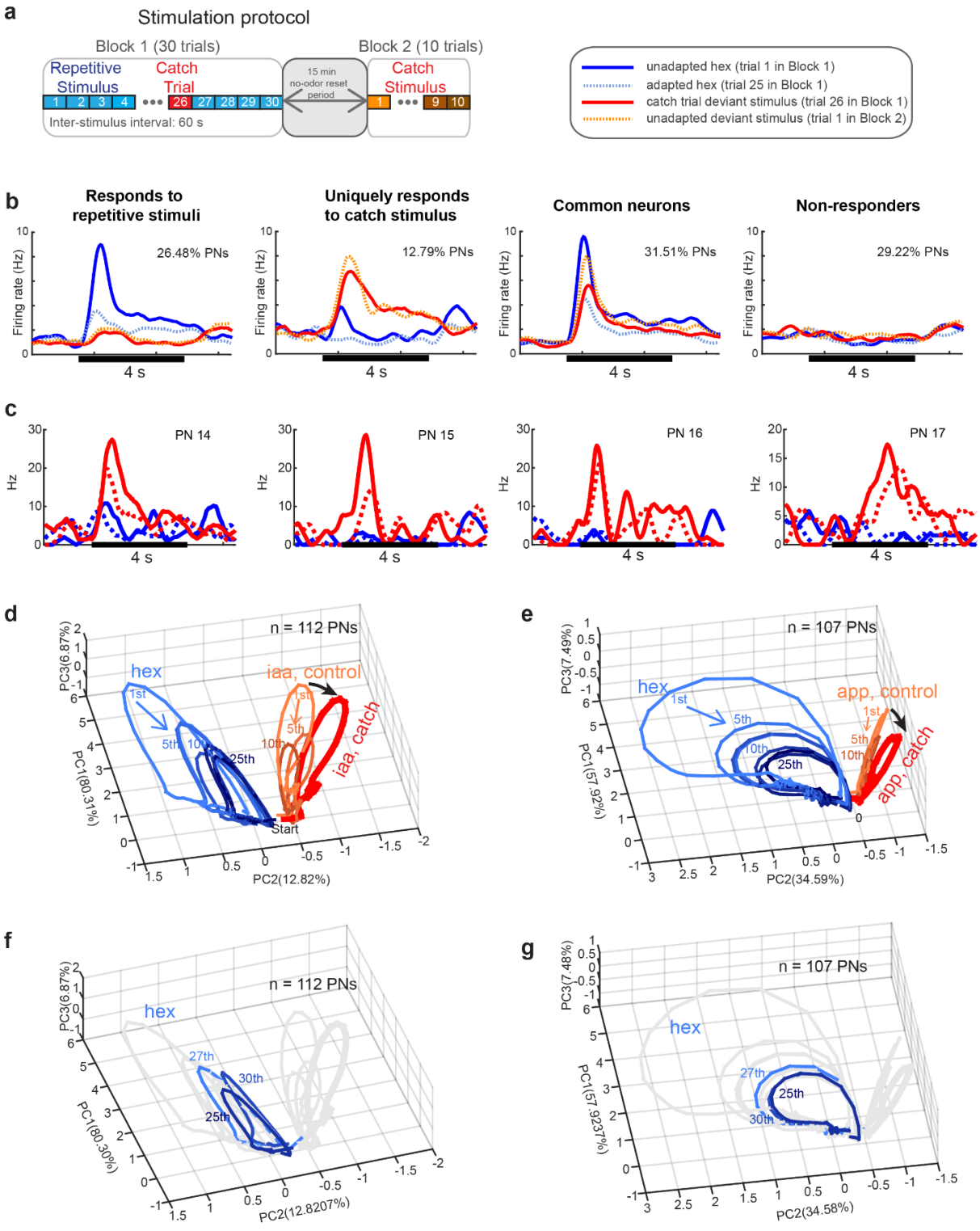

Figure. 3.7: Contrast enhancement of ensemble responses to the deviant stimulus.
(a) Experimental setup: Two blocks of trials were used. First, a block of 30 trials where one odorant (*hex*) was presented in all trials except the 26th trial (the catch trial). A deviant stimulus (iaa or app) was presented during the catch trial. After a 15-minute no-odor reset period, the second block of ten trials of deviant stimulus was presented. This was done to determine the unadapted (first trial) and adapted (later trials) responses of the same set of PNs to the stimulus used in the catch trial.
(b) PNs responses were categorized into four different groups and shown: activated by the repetitive stimulus alone, activated by the deviant stimulus alone, responds to both stimuli, and non-responsive to either stimulus. PN responses during four trials are compared in each plot: pre-adapted response to repetitive stimulus (first trial in block 1; solid blue traces), adapted response to the repetitive stimulus (the twenty-fifth trial; dashed cyan traces), response to the deviant stimulus during the 'catch trial' (twenty-sixth trial in block 1; solid red traces), and unadapted response to the deviant stimulus following the 15-minute no-odor reset period (first trial of block 2; dashed orange traces). Each panel shows the ensemble response averaged across all PNs belonging to one category. The fraction of PNs belonging to each response motif is indicated in each plot.
(c) Responses of four representative PNs (uniquely responds to catch stimulus) that have a stronger response during the catch trial than the unadapted responses evoked by the same stimulus are shown. In each panel, four trials are shown: solid blue trace – pre-adapted response to repetitive stimulus (i.e., the first trial in block 1), dashed cyan-trace – adapted response to the repetitive stimulus (twenty-fifth trial in block 1), solid red trace – response to the deviant stimulus during the 'catch trial' (twenty-sixth trial in block 1), and dashed red trace – unadapted response to the deviant stimulus following the 15-minute no-odor reset period (first trial of block 2).
(d, e) Similar trial-by-trial trajectory plots as in **Figure. 4**. PN ensemble response during each trial is shown as a closed-loop response trajectory. Ensemble PN response to the repeated stimulus is shown in blue (hex; block 1 – trials 1 - 25). Orange response trajectories are those elicited by *iaa* or *app* during block 2 trials. The numbers next to the trajectories indicate the trial number, and a color gradient from light to dark indicates early and late trials, respectively. The PN response trajectory elicited by *iaa* or *app* during the catch trial (block 1 – 26th trial) is shown in red. The black arrows indicate the shift in the direction of PN response trajectories during the catch trial.
(f, g) Trial-by-trial trajectory showing a modest increase in the trajectory length observed during the trials following the catch trial (27th and 30th trials) when the repetitive stimulus was presented again.

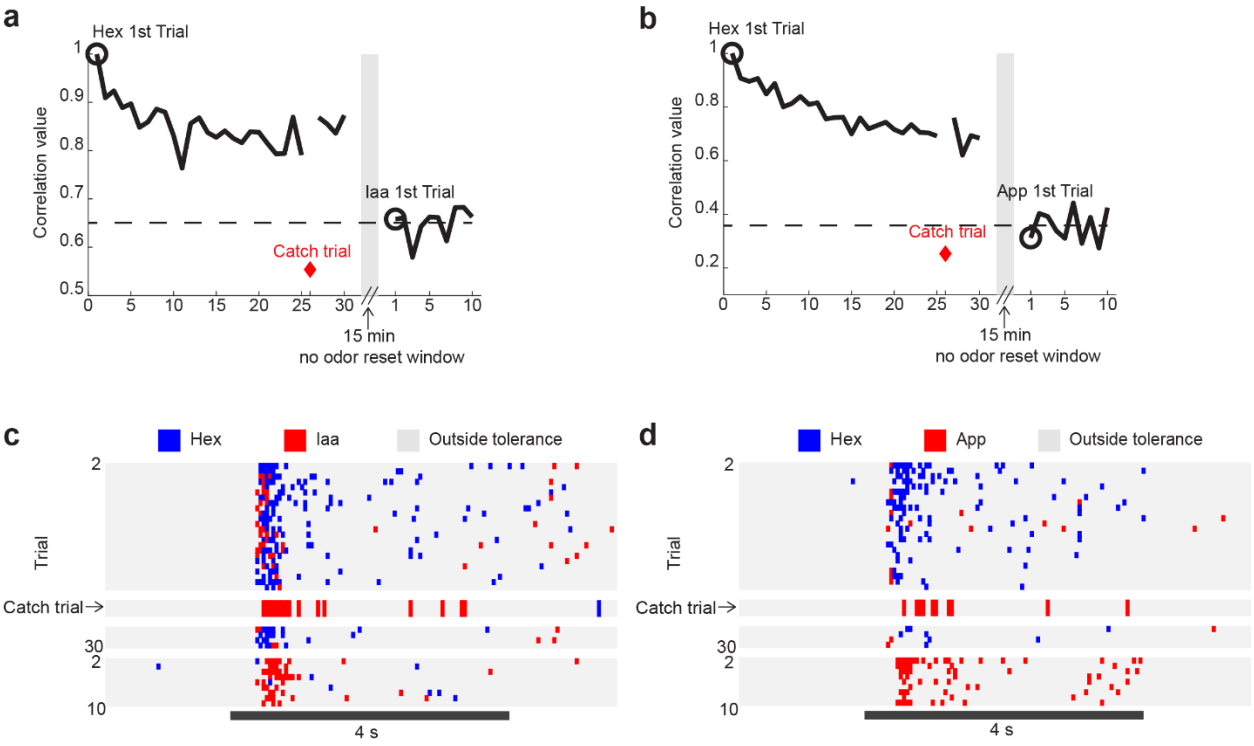

Figure. 3.8: Neural responses to the deviant stimulus can be robustly decoded.

(a) The correlation value (a measure of similarity) between the mean ensemble neural response in each trial with the neural activity evoked during the first presentation of the recurring stimulus (*hex*) is shown. Note that hex was repetitively presented during all but the twenty-sixth trial ('catch trial') in the first 30 trial block. During the 'catch trial', a deviant stimulus (isoamyl acetate; iaa) was presented. Following the 30-trial block, no odorant was presented for 15 minutes to allow the antennal lobe circuit to reset. Subsequently, ten trials of isoamyl acetate (*iaa*) were presented after this reset period. The dashed line shows the mean correlation value between the ten trials of isoamyl acetate presented during the second block of trials with the response to the first trial of *hex* in block 1.

(b) Similar plot as panel **(a)**, but during 'catch trial', a different stimulus (apple; *app*) was presented.

(c, d) Classification results for neural responses during block 1 and block 2 trials are shown. In this analysis, only the neural responses in the first trial of hex presentation (trial 1 of block 1) and the first trial of the deviant stimulus presentation (trial 1 of block 2) were used as responses templates to be pattern matched. The classification results for the remaining 38 trials are shown. The color of each pixel schematically indicates the results of the classification analysis: blue – pattern match with the templates of the repetitive stimulus (i.e., *hex*), and red – pattern match with the templates of deviant stimulus (i.e., *iaa* for panel **c** and *app* for panel **d**). The 4 s odor presentation period is indicated as a black bar along the x-axis. Neural responses in any time bin

outside the angular tolerance are indicated as gray pixels (i.e., not pattern matching well with any of the response templates).

3.2.6 Activity-dependent plasticity in single projection neurons

What mechanisms could underlie the changes in spontaneous spiking activity and stimulus-evoked responses in individual PNs? To understand this, we performed intracellular recordings from individual PNs and monitored spiking activity before, during, and after current injections (**Figure 3.9**). We found that the PN firing rates following a positive current pulse decreased below the pre-pulse activity levels (**Figure 3.9a**). However, for the same neuron, following a negative current pulse, the observed post-pulse activity levels were greater than the pre-pulse firing rates (**Figure 3.9b**). Thus, it appears that the spontaneous PN activity is not constant, but changes based on recent response history: a period of intense firing is followed by a prolonged period of low spontaneous activity (**Figure 3.9a right panel**), whereas following an epoch of hyperpolarization, the spiking activity increases compared to the pre-pulse level (**Figure 3.9b right panel**).

Next, we examined the response of individual PNs to back-to-back current pulses to determine whether the PN's response history can alter its response to subsequent inputs of equal magnitude (**Figure 3.9c**). Our results indicate that the response to the first pulse in the sequence

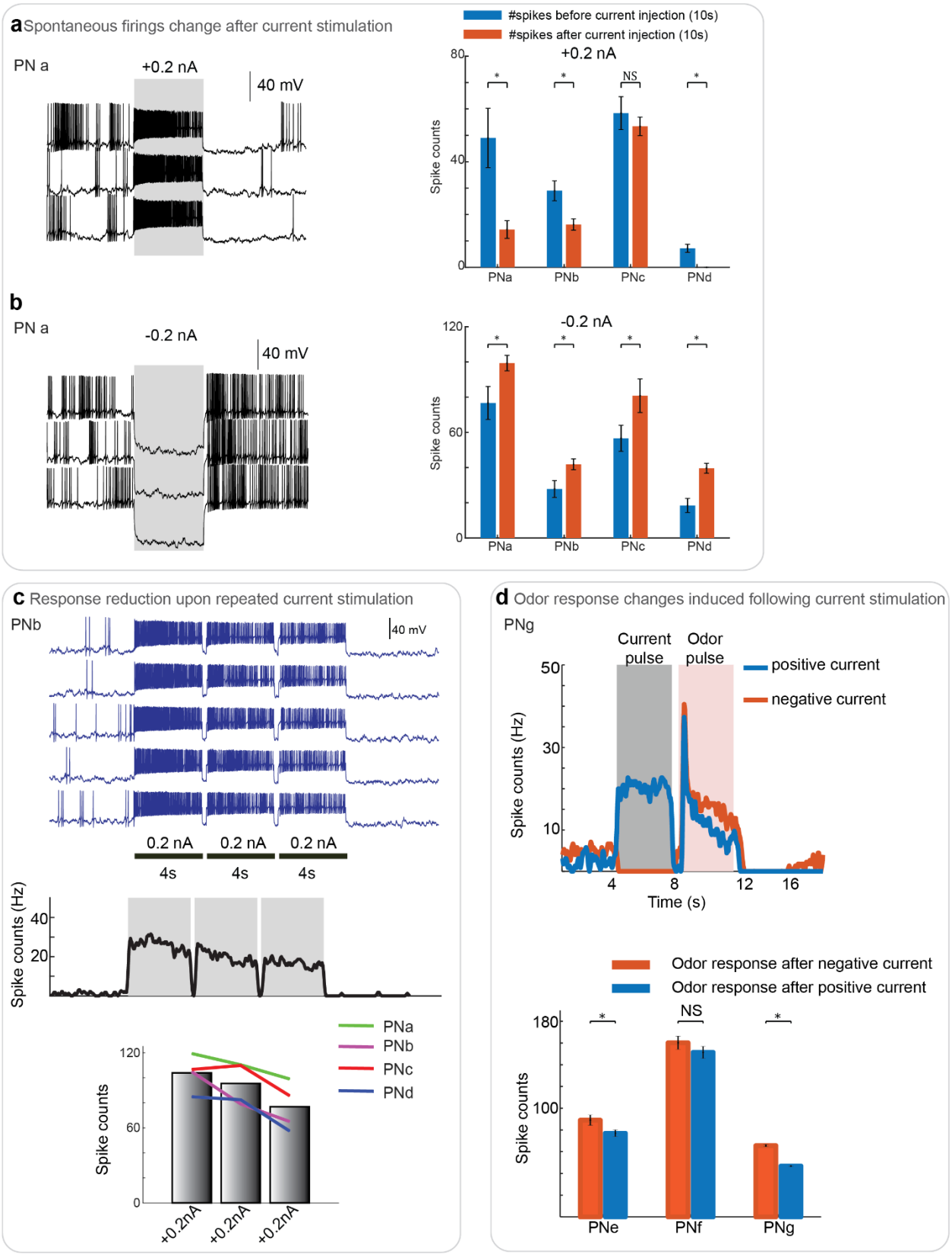

Figure 3.9: Activity-dependent plasticity in individual projection neurons

(a) Intracellular voltage traces revealing PN activity before, during, and after a 4 s current pulse (+0.2 nA; gray box). Each row corresponds to one trial, and current pulses in successive trials were 60 s apart. Right panel: Bar plots comparing PN spike counts during pre- (blue) and post- (orange) current injection periods. The height of the bar indicates the mean of spike counts, and the error bar indicates s.e. (standard error) across trials. Asterisks indicate a significant decrease in spike count (*P < 0.05, NS: P > 0.05, paired t-tests, *n* = 3 trials for PNa and *n* = 5 trials for PNs b-d).
(b) Bottom panel, the similar plot as in the top panel but showing similar results but for a negative current injection (-0.2 nA). Note, asterisks in the right panel indicate a significant increase in spike count.
(c) Top panel, intracellular voltage traces recorded from a PN are shown. Three consecutive positive current input of +0.2 nA (each 4s in duration) separated by a 250 ms IPI were used to evoke a firing response. Results from five consecutive trials are shown to illustrate repeatability. Middle panel, trial-averaged firing rates into 50 ms time bins are plotted as a function of time. Bottom panel, bar plot comparing trial-averaged spike counts in each of the three current injection pulses is shown. The height of the bar indicates the mean across four PNs, and individual PN responses are indicated using lines of different colors.
(d) Top panel, firing rates of a PN to a non-overlapping sequence of a 4 s current injection pulse followed by 4s odor presentation (500 ms gap) is shown. The blue line corresponds to the trial-averaged PN firing rates when a positive current (+0.1 nA) was injected before odor pulse (*hex* 1%), and the red line corresponds to the case when negative current (-0.1 nA) was injected before odor pulse (again *hex* 1%). Bottom panel, trial-average spike counts, elicited by the odorant is shown as bar plots. Red bars correspond to odor responses (*hex* 1% for PN e, g and citral1% for PNf) following a negative current pulse (-0.2 nA for PNe, -0.1 nA for PN f, g) and blue bars correspond to mean response to the same odorant following a positive current pulse (+0.2 nA for PNe, +0.1 nA for PNf, g). Error bar indicates s.e. (standard error) across trials. Asterisks indicate a significant decrease in spike count (*P < 0.05, NS: P > 0.05, paired t-tests, *n* = 5 trials).

was the strongest and the spike count reduced systematically for the second and the third pulse in the sequence (**Figure 3.9c middle and bottom panels**). When the second and third pulses were replaced by an odorant pulse, we found that the response to the odorant following a positive current pulse was weaker than the response to the same odorant when it was received after a negative pulse that hyperpolarized the cell (**Figure 3.9d**). More importantly, we found that these changes in PN

spontaneous activity following current injections, induced by both positive and negative, persisted for tens-of seconds after the end of the stimulation period (**Figure 3.10**).

Taken together, these results suggest that there may be a cell-intrinsic form of PN response plasticity that could contribute to spontaneous spiking activity, gaining a negative correlation with stimulus-evoked responses, reduction in response to a recurring stimulus, and enhancing responses to a novel stimulus.

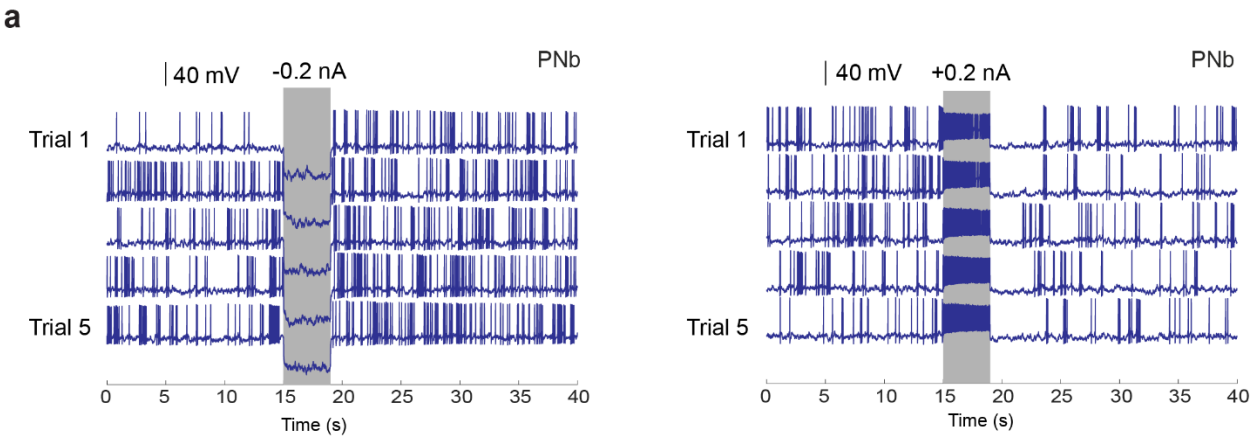

Figure 3.10: Persistent changes in PN spontaneous activity following current injections. **(a)** Intracellular voltage traces are plotted similarly as in **Figure.11a, b.** The PN spiking activity during the entire 40 s trial is shown for PNb. The inter-trial-interval was 20 s. Left panel shows the spiking activity before, during, and after a negative current pulse (-0.2 nA). The right panel shows a similar plot but for a positive current pulse (+0.2 nA). Note that the changes in firing rate due to current injections persist for tens of seconds until the end of the trial.

3.2.7 A simple linear model for adaptation and contrast enhancement

To summarize our findings, we visualized the mean odor-evoked ensemble response in the first trial (i.e., the unadapted response) and the average spontaneous activity observed in each trial during the pre-stimulus period (**Figure 3.11a**). Consistent with our interpretation so far, the spontaneous activity vectors progressively re-oriented towards the opposite direction of the odor-evoked response vector (**Figure 3.11a**). Note that a linear combination of the unadapted

ensemble response with the spontaneous neural activity preceding stimulus in a trial would lead to a suppression of response to the recurring stimulus, thus matching observed results (**Figure 3.11b**). On the other hand, adding ensemble response evoked by a novel stimulus (red vectors) to the spontaneous activity altered by the recurring stimulus should increase the angular distance between the summated vector (brown vectors) and the recurring stimulus response (blue vector). This was precisely what was observed during the catch trial (**Figure 3.11c, d)**. In sum, these results indicate that a simple linear model that considers both the ongoing activity and the unadapted antennal lobe response to the odorant can explain the changes in stimulus-evoked responses observed for a recurring or a novel stimulus.

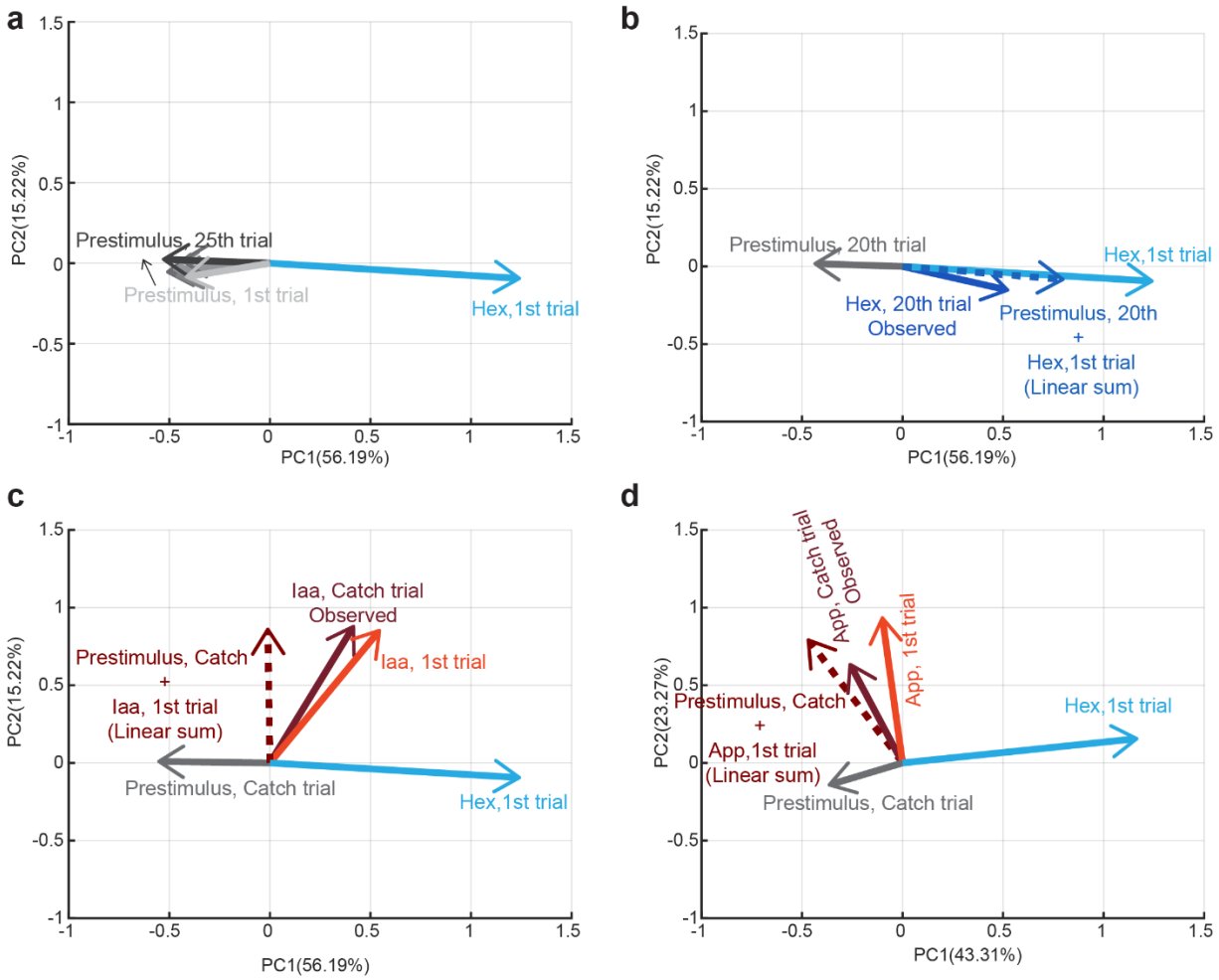

Figure 3.11: A linear model for repetition suppression and novelty contrast enhancement
(a) The average odor-evoked ensemble response observed in the first trial and the average baseline activity during the pre-stimulus period observed in different trials were visualized using principal component analysis. After *hex* was repeatedly presented, note that the baseline response vectors become more anti-correlated with the stimulus-evoked response vector.
(b) The average baseline activity vector and odor-evoked response vector observed in the 20^{th} trial after dimension reduction are shown. For comparison, the average first trial odor-evoked response is also shown. The dashed line shows a linear vector addition of the 20^{th} trial's baseline activity vector and odor-evoked response vector in the first trial.
(c) The average baseline activity and the odor-evoked response observed in the catch trial are shown after PCA dimensionality reduction. The odor-evoked response in the first trial of the second block (*iaa*, 1^{st} trial) is also shown. A linear sum of the baseline activity in the catch trial and the *iaa* response during the first trial is shown as a dashed brown vector. The actual ensemble response observed during the catch trial is shown as a solid brown vector. Note that the angular distance between the *iaa* response vector during the catch trial and the *hex* response vector increases.
(d) Similar plot as panel **(c)** but when the *app* was used as the catch trial stimulus.

3.3 DISCUSSION

The response elicited by a sensory stimulus often reduces when the same stimulus is repeatedly encountered. This form of adaptation is found in most sensory systems [72, 134-139], and is thought to allow humans and other animals to attend to other more salient or novel stimuli in their environment [99, 140-142]. However, could diminishing the neural response to the recurring stimulus potentially confound other pertinent information about the same adapting stimulus, such as its intensity, or alter how information regarding other stimuli are transmitted? Our results indicate that adaptation does not lead to a loss of stimulus-specific information. Although neural response strength reduced with repetition, information about the odorant identity and intensity could be more efficiently encoded (i.e., with fewer spikes). Further, adapting to one stimulus altered how other stimuli were processed by the neural circuit. The response features that were unique to the deviant stimulus were unaltered.

How different are these results from prior work on self- and cross-adaptation? Exposure to a stimulus reduces sensitivity to subsequent exposures of the same stimulus and to a lesser degree

for other cues as well [138, 139, 143]. The fundamental question investigated in this study is not about the information lost due to adaptation, but what is retained after adaptation and whether it could allow for stable representation of stimulus identity and intensity. While preserving information to decode stimulus identity from being corroded by cross adaptation should be a ubiquitous requirement in most sensory systems, the need to preserve intensity information may depend on whether the odorant elicits varying behavioral response/percepts at different concentrations. For example, molecules such as skatole and indole, which smell like feces at high intensity, have been reported to be floral at low intensity. Would these percepts change with adaptation? It is logical to expect that no matter how much one is exposed to high-intensity vapors of skatole, it would still not smell floral and *vice versa*?

Where does the memory of a recently encountered stimulus reside? While olfactory sensory neuron responses have been shown to diminish upon prolonged exposures, they recover when the stimulus exposure is intermittent with large temporal gaps between consecutive exposures (on the order of tens of seconds [89]). Electroantennogram (EAG) recordings from the locust antenna also revealed that the magnitude of the EAG signals recover entirely when given a minute to recover (data not shown). However, previous results have shown that individual ORNs have responses that tend to outlast stimulus durations, and some have OFF responses following termination of odor pulse [33, 144, 145]. Such prolonged stimulus-evoked responses can make the post-stimulus activity correlated with the stimulus-evoked activity (data not shown). Therefore, the ORN response diversity may not be necessary for response suppression to subsequent encounters of the same stimulus, especially with long ISI as used in this study [89]. However, if the ORN OFF responses persist for long periods, contrast-enhancement of response to a novel stimulus may originate right from the periphery.

Our results also indicate that the responses in the second relay center, the antennal lobe, continue to diminish even for temporally discontinuous encounters of the recurring stimulus with long ISI. One possible mechanism underlying these results is that the synapses between the olfactory sensory neurons and the antennal lobe PNs could depress to mediate adaptation [146]. Our results reveal that although responses to the repeating odorant reduce in many PNs, the spiking activity recovers to higher response levels when a deviant stimulus is presented (**Figure 3.7b, c; unique responders**). This observation is at odds with the suggestion that synaptic depression might be a possible basis for response suppressions in PNs. Alternately, since locust PNs are multi-glomerular, it is possible that sensory input for different odorants is transmitted onto PNs through different ORN-PN synapses. In addition to recovery from inhibition, our results also indicate that some PN responses to the deviant/unexpected stimulus during the catch trial were stronger than the unadapted responses evoked by the same stimulus immediately after a 15 min no-odor reset window (**Figure 3.7c**). These latter results cannot be explained by the depression of ORN-PN synapses and indicate that some aspects of this short-term memory may also reside within the antennal lobe neural network.

Consistent with previous findings[72], our data also indicate that PN response changes were largest in the first few trials. However, we found that most PN spiking responses continued to change, albeit modestly, even after twenty repetitions of the same stimulus (**Figure 3.4**). As can be expected, compared to the individual PN responses, the ensemble response profiles remained relatively consistent across trials (**Figure 3.5**). As a result, although the overall response strength diminished over trials, the combination of PNs activated robustly encoded both the stimulus identity and intensity (**Figure 3.6**). Intuitively, the direction of the PN ensemble response vectors varied with stimulus identity and intensity and therefore robustly encoded this information.

However, the length of these vectors diminished over trials (as visualized by the length of the trajectories shown in **Figure 3.5a-d, Figure 3.12**) but did not confound information about stimulus intensity. Such an encoding scheme could allow the adaptation-invariant representation of stimulus intensity. These results are consistent with earlier findings[76] and extend them by including both unadapted and adapted responses (i.e., all trials) for analyses.

In addition to changes in stimulus-evoked activity, we also found that the spontaneous activity in individual PNs changed depending on the identity of the odorant that was repeatedly presented (**Figure 3.2b**). The ensemble-level baseline PN responses during two non-overlapping epochs when two different odorants were presented resulted in two distinct spontaneous activity clusters (**Figure 3.2c**). A prior imaging study reported that spontaneous activity in pairs of glomeruli (where PN dendrites receive sensory inputs) activated by an odor exposure increased following termination of the stimulus [147]. In this study, we focused on understanding the similarity between the odor-evoked ensemble response and the change in spontaneous activity that persists after odor termination and found a negative correlation between the PN ensemble responses during these epochs (**Figure 3.1**). Note that the spontaneous ensemble PN activities in the very first trial were random. However, subsequent evolution after the first encounter with a repetitive stimulus reduced the correlation between neural activities observed in these two epochs (**Figure 3.2d, Figure 3.11, Figure 3.12**).

What could be the neural basis for this short-term memory? Prior work has shown that the facilitation of recurrent inhibition onto PNs can explain behavioral habituation in fruit flies[148, 149]. Further, enhancement of odor-specific inhibition was hypothesized to create a sensory memory that is a ‘negative image’ of the stimulus. This short-term memory can selectively impede the transmission of a familiar stimulus[99]. Indeed, our result is largely consistent with this idea.

Sensory memory of a repetitive stimulus caused the spontaneous activity in the network to progressively become negatively correlated with the odor-evoked response (**Figure 3.1, 3.11**). Further, facilitation of inhibition has been shown to entrain oscillatory synchronization of neural activity in the antennal lobe [72]. Since both odor-evoked oscillations and spike rate reduction can be mediated by facilitating inhibition in this circuit, it is possible that the exact mechanism may contribute to both these results.

In addition to other well-characterized mechanisms that may contribute to repetition suppression and novelty contrast enhancement, we found a cell-intrinsic form of plasticity in the antennal lobe projection neurons. A projection neuron's spontaneous spiking activity changes in an activity-dependent manner. Typically, the excitability increased following a period of hyperpolarization and decreased after a bout of intense spiking. Such bi-directional control of individual neuron's excitability has recently been reported in the mice brain stem and suggested as a plausible mechanism for controlling vestibulo-ocular reflex [150, 151]. Our results reveal that this simple mechanism observed at the level of individual neurons can confer a negative correlation to the activity that persists following the stimulus termination. Further, this negatively correlated ensemble activity, when linearly combined with a constant sensory input driven by sensory neurons, can provide a potential model for both repetition suppression for recurring stimulus and contrast enhancement for novel stimuli.

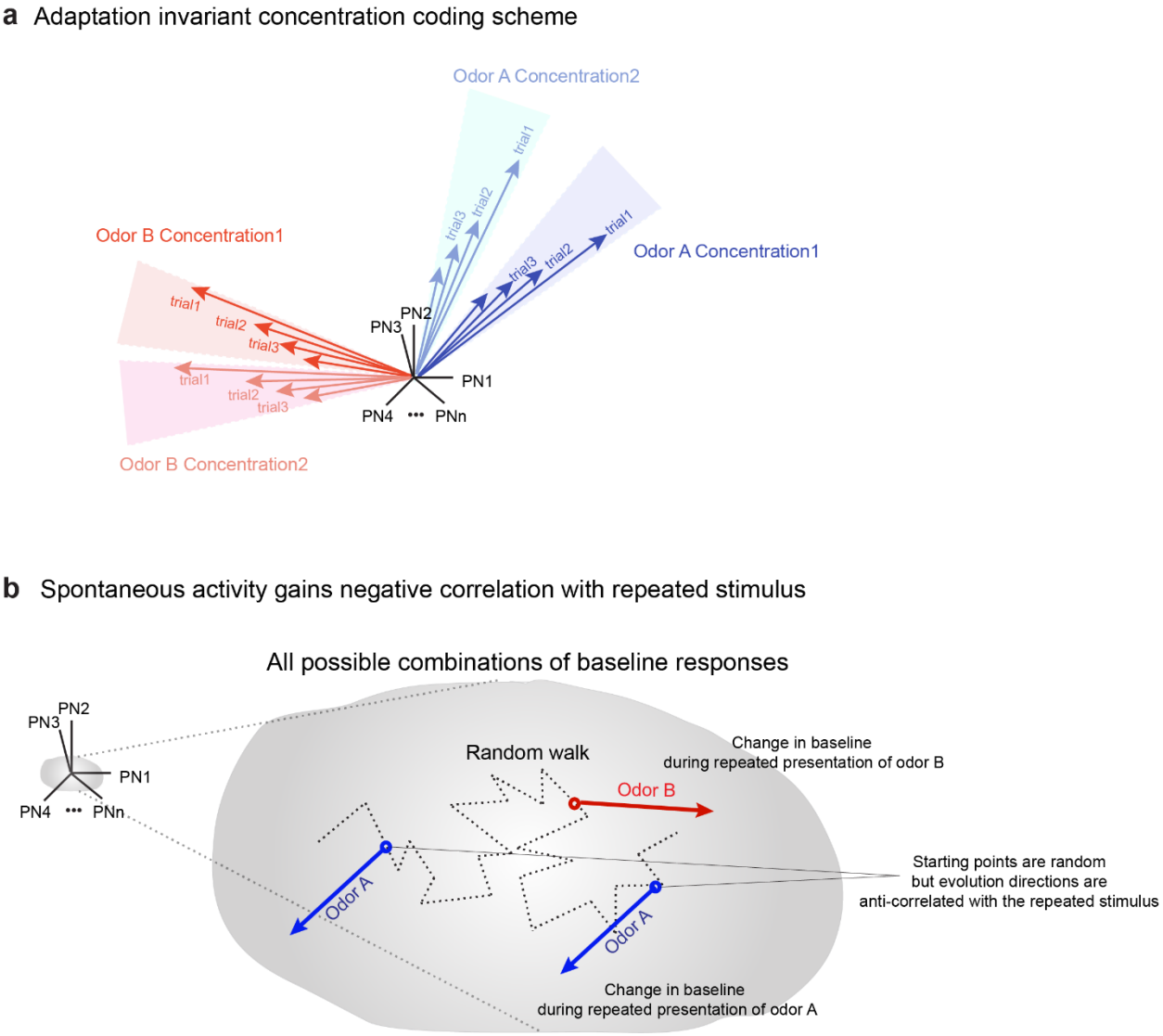

Figure. 3.12: Schematic representation of the main ideas of the chapter.
(a) A schematic showing how odor identity, concentration can be encoded in an adaptation invariant manner. The direction of the high-dimensional vector is determined by the combination of the neurons activated, and the response strength determines the length of the vector. Our results indicate that the ensemble of PNs activated changes subtly with stimulus intensity and drastically with stimulus identity. Although the response strength reduces upon repetition, the combination of PNs activated is maintained.
(b) A schematic showing how baseline ensemble neural responses change upon repeated stimulus exposure. Without any odor stimulus, there is some inherent variability in the ensemble PN baseline response, which can be represented as a random walk in the high dimensional state space (dotted line). When an odor stimulus is encountered repeatedly, the ensemble PN baseline changes in a specific direction in the state space. The observed changes in the baseline activity are stimulus-specific (red and blue arrows). However, note that repeated encounters of the same

stimulus results in similar shifts in the baseline, but the starting points in the state space are different (indicated using two blue arrows but with different starting points)

3.4 Author Contribution

Barani Raman conceived the study and designed the experiments/analyses. Lijun Zhang and Chao Li did all the analyses. Lijun Zhang generated all the figures. Debajit Saha and Alex Chen performed the electrophysiological recordings. Srinath Nizampatnam performed the patch-clamp experiments. Barani Raman wrote the paper taking inputs from all the authors and supervised all aspects of the work. Lijun Zhang, Alex Chen, Debajit Saha and Srinath Nizampatnam are equally contributing first authors.

This research was supported by an Office of Naval Research grant (N00014-16-1-2426, N00014-19-1-2049), an NSF CAREER grant (#1453022) and a NSF CRCNS grant (#1724218) to B.R.

Chapter 4: Temporal Organization of Odor-evoked Responses in a Fly Olfactory Circuit: Inputs, Outputs and Idiosyncrasies

4.1 Introduction

Most neuronal networks consist of many sub-types of neurons that interact through different microcircuits and actively reorganize the information they receive. To fully understand the information processing carried out, at a bare minimum three pieces of information are essential. First, it is necessary to understand the input received by the network. Second, to understand what computations arise from which microcircuit, it is necessary to follow this input signal as it propagates from one processing compartment to the next. And third, it is necessary to understand how different neuronal subtypes that are present in these circuits contribute to the information processing. An additional layer of investigation could be added by comparing how information is represented by equivalent circuits in different individuals. This would allow us to understand the generic rules of signal processing and information transformation and help identify any idiosyncratic features that may be utilized in different individuals. Understanding such idiosyncrasies in neural encoding can arguably help us better understand a source of variance in behavioral outcomes observed across individuals. In this chapter, we dissect how odor signals are organized and processed as it propagates through the fruit fly (*Drosophila melanogaster*) antennal lobe neural network.

In the fruit fly olfactory system, vapors from volatile chemicals are transduced into neural responses by olfactory receptor neurons (ORN) present in the antenna that then transmit this

information to a region called the antennal lobe (analogous to the mammalian olfactory bulb). The ORNs of the same type, i.e., expressing the same receptor–co-receptor gene combination, send their axons to either one or two spherical structures of neuropil called glomeruli in the antennal lobe[152, 153]. The ORN activity drives responses in three major types of neurons in the antennal lobe: GABAergic local neurons (LNs), cholinergic projection neurons (excitatory PNs or ePNs) and GABAergic projection neurons (inhibitory PNs or iPNs). The local neurons are diverse[154] and play important roles in processing sensory signals within the antennal lobe[155, 156] . However, LNs do not send their processes outside the antennal lobe, and thus only the activity ePNs and iPNs constitute the outputs from this olfactory neuronal network.

Notably, the ePNs and iPNs differ in how they receive inputs and transmit their output. The ePN dendrites innervate a single glomerulus and therefore receive input from a single ORN type[153]. The ePNs project their axons onto both mushroom body (a center associated with learning and memory[157, 158]) and lateral horn (a region with a putative role in driving innate behavior[159, 160]. In contrast, iPNs dendrites are multi-glomerular and therefore integrate information distributed across several different ORN types. The iPN axons are also exclusively sent to the lateral horns. The ePNs and iPNs can influence each other's activity through chemical synapses[161]. While the importance of the ePN and iPN activity for odor recognition is well established[162-164] , how the ePN and iPN activities are spatially organized and patterned over time to facilitate odor recognition remains poorly understood.

In this study, we used an *in vivo,* light-sheet, volumetric, calcium-imaging technique to examine this issue with high spatial and temporal resolution. We monitored the odor-evoked signals at the ORN axons entering the antennal lobe (input), the responses they drive in ePNs dendrites located within the antennal lobe, and ePN and iPNs axons (output) entering mushroom

body calyx and lateral horn (iPNs only project to the latter). Using this approach, we examined how odorant-evoked responses are patterned over time in each of these neural populations. Comparison across flies helped understand generic odor coding principles and how they might arise from idiosyncratic processing mechanisms utilized within the antennal lobe network. Lastly, we examine odor-evoked responses patterns and idiosyncratic processing features across different stimulus trials within the same fly.

4.2 Results

4.2.1 Light-sheet imaging of odor evoked neural activity

We used a custom-built light-sheet imaging setup [165] to monitor nearly in real-time calcium signals (GCamp6f) from olfactory sensory neurons expressing the *orco* co-receptor (ORNs), and their two downstream targets, excitatory GH146 projection neurons (ePNs) and inhibitory Mz699 projection neurons (iPNs) (**Figure 4.1a - c**). In each fly, one of these three neural populations was labeled (**Figure 4.1d**). While the axonal outputs alone were monitored for ORNs and iPNs (as GCamp6f expression levels were weak in the antennal lobe for the Mz699 line), both dendritic and axonal calcium signals were monitored for ePNs (AL, LH, and Calyx, GH146 line). This approach allowed us to compare the dendritic inputs in the antennal lobe with the functional signals reaching the two downstream targets: mushroom body calyces and lateral horns. The responses of ORNs, ePNs, and iPNs were probed to a panel of six odorants with two concentrations each. The odor panel was chosen to ensure diversity in functional groups, behavioral valence, activation patterns, and concentrations. The light-sheet images acquired were segmented using an unsupervised non-negative matrix factorization method. Note that the ROIs corresponded to glomeruli for Orco-ORN axons and ePN dendrites (**Figure 4.2a;** top row), and ePN and iPN axonal

boutons in calyx (CX) and lateral horn (LH) (**Figure 4.2a**; bottom row). A quick summary of the number of ROIs extracted from each fly is listed in **Figure 4.1c.**

In addition to large spatial coverage, we also acquired images rapidly (4 Hz sampling rate) to characterize odor-evoked, spatiotemporal response dynamics across the entire population of a specific type of olfactory neuron (**Figure 4.2**). Consistent with earlier reports[166], we found that each odorant activated a unique combination of ORNs. For most ORNs, the sensory input lasted the duration of the odor response, and for certain odorant-ORN combinations, the unabated response persisted and outlasted the stimulus duration (**Figure 4.2b**; for example, *1o3ol04* and *Acet04*). In a few ORNs, substantial reduction in calcium signals were also evident during the odor presentation (ethyl acetate (*EA*) and ethyl butyrate (*EB*)).

In the downstream antennal lobe level, ePN dendrites showed richer response dynamics for all odorants (**Figure 4.2c**). An increase in calcium signals after stimulus termination (i.e., 'OFF responses') was observed in many glomeruli. Consistent with prior results[167], we also observed that odorants that evoked weak ORN inputs had amplified responses at the level of ePN dendrites (e.g., *Bzald04*). We also found the ePN signals attenuated more rapidly. As noted earlier, ePNs send axons to both the mushroom calyces and lateral horns, whereas iPNs project only to lateral horns. We found that activation patterns of ePN and iPN axons entering these higher centers were broadly distributed across several boutons. The ePN and iPN axonal responses tended to be more transient than those observed at the level of ePN dendrites. Together, these results suggest that active signal transformation occurs between input and output compartments of these neurons. The activation became stronger for all odorants at the higher concentration but nevertheless remained highly transient and attenuated rapidly (**Figure 4.3**). These observations remained consistent when data from across the flies were compared. Primarily, we sought to understand how sensory signals

are temporally represented and transformed at the input and output of the antennal lobe. More importantly, how sensory signals are processed across multiple flies.

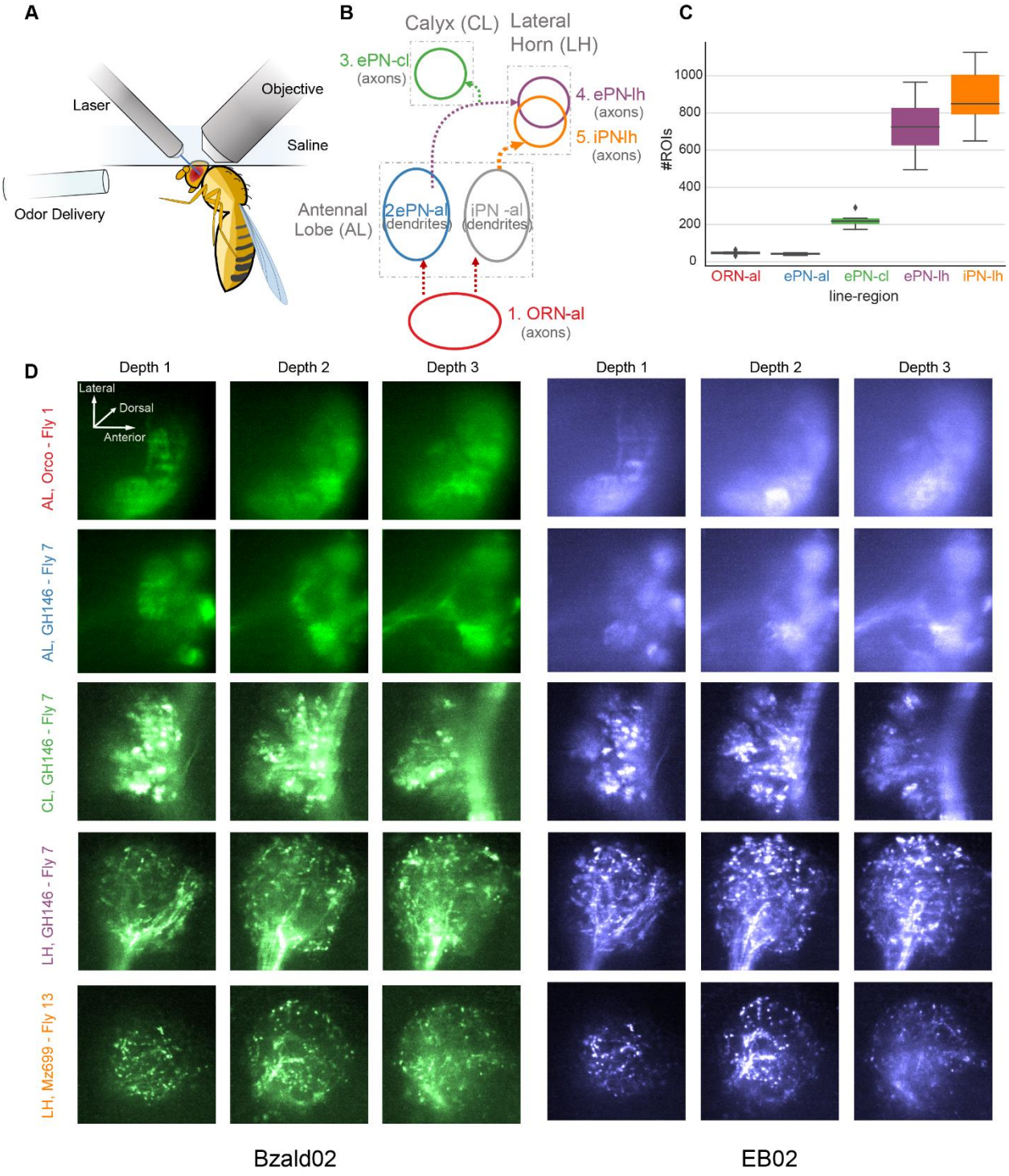

Figure 4.1: **Light-sheet imaging for volumetric in vivo characterization of odor-evoked responses at the input and outputs of the antennal circuitry.**
(a) A schematic of the experimental setup. The fly is mounted on a custom mounting block with its antennae exposed to an air stream and brain immersed in saline. At each scanning step, a whole-brain plane is illuminated by a light-sheet with two wavelengths (488 nm and 561 nm). The fluorescent signals are collected by the objective and the downstream optical components.
(b) Fly lines labeling any one of the following three distinct neural populations were used in our experiments: cholinergic ORNs expressing Orco co-receptor (ORNs), cholinergic projection neurons (ePNs), and GABAergic projection neurons (iPNs). For ORNs and iPNs, axonal activity alone was monitored. For ePN, both dendritic responses in the antennal lobe and axonal responses transmitted onto mushroom body calyx and lateral horns were near-simultaneously monitored.
(c) The number of regions of interest (ROI) extracted by a constrained non-negative matrix factorization algorithm is shown for different regions. Both the median and the interquartile ranges (IQR, 50%) are shown. Whisker lengths are 1.5 IQR past the low and high quartiles. Points out of this range were regarded as outliers.
(d) Maximum responses observed during the Bzald0202 presentation window are shown for each optical plane. Each row shows changes in calcium activity from a labeled neural population at an anatomical location. Each column shows responses monitored at one depth of imaging stacks.
(e) Similar plots as shown in panel D but now showing responses to EB02.

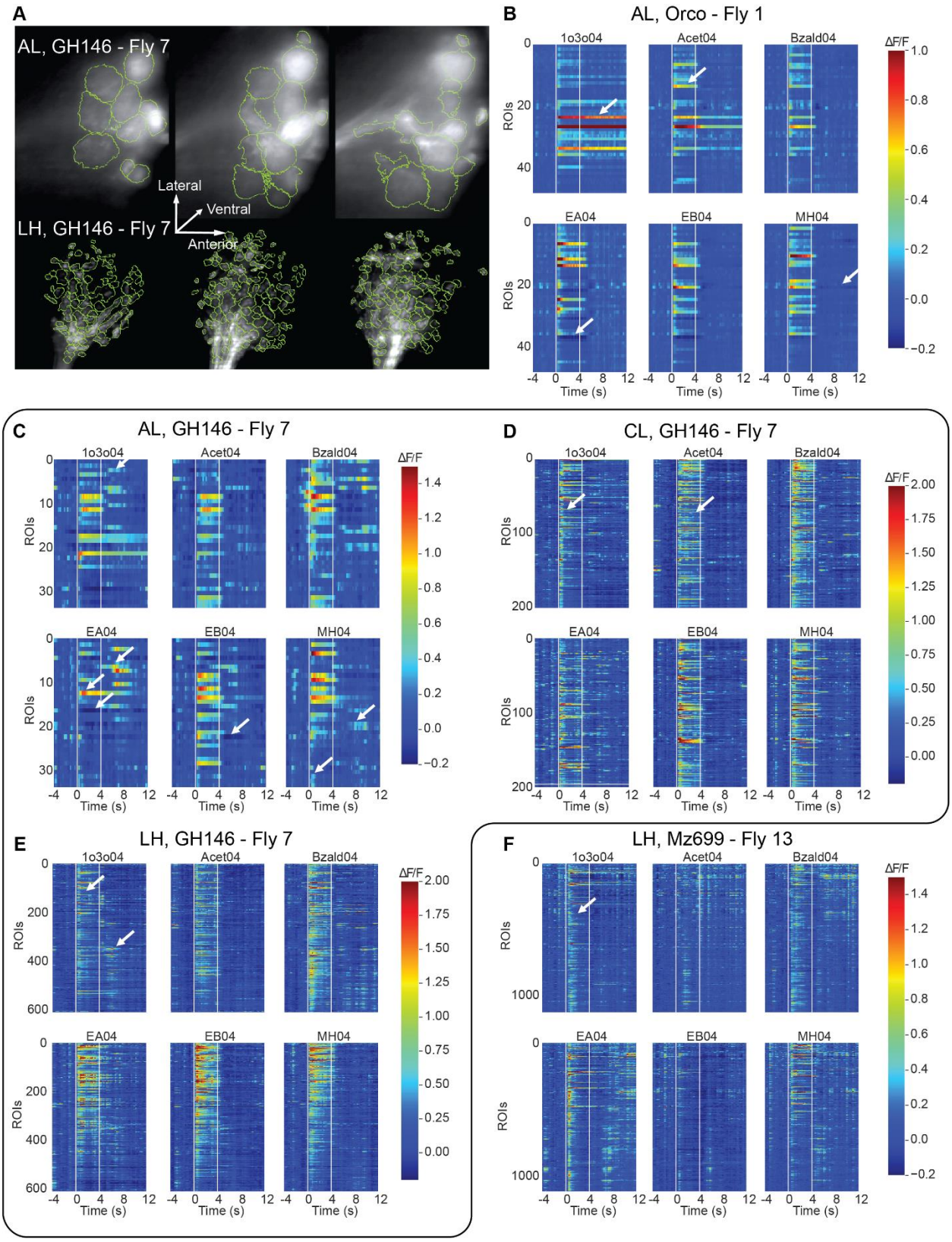
A
AL, GH146 - Fly 7
Lateral
Ventral
LH, GH146 - Fly 7
Anterior
B
AL, Orco - Fly 1
1o3o04
Acet04
Bzald04
EA04
EB04
MH04
ROIs
Time (s)
ΔF/F
C
AL, GH146 - Fly 7
D
CL, GH146 - Fly 7
E
LH, GH146 - Fly 7
F
LH, Mz699 - Fly 13

Figure 4.2: **Extraction of spatial and temporal patterns of odor-evoked neural activity.**
(a) Region-of-interest (ROI) masks extracted by an unsupervised non-negative matrix factorization method are overlaid on top of raw calcium signals recorded from ePN dendrites in the antennal lobe (top panel) and ePN axons entering the lateral horn (bottom panel). Three panels are shown characterizing odor-evoked responses and ROI masks extracted at three different depths. Note the mask contours match the anatomical structures (glomeruli and axonal boutons) in both regions very well.
(b through **f)** Representative responses to a panel of six odorants are shown as a data matrix. Calcium signals from individual ROIs extracted in each fly line/region are shown: olfactory receptor neurons in the antennal lobe (**b**); excitatory projection neuron dendrites in the antennal lobe (**c**); excitatory projection neurons axons in the mushroom body calyx (**d**); excitatory projection neuron axons in the lateral horn (**e**); inhibitory projection neuron axons in the lateral horn (**f**). The warmer color indicates stronger excitation, whereas cooler colors indicate inhibition. In each panel, each row represents the temporal response of one ROI arranged in the order from dorsal to ventral. All the ROIs across different depths were pooled together and shown in the plot (from dorsal at the top to ventral planes at the bottom of each data matrix). Y-axis indicates the ROI numbers. White arrows annotate the typical response dynamics.

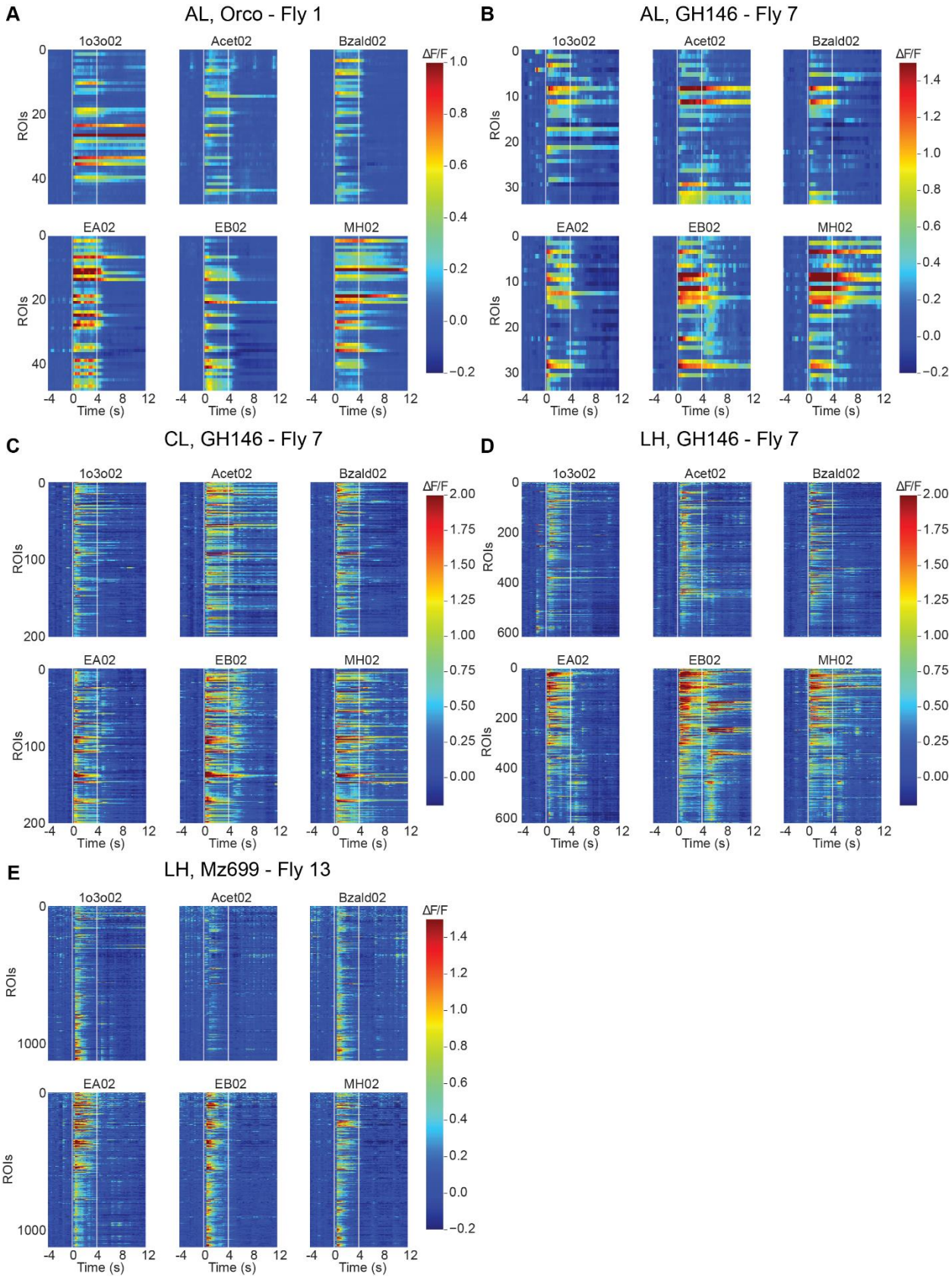
A
AL, Orco - Fly 1
1o3o02
Acet02
Bzald02
EA02
EB02
MH02
ROIs
Time (s)
ΔF/F
B
AL, GH146 - Fly 7
C
CL, GH146 - Fly 7
D
LH, GH146 - Fly 7
E
LH, Mz699 - Fly 13

Figure 4.3: **Temporal responses in higher concentrations.**
(a to **e)** Similar to **Figure 4.2 (b** to **f),** Representative responses to the same six stimuli but delivered at a higher concentration are shown.

4.2.2 Temporal patterning of odor-evoked responses

Next, we sought to examine how these odor-evoked responses are patterned over time at a population level. Our results indicate that spatial patterns of activity in the antennal lobe, both at the level of *Orco* axons (**Figure 4.4**) and ePN dendrites (**Figure 4.5a**), were highly similar immediately after the onset of the odorants. However, these spatial patterns of neural activity evolved to become more distinct over time.

To quantify this observation, we computed the cosine similarity between responses evoked by different odorants at a specific time point during stimulus presentation (**Figure 4.5b**). As can be observed, the responses evoked by different odorants at all five neural processes (Orco axons, ePN dendrites, ePN axons entering calyx and lateral horn, iPN axons entering lateral horn) had a high correlation immediately after the onset of the stimulus. However, over time these correlations reduced, and responses evoked by different odorants became more distinct from each other (i.e., lower correlations/similarity).

These observations were further corroborated when pairwise similarities between odorants across flies were examined (**Figure 4.5c**). Note that pairwise similarities between most odorants immediately after onset were high in all three lines examined (tick marks shown below the probability density functions in **Figure 4.5c**). Before onset of any two stimuli, the pre-stimulus activity showed wide dispersion of cosine similarity values with a mode near zero, indicating randomness in signals recorded during this period. Immediate after odor onset, the distribution shifted right, indicating an increase in odor similarity across pairs of odorants and observed in all

flies examined. With the progression of time, the distribution of pairwise cosine similarities shifted leftwards (i.e., towards lower values), indicating decorrelation of odor-evoked responses.

The evolution of mean pair-wise correlation across odorants over time showed variable reduction rates in each individual fly examined (**Figure 4.5d**). As can be expected, in all three neural populations, low concentration stimuli decorrelated faster and more than responses to the same set of stimuli evoked at a higher concentration (**Figure 4.5e**). Interestingly, only in the ePN axonal projections, the speed of response decorrelation was comparable at both low and high concentrations. This result directly suggests that some additional modification of response patterns occurred in this neural population to rapidly make the neural activity evoked by each odor more distinct from others (**Figure 4.5e**).

Taken together, these results indicate that the odor-evoked response patterns and the discriminatory information needed for selective recognition evolve over time in the early fly olfactory circuits. Consistent with findings from other model systems[63, 168, 169], the observed temporal patterning made odor-evoked response patterns to become different from the initial stimulus-evoked activity but also more distinct when compared to other odorants.

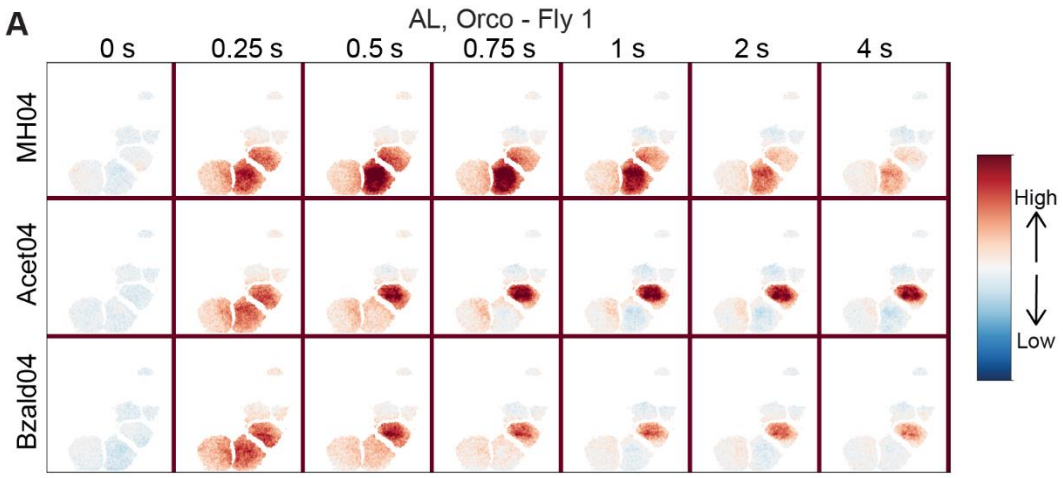

Figure 4.4: **Odor-evoked responses decorrelate over time.**
(a) Change in fluorescence signals (ΔF/F) for a few representative ROIs on a single optical plane at the level of *Orco* axons are shown as a function of time since odor onset (shown at the top of the panel). Each row reveals responses evoked by an odorant.

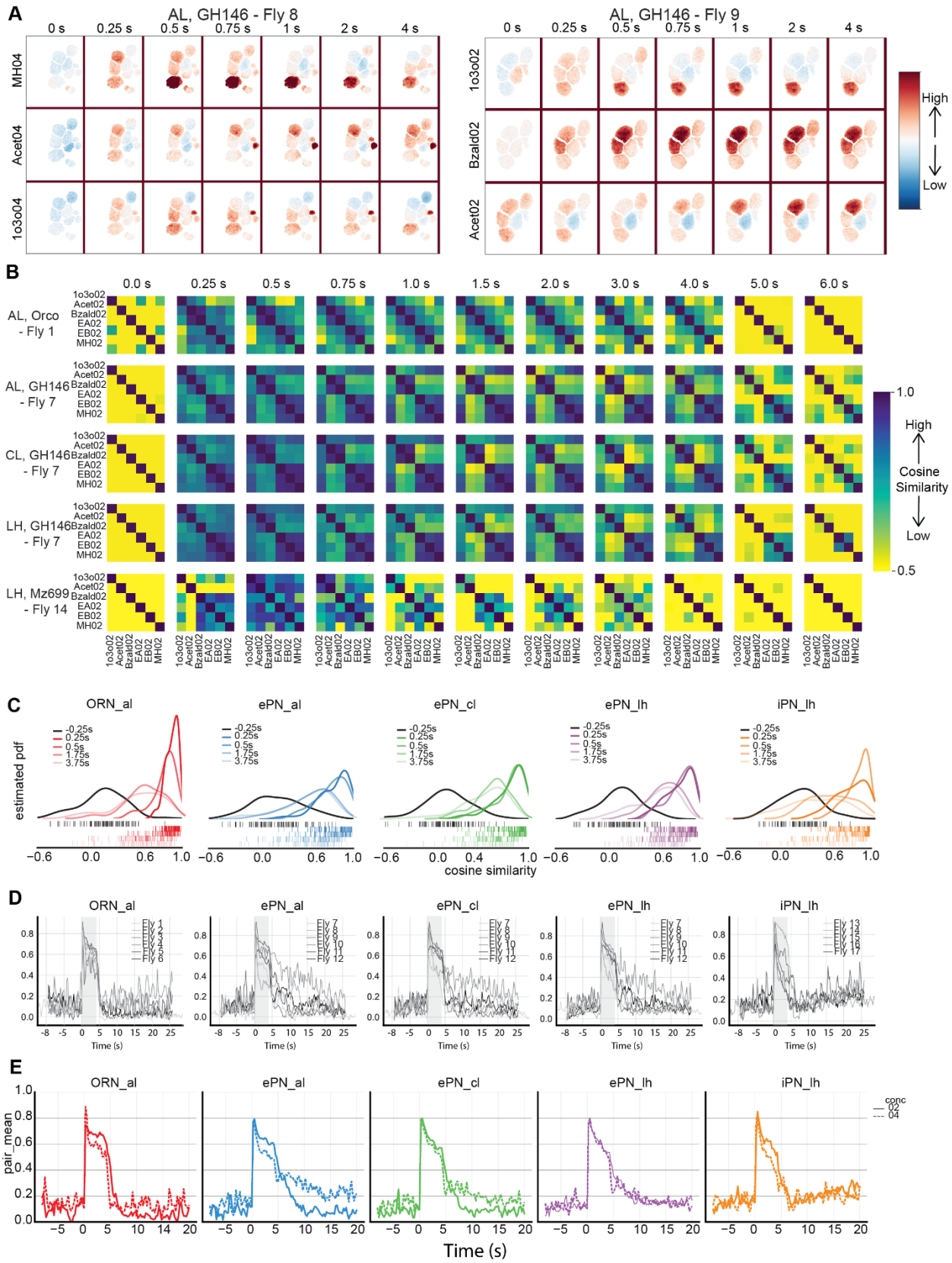
A
AL, GH146 - Fly 8
AL, GH146 - Fly 9
0 s
0.25 s
0.5 s
0.75 s
1 s
2 s
4 s
MH04
Acet04
1o3o04
1o3o02
Bzald02
Acet02
High
Low
B
0.0 s
0.25 s
0.5 s
0.75 s
1.0 s
1.5 s
2.0 s
3.0 s
4.0 s
5.0 s
6.0 s
AL, Orco - Fly 1
AL, GH146 - Fly 7
CL, GH146 - Fly 7
LH, GH146 - Fly 7
LH, Mz699 - Fly 14
1o3o02
Acet02
Bzald02
EA02
EB02
MH02
1.0
High
Cosine Similarity
Low
0.5
C
ORN_al
ePN_al
ePN_cl
ePN_lh
iPN_lh
estimated pdf
-0.25s
0.25s
0.5s
1.75s
3.75s
cosine similarity
D
ORN_al
ePN_al
ePN_cl
ePN_lh
iPN_lh
Time (s)
E
ORN_al
ePN_al
ePN_cl
ePN_lh
iPN_lh
pair_mean
conc
02
04
Time (s)

Figure 4.5: **Odor-evoked responses decorrelate over time**
(a) Similar plot as **Figure 4.7**, Change in ePN dendrites fluorescence signals (ΔF/F) for a few representative ROIs on a single optical plane in the antennal lobe are shown as a function of time since odor onset (shown at the top of the panel). The right panel shows the evolution of odor-evoked responses in the antennal lobe ePN dendrites observed in another fly.
(b) Pattern similarity matrices for a representative fly for each labeled fly line/region are shown. Each element in the matrix is the cosine similarity value between a pair of odorants. Hot colors indicate stronger similarity, and cooler colors indicate weaker similarity. Each row reveals how pairwise odor similarities evolve over time. Again, time since odor onset is indicated at the top of the panel. In total, pairwise similarity matrices at eleven time points are shown. Odor stimulus was presented from 0.0 sec to 4.0 sec. Note that similarity matrices start with higher pattern similarities (cooler/blue colors) and gradually decorrelate over time (hotter/yellow colors). This can be observed in all five rows corresponding to responses observed in ORNs, ePN dendrites, ePN axons in the calyx, ePN axons in the lateral horn, and iPN axons in the lateral horn.
(c) Distributions of pairwise pattern similarity (cosine distance) obtained using kernel density estimation are shown. Each curve shows pairwise pattern similarity distribution at one time point. In each panel, response similarity distributions are shown for five different time points before and during stimulus presentation. Tick marks shown below the distributions represent the pairwise similarity between every pair of odorants and across flies. Ticks are color-coded following the same scheme used for the distributions shown on the top.
(d) Mean pair-wise cosine similarity in each region is shown as a function of time. Each trace shows the mean cosine similarity value across all odor pairs for each individual fly. The color bar indicates the 4 s duration when the odorant was presented. Five panels are shown to illustrate results from the three fly lines used in the study.
(e) Mean pair-wise cosine similarity as a function of time is shown. Two traces, corresponding to the two concentrations of odorants used, are shown tracking changes in mean cosine similarity across odorants/flies.

4.2.3 Idiosyncratic processing underlies how odorants are segregated over time

Given that the initial olfactory circuits have been reported to be stereotyped across flies[152, 170-172], it would be reasonable to expect the variability across flies in these peripheral neural circuits to be low. However, our results (**Figure 4.5d**) indicate that decorrelation of odor-evoked responses occurs at different rates in different flies. We also observed some glomeruli respond to the same stimulus but with different temporal patterns. To further examine this issue, we compared how similarity between pairs of odorants evolved over time in different flies more thoroughly (**Figure 4.6a**). Note that the hot colors indicate high correlations/similarity, and cool colors indicate

negative correlations. Also, clearly observable in the correlation plots shown for the two representative flies is the initial vertical band of high correlation immediately after odor onset. However, note that the correlation between different stimulus pairs transformed rapidly. Bands of highly correlated responses observed immediately after odor onset (show using hotter colors) transitioned to dissimilar responses (less hot colors) at varying points in time. More importantly, the pairwise odor correlation patterns differed between flies indicating that although the odor responses became more distinct, which pairs of odorants became separable, at which point in time depended not only on the odorants but also varied from one fly to another.

To further quantify this result, we computed and plotted the standard deviation in pairwise odor response correlations across flies (**Figure 4.6b**). The high standard deviation would identify pairs of odorants that were decorrelated differently in different flies. Our results indicate that some odor pairs were indeed processed in a relatively conserved manner across flies (identified using arrowheads), whereas many differed starting from the activity they evoked at the level of ORN axons. The standard deviation between flies was relatively less at the level of ePN axons compared to their dendritic activity, whereas the multiglomerular iPNs had higher levels of variability even though they integrated inputs from multiple different ORNs. These results indicate that while odor-evoked response patterns decorrelated to become more distinct over time in all flies, this computation was performed in an idiosyncratic fashion.

To illustrate the variability across flies, for each stimulus pair, we plotted the median response similarity (**Figure 4.6c;** median over time and each row shows variance across flies for each odor-pair). Our results indicate that the attractive odorants (indicated using arrowheads at the bottom of the panel) were more reliably represented across flies and evoked fewer variable responses in ORNs and ePNs. Overall, the variability was reduced at the level of ePN axonal

responses in the calyx and lateral horns. In sum, these results indicate that odor-evoked responses, even in the early olfactory circuits, are not stereotyped for most odorants.

We wonder if we can further compare odor responses between flies in a precise manner. We have identified nine glomeruli from ePN dendrites in the antennal lobe across different flies. To obtain such glomeruli, we first registered the same ROIs across flies and assigned registered ROIs into specific glomeruli based on flies' atlas map. **Figure 4.7** shows an example of identified glomeruli from our calcium imaging data and corresponding confocal imaging atlas map. Note that the light-sheet imaging illuminates the antennal lobe at a different angle than what would be conventionally done with 2Photon or 1Photon illumination done in confocal microscopes. Therefore, the shape of some glomeruli would differ from those published in anatomically atlas. With nine glomeruli identified across all flies **Figure 4.8**, we can further compare temporal odor responses and verify our observations. We found that responses preference remains similar across different flies (**Figure 4.9**). However, glomeruli may elicit responses with different temporal patterns across flies. Some flies may respond more transiently (Or92a, EB02, fly 7 and 9), while others have more lasting responses (Or92a, EB02, fly 8). This observation further confirms different flies respond with idiosyncratic features.

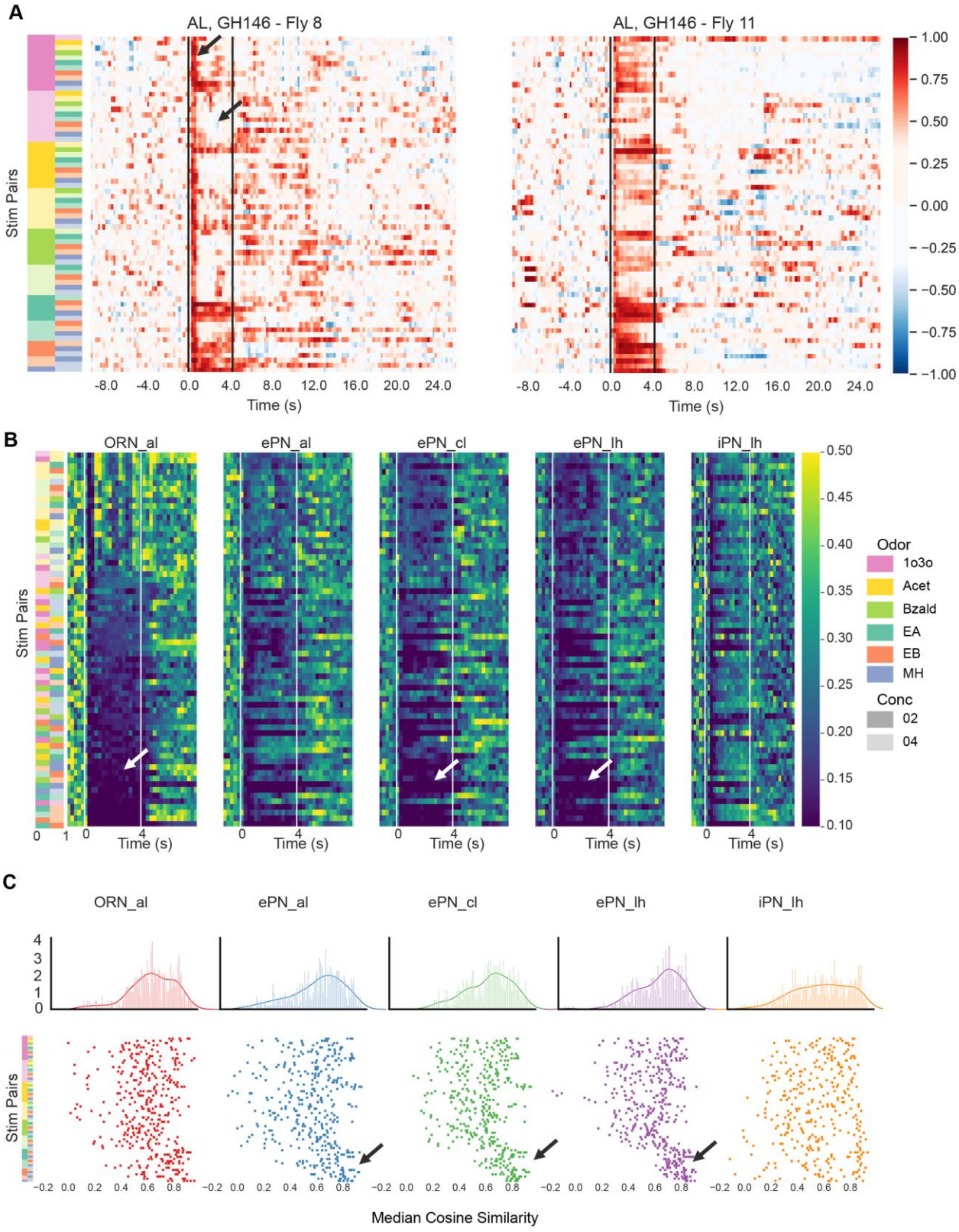

Figure 4.6: Pairwise odor similarities vary across flies.

(a) Pairwise cosine similarities of ePN dendritic responses and how they evolve as a function of time are shown as a heatmap. Each row tracks response similarity between one odor pair, and each column represents one time point. The identity of each stimulus pair tracked in a given row is indicated using a color bar on the left of the heatmap. The four-second odorant presentation window is indicated using black vertical lines. Hotter colors indicate more similarity and cooler colors indicate less similarity. The right panel shows the evolution of pairwise cosine similarity for the same pairs of odorants (ordered as shown on the left panel) but in a different fly.
(b) For each odor pair, the standard deviation in pairwise odor similarity across individuals was calculated and plotted as a function of time. Hot regions in the heatmap show the standard deviation of the cosine similarity across individual fly was greater (i.e., more variability across flies). Similar plots but characterizing variation in pairwise odor similarity in the five fly-line/regions studied are shown. The color bar on the left identifies the odor pair tracked in each row. Note that the rows are sorted in descending order based on standard deviation values observed in the ORN level.
(c) The median cosine similarity during the 4s stimulation period for each stimulus pair, and for each fly, is shown as a scatter plot (bottom). Therefore, each marker represents median pairwise odor similarity observed in a single fly, and each row tracks variation across flies. The identity of the odor pairs corresponding to each row is indicated using the color bar on the left. Tighter packing of individual markers along a single row indicates responses observed across individual flies were highly reliable. The overall distribution across odor pairs and flies is shown on the top.

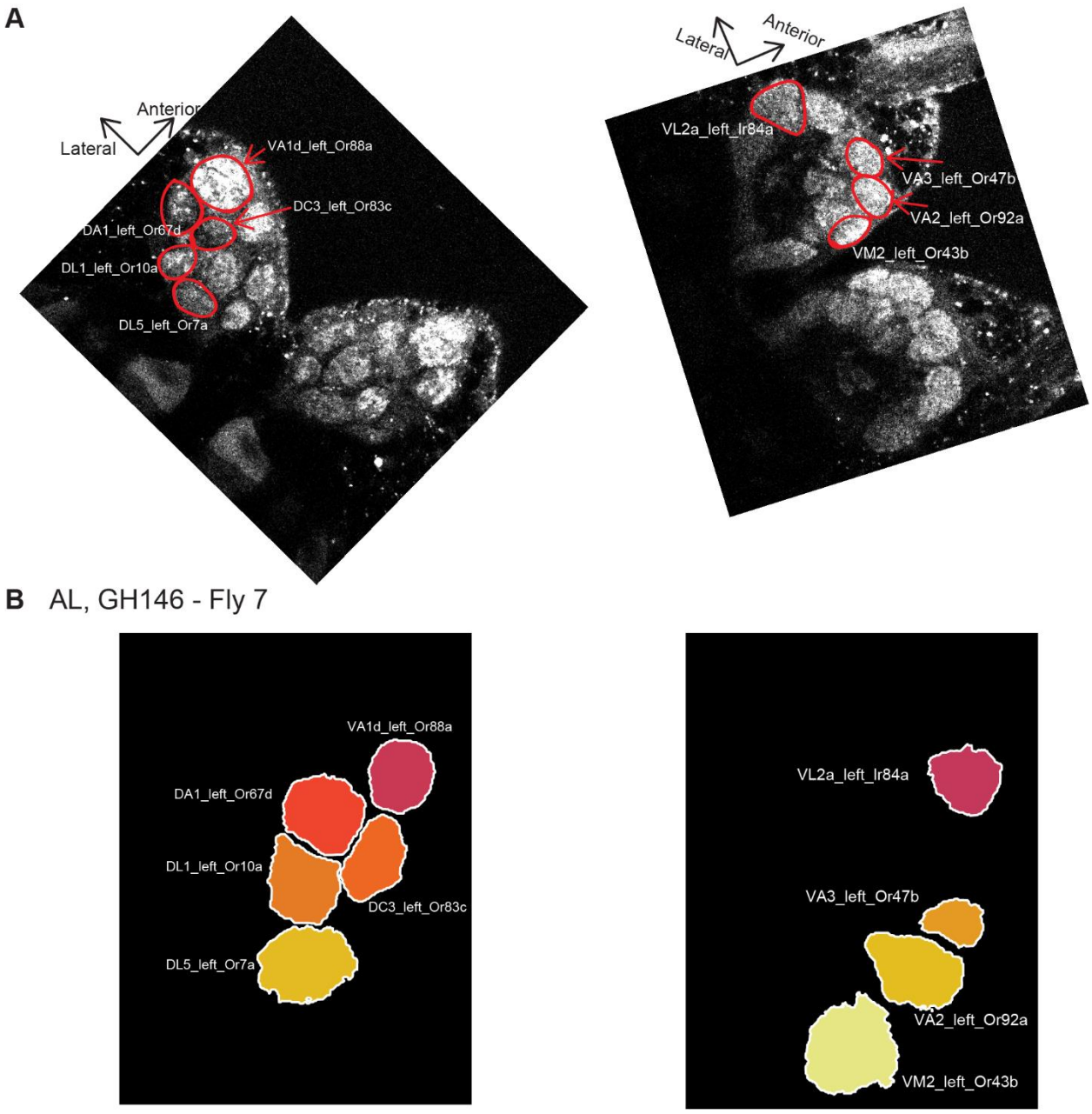

Figure 4.7: **Identified glomeruli examples.**
(a) Left panel, glomeruli from antennal dendrite identified from a confocal imaging setup as atlas map in one plane. The red region indicates the specific glomeruli we identified from our functional dataset. The name of each glomerulus is also shown. Right panel, another four glomeruli in the deeper plane were identified and shown.
(b) The glomeruli identified from functional imaging of one example fly. The images were segmented first and then assigned to the ground truth glomeruli identified from the atlas map by matching the relative size and shape. The Left and right panels show two different planes of images recorded.

AL, GH146 - Fly 7

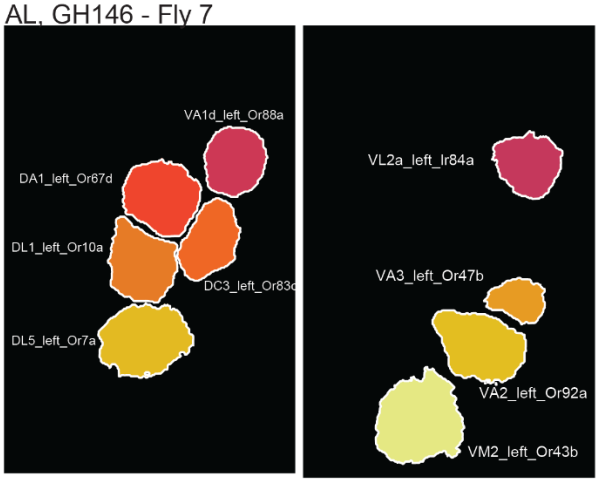

AL, GH146 - Fly 8

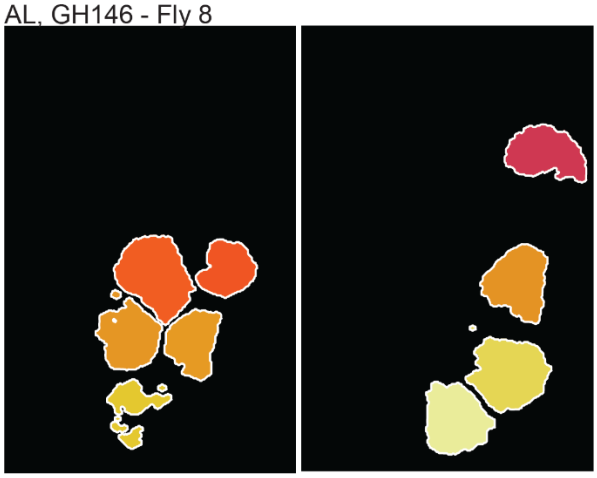

AL, GH146 - Fly 9

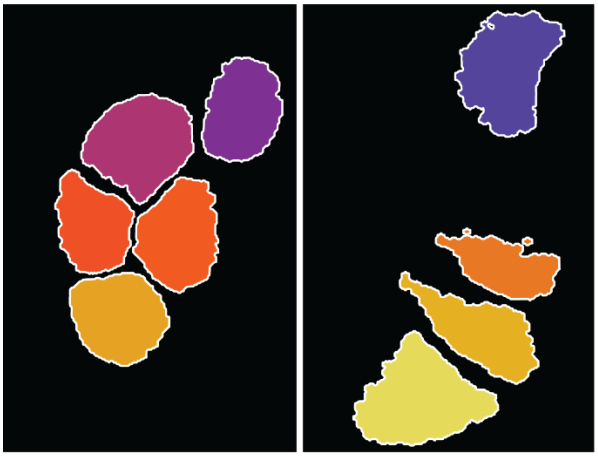

AL, GH146 - Fly 10

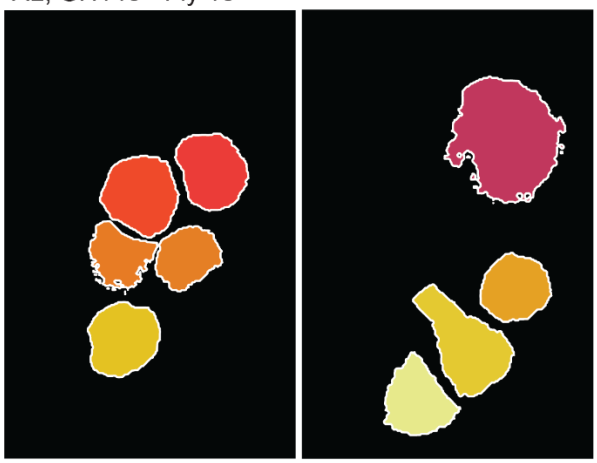

AL, GH146 - Fly 11

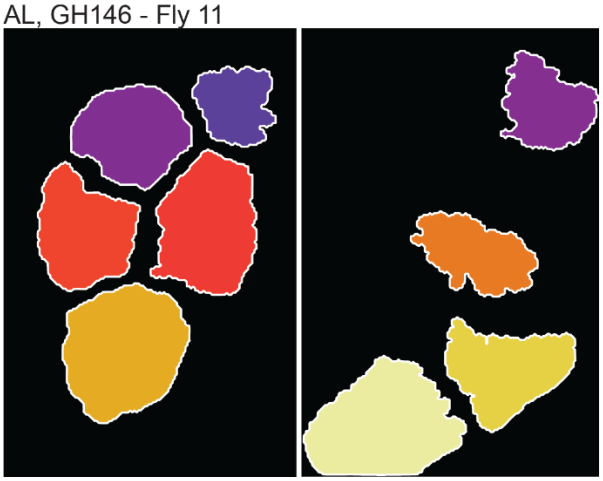

AL, GH146 - Fly 12

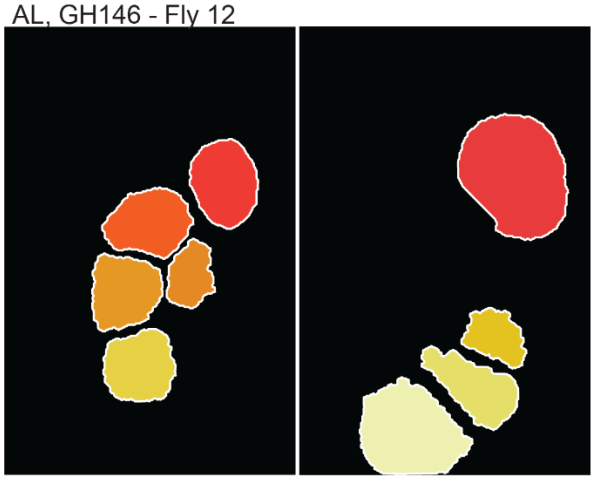

Figure 4.8: **Identified glomeruli across all flies.** Glomeruli identified for two planes in each GH146 labeled fly are shown. Each sub-panel shows nine identified glomeruli in two planes as **Figure 4.4b**.

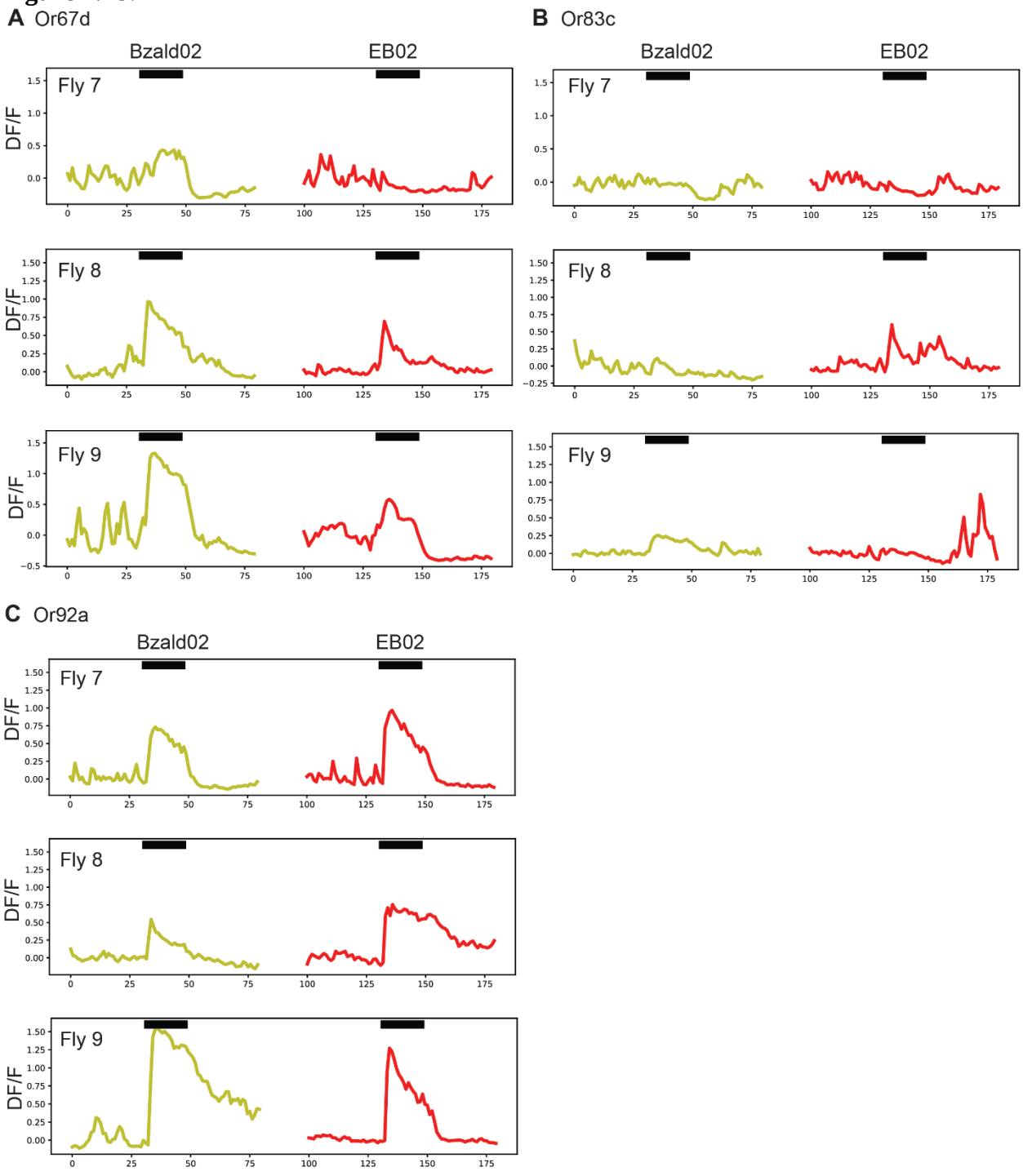

Figure 4.9: **Comparing temporal responses of the same glomerulus across flies.**
(a) Temporal responses (DF/F) of Or67d to odorants Bzald02 and EB02 are shown. Different rows show Or67d responses in 3 different flies. The odor presentation period was indicated with a black bar.
(b, c) Similar plots as panel **a**, but show the temporal responses of glomerulus Or83c and Or92a.

4.2.4 Idiosyncratic processing under short-term memory

We compared the neural responses of the first and second trial of stimulus presentation by directly plotting the ensemble responses after dimension reduction using PCA (**Figure 4.10)**. We found, consistently across all sub-regions and neuronal types, the responses still evolve within the same manifold for the same stimulus identity like what we have observed in PNs responses in the locust antennal lobe. Similarly, the responses decrease after the very first trial of odor presentation. However, responses from iPN tend to have more reduction compared to other responses regions. This indicates the adaptation already starts from olfactory sensory neurons, but processing from network interactions further increases the reduction of the response, resulting in more adaptation in downstream neurons.

Next, we examined if the decorrelation effect observed remains the same under the short-term memory. We compared the pairwise correlation between odor-evoked responses observed across trials within a single fly, and across observations made in different flies (**Figure 4.11a, b;** for GH146 PN responses in the antennal lobe). Note that each heatmap matrix still has the following structure: (i) each row reveals similarity between a specific odor pair before, during (between the vertical lines) and after stimulus presentation window, (ii) different rows correspond to different pairs of odorants, (iii) hotter colors indicate higher similarity in odor-evoked responses, and cooler color indicates dissimilarity. As can be noted, the spontaneous activity, i.e., odor-evoked responses during the period before stimulus onset, is random. However, after stimulus

onset, the similarity between odor pairs increases for almost all odor pairs (initial column of hot color after odor onset). Subsequently, the similarity between different odorant pairs decreases at different rates as the stimulus is sustained. It would be worth pointing out that the pairwise correlation heatmaps are strikingly similar across two trials of recordings made from a single fly (**Figure 4.11a or b;** left vs. right column). However, note that the correlation patterns across different flies are qualitatively different (**Figure 4.11a vs b**). To quantify this result, we computed the Frobenius norm between the two pairwise odor correlation matrices. We performed this comparison for responses observed in two different trials within the same fly and between two trials across different flies. As expected, within fly response correlations were higher indicating stability of responses observed during different trials. Responses observed in different flies, while consistent across trials for each fly, had significantly lower levels of response correlations. This result also identifies the noise floor (variations across trials in the same fly) and how differences in odor-evoked response correlations observed across flies are significantly higher (**Figure 4.11c**).

Further, the evolution of mean pair-wise correlation across odorants over time showed variable reduction rates in each trial (**Figure 4.12**). The overall speed at which decorrelation between odorants occurred was accelerated during the second block of trials. Interestingly, ePNs dendrites and axons showed a stronger reduction compared to the other neuron population. This result suggests that a role of short-term memory was to expedite the speed of discrimination between odorants.

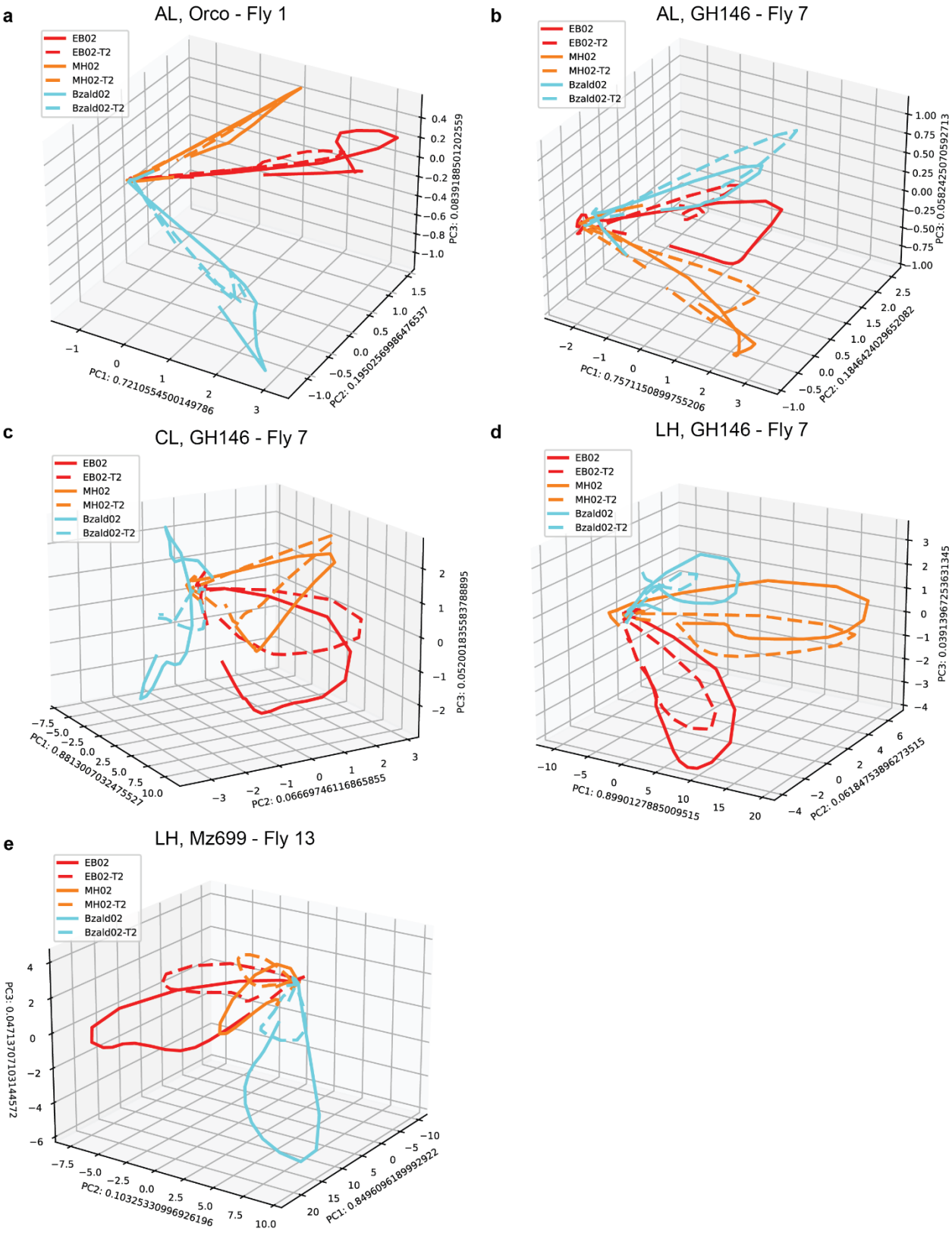
a
AL, Orco - Fly 1
EB02
EB02-T2
MH02
MH02-T2
Bzald02
Bzald02-T2
PC1: 0.7210554500149786
PC2: 0.19502569866476537
PC3: 0.08391885012025559
b
AL, GH146 - Fly 7
PC1: 0.7571150899755206
PC2: 0.18464240296520 82
PC3: 0.05824250705927 13
c
CL, GH146 - Fly 7
PC1: 0.8813007032475527
PC2: 0.06669746116865855
PC3: 0.05200183558788895
d
LH, GH146 - Fly 7
PC1: 0.8990127885009515
PC2: 0.06184753896273515
PC3: 0.03913967253631345
e
LH, Mz699 - Fly 13
PC1: 0.8496096189992922
PC2: 0.10325330996926196
PC3: 0.04713707103144572

Figure 4.10: Short-term memory across different microcircuits.
(a) Odor-evoked orco-AL ROIs response trajectories are shown after dimensionality reduction using PCA. Solid trajectory represents the responses from the first trial. The responses in the second trial are shown by dashed trajectories. In total, three different stimuli were shown.
(b, c, d, e) Similar trajectories plots as panel **a**, but from GH146-AL(**b**), GH146-Calyx(**c**), GH146-LH(**d**) and Mz699-LH(**e**) are shown.

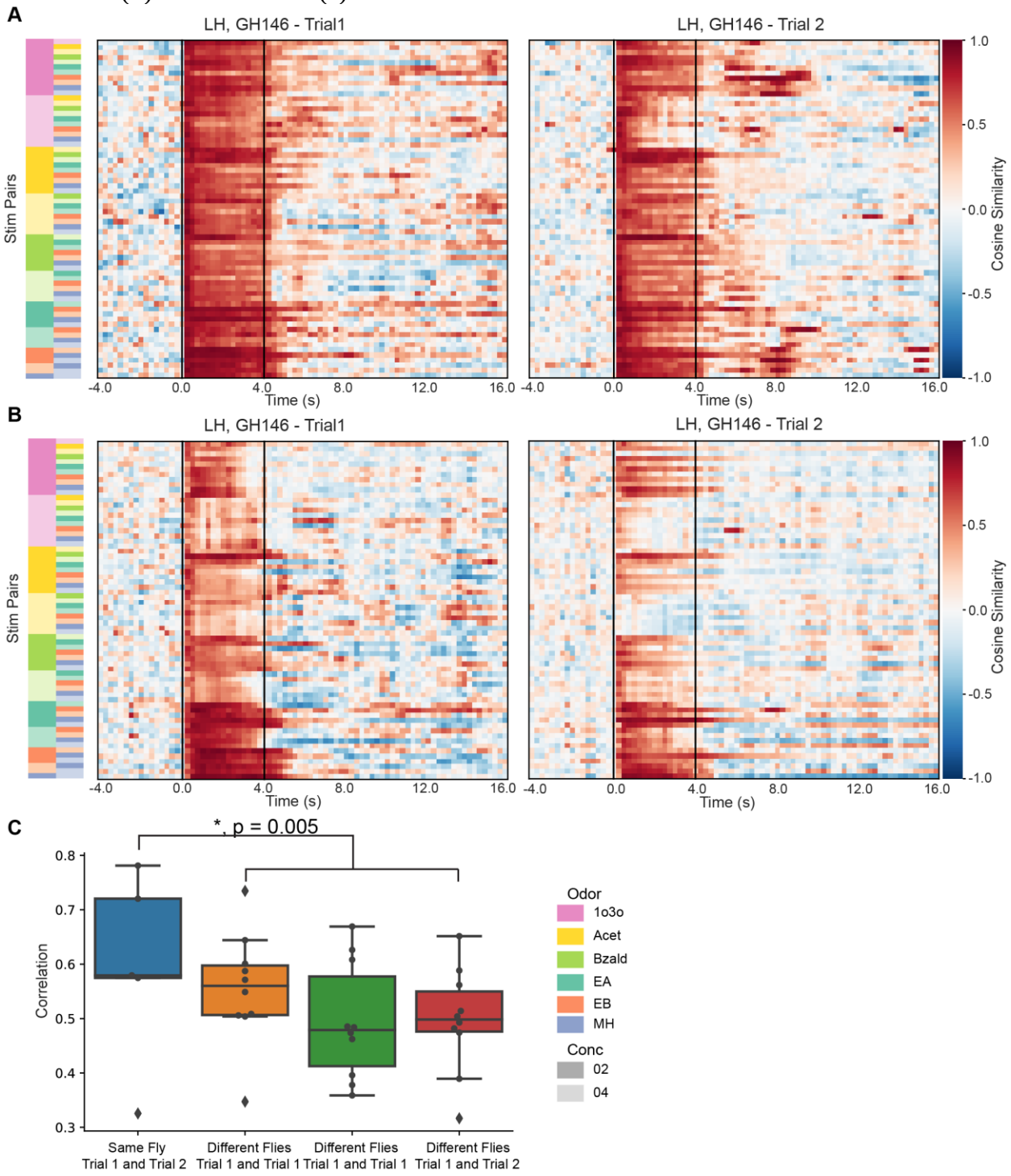

Figure 4.11: Within-fly vs. across-flies comparison.
(a) Both panels show similar pairwise cosine similarities matrices as panel Figure 4.9a, but the matrices are obtained from responses of two trials within the same fly.
(b) Similar plot as panel a, but neural responses correlation matrices from another fly are shown.
(c) Within fly variation was quantified by the correlation between cosine similarity matrix during the odor-evoked period across two flies. The distribution of correlation values was summarized by the bar plot. The first column shows the correlation of similarity matrix within fly across two trials. The second column shows the correlation distribution for the same trial (first trial) but across flies. The third column shows the correlation distribution of the second trial across flies. The last trial shows correlations calculated from different flies and different trials. Note that within fly correlations are significantly larger than across flies' variations.

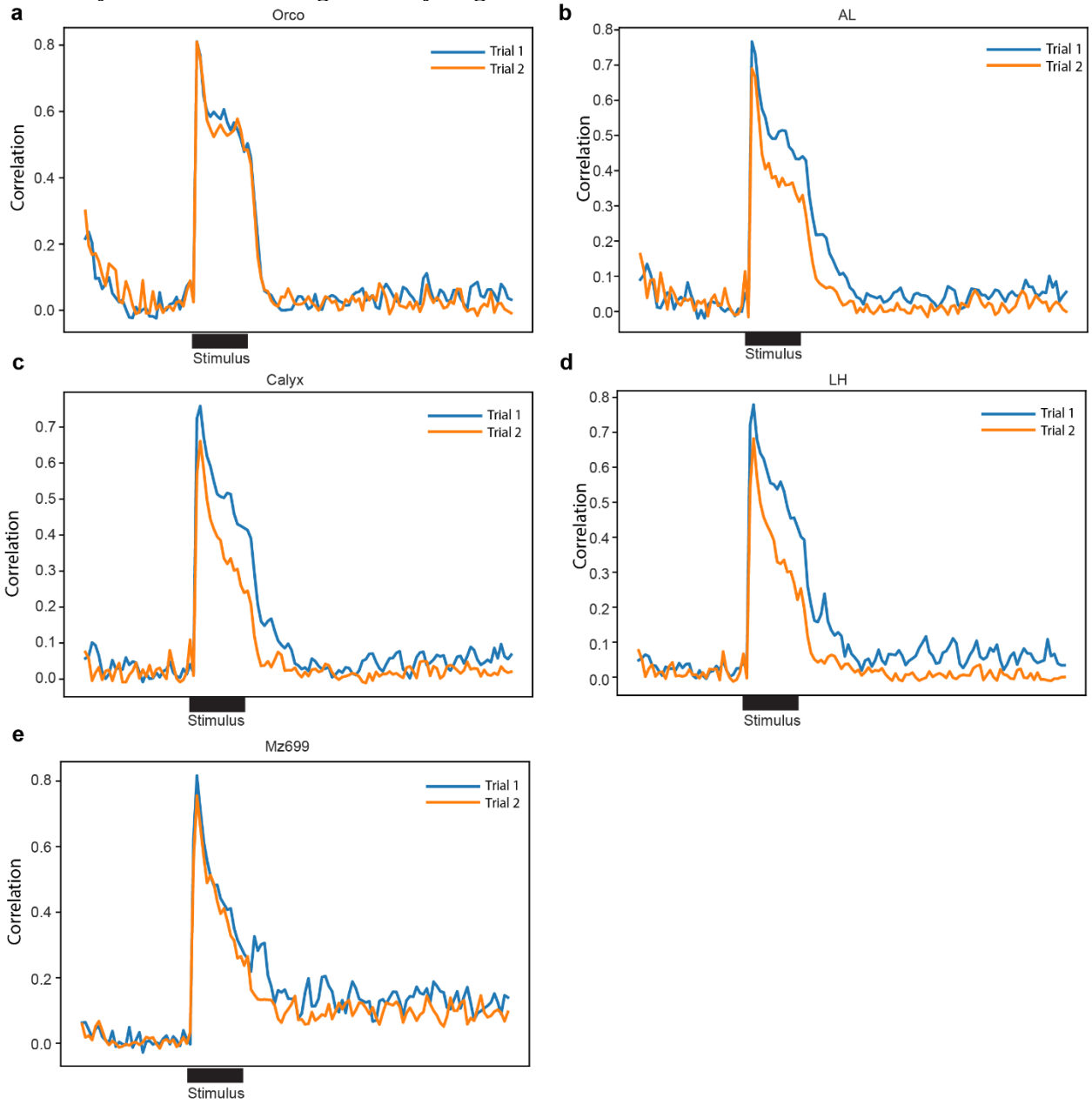

Figure 4.12: Mean pair-wise cosine similarity comparison across trials.
(a-e) Mean pair-wise cosine similarity traces as a function of time in each fly line/region are shown. For each trace in each neuronal population, the mean pair-wise cosine similarity was obtained by averaging across all stimulus pairs and all flies. Two traces, corresponding to the two trials, are shown tracking changes in mean cosine similarity due to short-term memory.

4.2.5 Stimulus evoked ON and OFF responses

Finally, we examined how stimulus-evoked responses were patterned after the stimulus termination (i.e., the stimulus-evoked OFF responses). We found that at the level of ORNs, two types of responses were observed after stimulus termination: continuation of the ON response and inhibition in new ROIs that did not have an ON response. Excitatory responses only during the OFF period were seldom observed at the level of sensory neuron responses (**Figure 4.13a**).

In comparison, the OFF responses observed at the level of ePN dendrites and ePN/iPN axons showed response patterns that were more orthogonal with respect to the ON responses (**Figure 4.13a**). ROIs that were active during the ON period returned to baseline activity levels or even below baseline level responses (i.e., inhibition) in many ROIs. Whereas ROIs that were not activated by stimulus exposure or even inhibited during the ON periods tended to have a strong OFF response.

To understand how dissimilar the neural responses were observed during and after stimulus termination, we performed a cross-correlation analysis. A snapshot of activity across all ROIs was regarded as a high-dimensional vector. The similarity between each response vector with every other response vector that was observed over time was computed and shown succinctly as a correlation matrix (**Figure 4.13b**). Hot colors were used to indicate high correlation/similarity and cool colors to indicate negative correlation/dissimilarity. Note that while response vectors observed during odor presentations (i.e., the ON responses) were well correlated amongst

themselves, the responses observed after odor termination (i.e., the OFF responses) poorly correlated with these ON responses (arrowhead). This relationship between the ON and the OFF responses was observed in all three neural populations and every fly studied.

To quantify how much the OFF patterns deviated from the ON patterns, we computed the angles between the mean population vectors during the ON and OFF periods (**Figure 4.13c**). Consistent with the interpretation of the correlation plots, for most odorants, the ON and OFF response vectors evoked by the same odorant had an angular similarity in the 60°– 100°range (closer to 0° indicates similar responses and 90° indicates orthogonal responses).

Finally, we examined whether the response patterns evoked after odor termination are as diverse as those observed during stimulus presence. To compare pattern diversity, we used the number of principal components that were required to capture 90% of the total variance of the data (can also be thought of as a measure of intrinsic dimensionality of the dataset; **Figure 4.13d**). Surprisingly, compared to the ON responses, our results indicate that the OFF patterns were more diverse and needed more principal components to capture the same amount of variance in the response patterns observed.

In sum, our results indicate that for most odorants, another round of diverse response patterns were observed following stimulus termination. More importantly, these response patterns were dissimilar to the odor-evoked ON responses and were a common encoding feature in all three neural response populations and all flies studied.

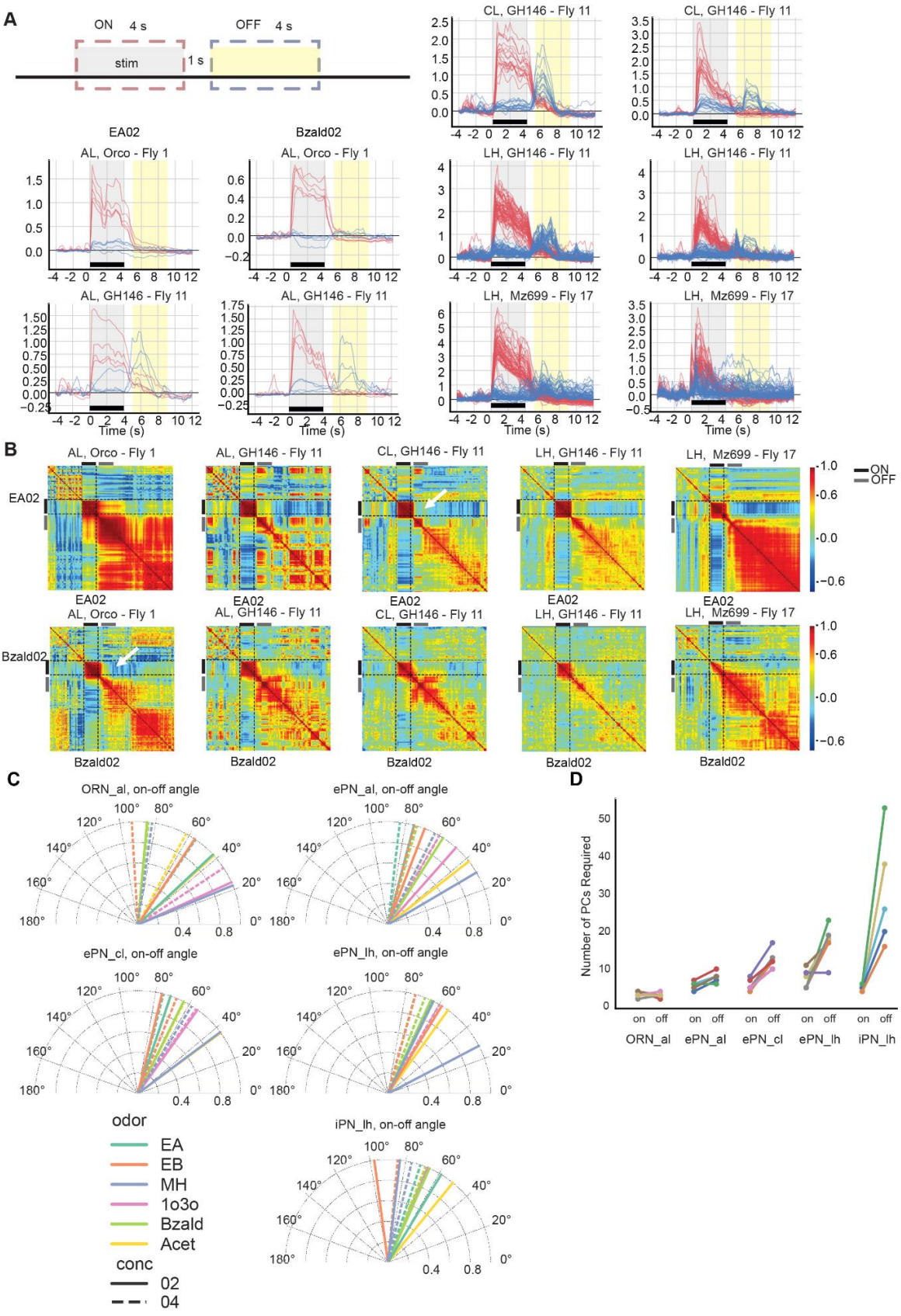
A
ON 4 s
OFF 4 s
stim
1 s
EA02
Bzald02
AL, Orco - Fly 1
AL, GH146 - Fly 11
CL, GH146 - Fly 11
LH, GH146 - Fly 11
LH, Mz699 - Fly 17
Time (s)
B
ON
OFF
C
ORN_al, on-off angle
ePN_al, on-off angle
ePN_cl, on-off angle
ePN_lh, on-off angle
iPN_lh, on-off angle
odor
EA
EB
MH
1o3o
Bzald
Acet
conc
02
04
D
Number of PCs Required
on off
ORN_al
ePN_al
ePN_cl
ePN_lh
iPN_lh

Figure 4.13: Odor evoked ON vs. OFF responses.
(a) The top and bottom 5% of traces sorted by the mean amplitude during stimulus are shown, with the top 5% in red, and the bottom 5% in blue. The ON and OFF response windows are schematic schematically identified in the plot. Responses evoked by two representative odorants in each of the five fly-line/region combinations are shown.
(b) Evolution of correlation between neural activity before, during and after odor exposure are shown as a heatmap. The black bar on the left and top indicates the time period when the stimulus was delivered. Hot colors indicate high similarity and cool colors indicate low similarity. Note that each non-diagonal pixel represents the similarity between ensemble ROI activities in one time bin versus those in another time bin. One row or column represents the correlation between one ensemble ROI activity vector with all other ensemble ROI vectors. Correlation heatmaps for two representative stimuli are shown for all three fly lines and five locations imaged.
(c) Angle between mean ON and OFF response patterns evoked by each odorant is shown. Different colors represent different stimuli, and the line style represents the two concentration levels.
(d) The number of principal components needed to account for 90% of the data variance during ON and OFF response periods are plotted as a pair of points for each fly line/regions. Colors indicate individual flies.

4.3 Discussion

We sought to understand how sensory input from olfactory receptor neurons is temporally reformatted by two different downstream neural populations: ePNs and iPNs. While ePNs are cholinergic and receive input from a single glomerulus [153] , iPNs are mostly GABAergic and multiglomerular [173]. Further, while ePNs project to both calyx and lateral horn, iPN axons only innervate the lateral horns [163]. So, given the differences in the nature of input received (from one vs. many types of ORNs), and the downstream centers they feed onto, it is reasonable to expect that the ePNs and iPNs use different transformations to reformat sensory information received. However, our data reveal that several temporal aspects of odor-evoked responses were strikingly similar in both these neural populations.

Our results indicate that the odor-evoked responses were dynamic and evolved over time at the level of sensory neurons and in both ePNs and iPNs. The initial responses immediately after the stimulus onset were strong but did not have much discriminatory information. Over time,

neural activity patterns evoked by different stimuli became more odor-specific. This decorrelation of odor-evoked responses over time was observed in all three neural populations examined. However, the trends observed (which odor pair became distinct when) varied even between the dendritic and axonal compartments of the same neural populations, and between flies. This result indicates that a generic computational function can be achieved in an idiosyncratic fashion in flies, and that the information transmitted to the calyx and lateral horns may be qualitatively different.

The decorrelation result is strikingly similar to what has been reported in other model organisms, particularly in zebra fish[63], with one caveat. We found that decorrelation already happens at the ORN level and gets accelerated downstream.

However, it is in stark contrast with a recent hypothesis put-forth for odor recognition that suggests initial responses carry information odor identity[174]. One possible explanation for the lack of odor-specificity at the stimulus onset could be that the neural activity immediately following stimulus presentation indicates stimulus presence and help with localization. Such localization signals have been reported in many other sensory systems[175]. We note that the responses immediately following this localization signal may still be extremely important for the fly to recognize the odorant.

Extraction of odor-specific information may happen in two different ways. First, the information may be refined in a systematic manner, such that the initial responses recognize odor groups and additional features are extracted to allow precise recognition (Odor present -> fruity -> tropical -> pineapple; analogous to a decision tree). In this case, a snapshot of activity during a later time point is sufficient to recognize the stimulus, while the initial responses may be utilized for other sensory computations. The second possibility is that features are extracted in a serial fashion, but the later responses need not be the most unique features. This latter scenario is

analogous to serial parsing of words (r·e·a·d· vs. r·e·e·l· vs. r·a·i·l· vs. m·e·e·t·). While the initial letters are still important for word recognition, the subsequent letters extracted are necessary but in isolation are not sufficient to allow precise recognition. In this case, an integration of all the features extracted might be necessary for stimulus recognition. Our results indicate that temporal patterning observed in the fly antennal lobe may be more analogous to the first scenario (i.e., pairwise similarity smoothly reducing over time), but achieved in an idiosyncratic fashion, indicating multiple different solutions may exist to this problem.

It would be important to point out that variations across different individuals could arise trivially due to unaccounted differences in experimental conditions between different experiments. However, we have identified the noise floor by finding much lower within fly variations compared to across fly variations (**Figure 4.11**). Further, our results reveal that not all results we observed varied across individual flies. Even in the temporal dimension, certain pairs of odorants evoked responses that were highly consistent (**Figure 4.6**). Such robustness in temporal features, at least for a subset of odorants, indicates that the variations observed in our dataset cannot be attributed solely to trivial differences in experimental conditions. It would be worth pointing out that such variations in neural responses could underlie differences in behavioral preferences in individual flies[176]. What variations are important and therefore get translated to mediate idiosyncratic differences in odor preferences, and what variations are squashed to underlie robust recognition needs further examination.

Finally, our results indicate that the stimulus-evoked responses do not stop after stimulus termination. At the level of sensory neurons, these are the persistence of activity, in some cases excitation and other inhibition, that was observed during the stimulus. However, in the ePN and iPN dendrites and axons, the responses often switched from one ensemble to another. Therefore,

stimulus ON and OFF responses were orthogonal to each other, and was observed in all flies. These results are consistent with those reported in other sensory systems, and in particular the locust olfactory system[177].

What is the purpose of these elaborate OFF responses? In cockroaches, such responses were observed directly at the level of sensory neurons and were thought to indicate a reduction in stimulus concentrations[178]. Such dedicated ON and OFF neurons were not found in flies. A single ROI in any region was able to respond during either ON or OFF periods depending on the odor. In a different study, it was reported that these OFF responses may indicate 'unsensing' of a stimulus (analogous to a pause after a tone or space after a word) and were found to be better predictors of termination of behavioral responses[179]. Furthermore, our results here indicate that the response patterns observed after stimulus termination were stimulus specific and more diverse than those observed during the stimulus presence period. Further, when odorants are encountered in sequences, the OFF response of the first stimulus was found to contrast enhance the neural activity evoked by the second stimulus. While these results are similar to the findings observed in locusts, the causal relationship between OFF responses and their behavioral contributions remains to be determined.

4.4 Author contributions

Haoyang Rong and Barani Raman conceived the study and designed the experiments/analyses. Haoyang Rong performed all the light-sheet experiments and collected the data. Lijun Zhang motion corrected the raw calcium imaging movies and extracted ROIs in collaboration with Haoyang Rong. Haoyang Rong performed temporal decorrelation data analysis with Lijun Zhang's assistance. Lijun Zhang performed across-trials analysis and identified common glomeruli across

flies. Haoyang Rong, Lijun Zhang, and Barani Raman wrote the paper taking inputs from all the authors. Yehuda Ben-Shahar and Tim Holy advised on the selection of fly lines and light-sheet imaging, respectively. Barani Raman supervised all aspects of the work.

This research was supported by NSF Neuronex grant (Grant# 1707221) and a NSF CAREER Award (Grant #1453022) to B.R.

Chapter 5: Invariant Odor Recognition with ON-OFF Neural Ensembles

5.1 Introduction

Robustly recognizing a sensory stimulus is a necessity for the survival and propagation of all animals. Since this capability is demonstrated in all sensory systems, it raises the following question: what is the neural basis that underlies this feat of pattern recognition? In the previous two chapters, we have examined how short-term memory alters odor processing in the antennal lobe network. As was noted interferences arose from changes in the sensory circuit due to plastic changes arising either from prior exposures or co-occurrence with other sensory cues. These changes can be regarded as intrinsic perturbations as the sensory stimulus encountered is the same, but the processing network of neurons have been altered some way or the other.

Additionally, most stimuli are encountered in a multitude of ways in natural environments. Often, stimulus features such as intensity, duration, and recurrence could vary. External perturbances due to changes in environmental conditions (such as changes in humidity or temperature), the presence of other competing cues, or the temporal context (i.e., when it is received in a stimulus sequence) could also change independently of the variation in stimulus-specific features. Given the complexity in carrying out the basic task of recognizing a stimulus, we wondered if there exists a computational framework that can compensate for all these disparate sources of variation and allow robust recognition of a stimulus. In this chapter, we will examine this issue using comprehensive datasets we have obtained in the locust olfactory system [8, 65, 67, 69, 76, 78, 122, 130, 179-183].

In the locust olfactory system, odorants activate olfactory receptor neurons in the antenna. This signal is transmitted downstream to the antennal lobe (analogous to the vertebrate olfactory bulb) where it drives responses in cholinergic projection neurons (PNs) and GABAergic local neurons (LNs). The interaction between PNs and LNs transforms the sensory input received into complex patterns of spiking activities distributed across ensembles of PNs that become the output of the antennal lobe circuit. Prior work has shown that information about the identity and intensity of an odorant is encoded by spatiotemporal PN activity patterns[76]. While individual PN responses were perturbed by manipulating stimulus dynamics[122, 184], stimulus history[77, 80], and presence of background chemicals[67], the ensemble neural patterns still allowed recognition of odorants. Behavioral evidences also support this interpretation and reveal that odorants can be recognized independent of background cues[67] and stimulus history[80].

It is worth noting that prior studies examined neural response variabilities that arose due to each of these perturbations in isolation. In natural contexts, such interferences could occur independently or in conjunction with one another. Could robust odor recognition still be achieved? Would an array of schemes that extract information from a variety of response features be necessary for compensating changes associated with each perturbation? Alternately, can the variable neural responses be decoded in a manner that can simultaneously allow invariant odor recognition independent of all these perturbations? If so, what neural response features would be important for achieving this result? We sought to examine these issues in this study.

5.2 Results

5.2.1 Robust odor recognition under short-term memory

In the locust antennal lobe, odor-evoked PN responses reduced over repeated exposures of the same stimulus. During the earlier trials of odor exposures, responses elicited at low intensities were comparable to those evoked during the later trials of the same stimulus but at a higher intensity (**Figure 3.5**). We found combinatorial PN activity profiles can still retain information about odor identity and intensity and is robust to changes that occur due to adaptation (**Figure 3.5, 3.6**). Can odorants still be robustly recognized independent of variations induced by short-term memory? We will study this question in this chapter.

To investigate this issue, we first pooled the ensemble activity across all PNs in a 50 ms time bin as a high-dimensional neural activity. To detect the presence of the target odorant and selectively recognize the identity of the target odorant, we trained a linear support vector machine classifier. As the stimulus was presented 25 times (25 trials), we used a leave-one-trial out scheme to train the classifier. For example, to test the presence of the last trial stimulus, we will use the responses in the first 24 trials to train the SVM classifier. **Figure 5.1** summarizes the result from a bin-by-bin, trial-by-trial classification analyses. Each tick represents the class label that was predicted in a given 50 ms time bin in a specific trial. If the ensemble neural responses were correctly recognized and predicted by the SVM classifier, that time bin will be labeled by the corresponding identity/intensities labels. This method allows us to precisely examine the recognition ability in a trial-by-trial manner.

For results shown in **Figure 5.1a**, we trained two different classifiers: one for recognizing Hex and another for recognizing Oct. The classification results clearly showed that all trials of introductions of the hex or oct, even in later trials, were correctly detected and recognized by the SVM classifier. More interestingly, during spontaneous activities window, some time segments

were also classified as Hex or Oct, indicating the altering of spontaneous activities due to short-term memory as discussed in Chapter 3.

Next, we examined robustness of odor recognition when we trained two different classifiers to discriminate between two different intensities of the same odorant. Note that the overall spiking activities during later trials of higher intensity odorant presentation were comparable to those during early trials of lower intensity odorant presentation. As can be noted in **Figure 5.1b**, the lower concentration of hex presentation can still be robustly recognized and separated for its higher concentration regardless of trials number. This result suggests that the odor identity and intensity information can still be robustly recognized under the perturbation of short-term memory.

We also applied SVM classifier to the catch trial dataset (**Figure 3.7**). In this dataset, to obtain the classification results during the first 25 trails of Hex or ten control trials of the catch odorant (Iaa or App), a similar leave-one-trial-out scheme was used to train SVM classifier. However, to obtain the results during catch trial (the 26^{th} trial after 25 trials of Hex repetition), both 10 control trials and first 25 trials of Hex were used as the training dataset. Similarly, after 25 trials of repetitive Hex presentation, the linear SVM classifier can still correctly recognize the responses evoked by deviant stimulus (Iaa or App) in the 26th catch trial (**Figure 5.1c, d**).

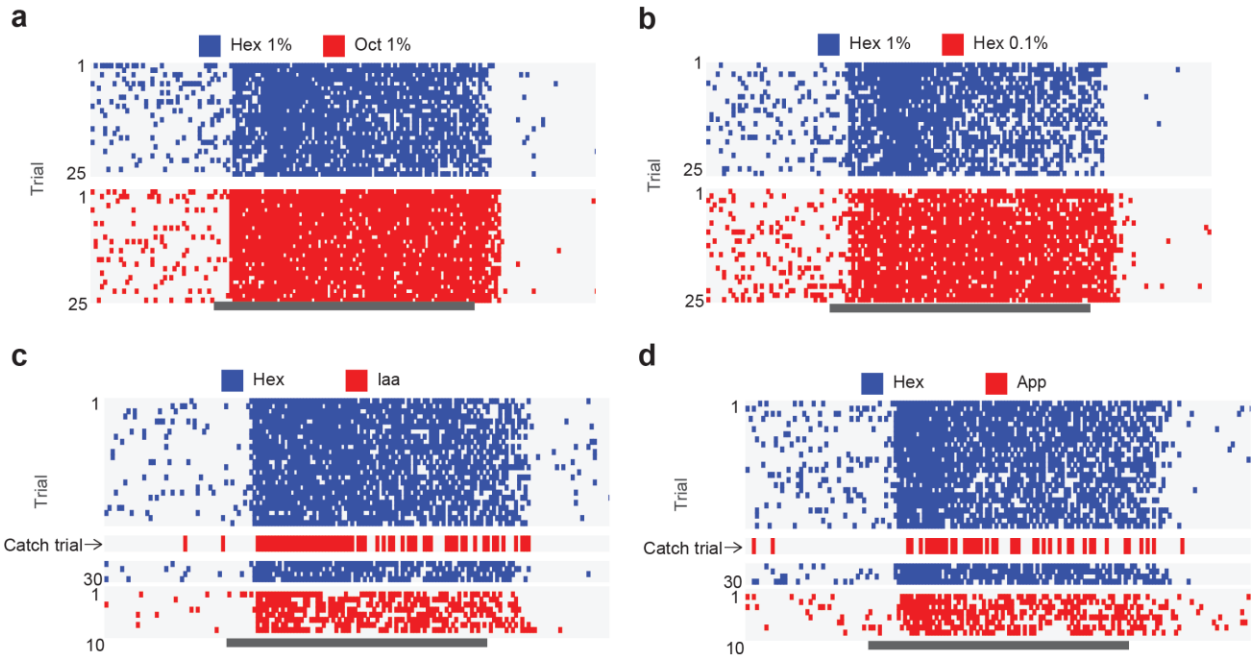

Figure 5.1 Robust odor recognition independent of perturbations from short-term memory.
(a, b) Linear SVM classification analysis results are shown in a bin-by-bin, trial-by-trial fashion. A leave one trial out scheme, in which if one trial is the target prediction trial, the remaining trials' neural response will be used as training data, was used to train the classifier. If the neural response was classified and assigned to the correct target class, a class label would be assigned (**a**, blue: Hex 1%, red: Oct 1%; **b**, blue: Hex 1%, Red: Hex 0.1%). The Gray bar indicates the stimulus presented period.
(c, d) Similar plots as panels **a** and **b**, but for catch trial dataset was used (**Figure 3.7**). To obtain the classification result of the catch trial, neural responses from the first 25 trials of Hex presentation and ten control trials of the catch odorant (Iaa or App) were used as the training set.

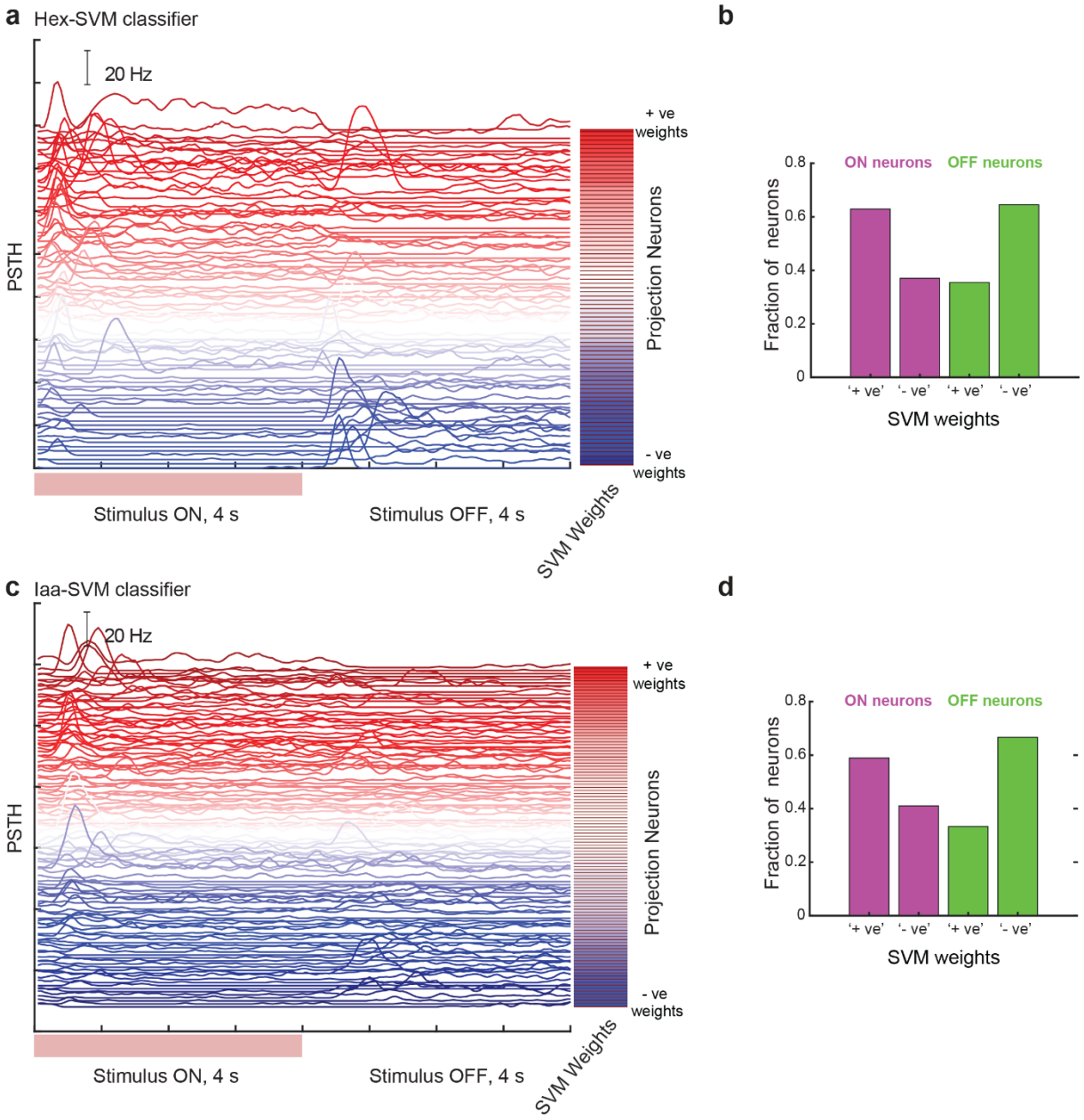

Figure 5.2 Comparison of weights and PNs' responsiveness.
(a) The PSTHs of each PN during 4 s solitary hex presentation and 4 s after stimulus termination are shown. Each trace shows PSTH of one PN. The PSTHs are sorted and color-coded based on the hex SVM classifier weights assigned to each PN (n = 80 PNs). The neurons assigned the most positive weights are at the top, and the most negatively weighted neurons are near the bottom. SVM classifier weights assigned to each PN are also schematically shown as a heatmap to the right.
(b) The fraction of ON and OFF neurons that received '+ve' or '-ve' weights are shown as a bar plot for comparison.
(**c, d**) Similar plots as panels a and b, but Iaa-SVM classifier with catch trial datasets were shown.

To understand why the classification results were robust, we examined the weights assigned to different PNs in the dataset (**Figure 5.2**). We sorted the PNs based on the weights assigned by the SVM classifier and plotted their average PSTH to the solitary target odor pulse (i.e., training data that was used). In **Figure 5.2a, b**, we showed the PSTHs and weights from Hex classifier and in **Figure 5.2c, d**, the PSTHs and weights from Iaa (catch odorant) were shown. Note that PNs with strong ON responses are at the top, and PNs with stronger OFF responses are at the bottom. The weights assigned to each PN by the hex-SVM (**Figure 5.2a**) or iaa-SVM (**Figure 5.2c**) classifier were shown next to the firing rate plots respectively to allow comparison. Our results indicate that ON responsive PNs received mostly positive weights, and the OFF responsive PNs were assigned negative weights (**Figure 5.2b, d**).

We wondered whether this simple approach would be sufficient to deal with more complex extrinsic perturbations such as those induced by varying recurring stimuli, background cues, distractor odorants and humid ambient conditions. In the following sections, we will systematically study the generalization of this approach for robust odor recognition.

5.2.2 Robust odor recognition in a behavioral assay

We began by testing our core hypothesis that locusts could indeed recognize an odorant in an invariant fashion. To do this, we used an appetitive conditioning assay (**Figure 5.3a**; left panel). In this assay, starved locusts were presented with an odorant (conditioned stimulus; CST) followed by a food reward (unconditioned stimulus; UST). The food reward is alone sufficient to evoke an innate extension/opening of sensory appendages close to the mouth of the locusts (called the maxillary palps). After training with six trials when CST and UST were delivered in an overlapping sequence, the ability of the locusts to recognize the CST was examined in an unrewarded testing phase. Opening of the maxillary palps following presentation of the CST was regarded as an

indicator of successful recognition of the trained odorant. Note that the palp opening response (POR) was selective to the CST (with a few caveats discussed below). Further, to make the readout quantitative, locust palps were painted with a non-odorous green paint, and the distance between the palps was tracked as a function of time (**Figure 5.3a**; right panel). Notably, the PORs remained consistent when probed multiple times with the CST in the unrewarded test phase thereby allowing us to examine the POR when we made a battery of perturbations.

First, we examined how PORs changed as we varied the duration of the stimulus. We found that the PORs initiated rapidly, and the palps were kept open for the duration of the odor pulse and terminated following cessation of the trained odorant. Although we trained locusts using a particular duration of CST pulse (4 s pulse of hexanol for results shown in **Figure 5.3b**), we found that POR duration was briefer for a shorter CST pulse, and the palps remained open for the entire duration of a longer CST pulse. These results indicate that locusts recognized the CST and maintained their responses to the trained odorant independent of the stimulus duration during training. Further, when two short, non-overlapping pulses of the CST were presented in quick succession, the locust palps opened, began closing, and again opened matching the dynamics of the stimulus delivery (**Figure 5.3b**; rightmost panel). The fact that the second CST pulse in the stimulus sequence elicited a POR comparable to the first pulse indicates that locusts could respond to the trained odorant robustly independent of variations in the stimulus delivery/encounters.

Could response to a stimulus change depending on what other cues were encountered recently? To understand this, we presented the CST in different non-overlapping sequences with a number of distractor cues. Note that the distractor cues terminate before the onset of CST, and are only used to determine if stimulus history can alter recognition performance. Our results

indicate that locusts could robustly recognize the trained odorant irrespective of the stimulus that was encountered before (**Figure 5.3c**).

Next, we wondered whether locusts trained to recognize a particular odorant could do so independent of the presence of other competing cues (**Figure 5.3d**). Note that locusts trained with a CST had a POR only when tested with the trained odorant (isoamyl acetate or iaa), and had no detectable POR response following the presentation of an untrained odorant (benzaldehyde or bzald). Presentation of the trained odorant (iaa) atop the untrained background cue (bzald) with different latencies did not alter the locust POR response to the trained odorant. In all the cases, a rapid and vigorous POR response was observed following the introductions of the CST, and the palps started closing upon the termination of the CST. Similar results were also reported when locusts trained with hexanol were tested by presenting hex alone or atop a background cue[67]. Taken together, these results indicate that the locusts could recognize the trained odorant in a background invariant manner.

Could changes in ambient conditions impact recognition performance? To understand this, we trained locusts in dry conditions (0% relative humidity). In the testing phase, we examined the ability of locusts to recognize the conditioned stimulus presented either in dry or humid (100% relative humidity) conditions. Our results show that locusts opened their palps to all the introductions of the conditioned stimulus in both dry and humid conditions (**Figure 5.3e; left panel**). The performance was near identical indicating a robust odor recognition that was invariant with respect to changes in ambient conditions. Similar results were also obtained when locusts were trained in humid conditions and tested in both dry and humid conditions (**Figure 5.3e; right panel**). These results indicate that locusts can recognize trained odorants independent of changes in ambient conditions.

The locust recognition performance under the battery of perturbations discussed is summarized in **Figure 5.4**. Taken together, these results support the idea that locusts could recognize an odorant independent of variations in stimulus features such as its duration and dynamics, and extrinsic features such as encounters with other distractor cues, presence of other competing cues, or changes in ambient conditions (**Figure 5.4b-e**). Furthermore, while locust responses were selective and the CST evoked the strongest response, locusts trained with one odorant also showed PORs to a select few other odorants (generalization; **Figure 5.4a**). These observations raise several questions regarding whether certain odor-evoked neural response features remain robust to such perturbations to invariant odor recognition, and whether achieving robust odor recognition also causes behavioral responses to generalize across odorants.

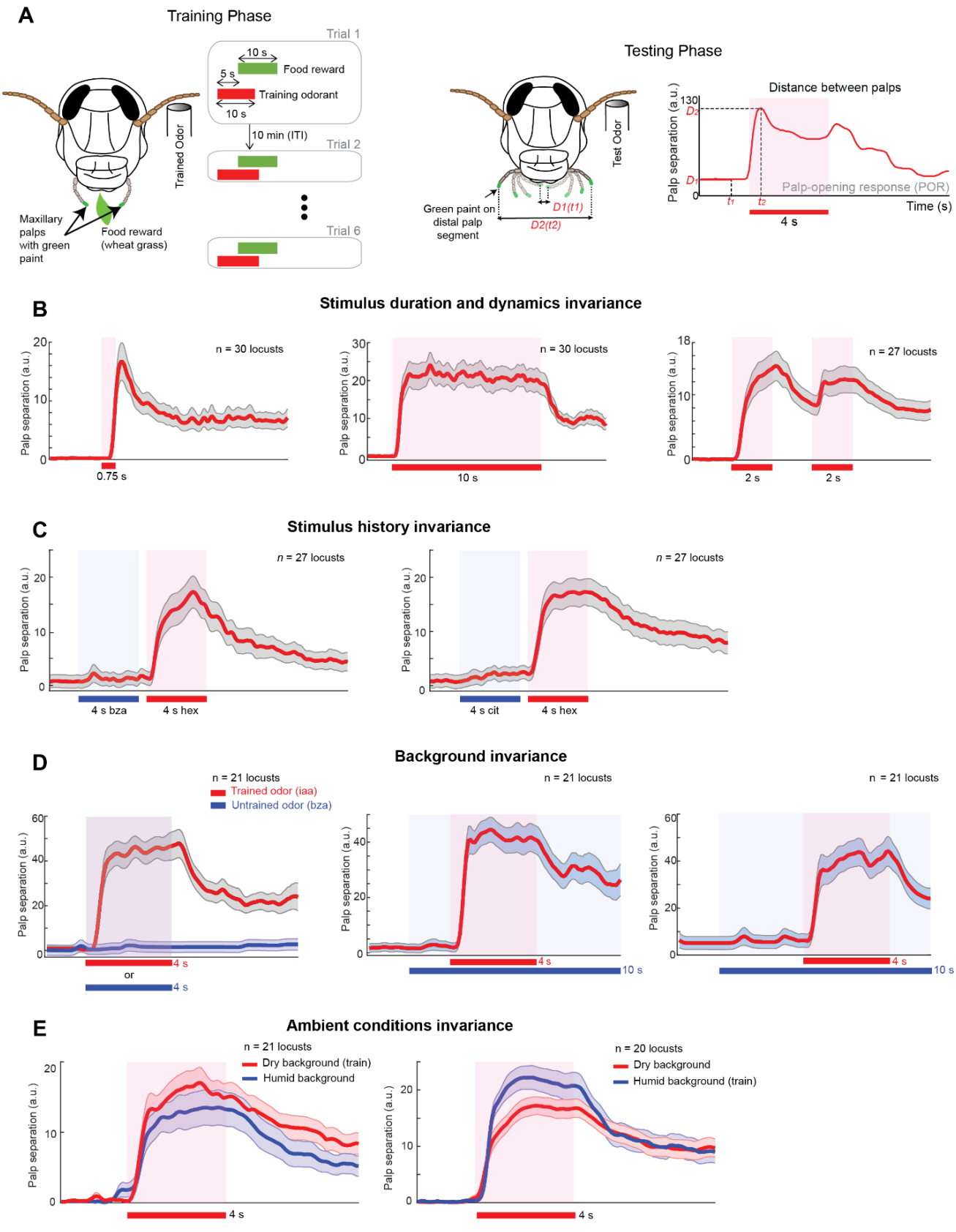
A
Training Phase
Trial 1
10 s
Food reward
5 s
Training odorant
10 s
10 min (ITI)
Trial 2
Trial 6
Trained Odor
Maxillary palps with green paint
Food reward (wheat grass)
Testing Phase
Test Odor
Green paint on distal palp segment
D1(t1)
D2(t2)
Distance between palps
Palp separation (a.u.)
130
D2
D1
0
t1
t2
Palp-opening response (POR)
Time (s)
4 s
B
Stimulus duration and dynamics invariance
n = 30 locusts
0.75 s
n = 30 locusts
10 s
n = 27 locusts
2 s
2 s
C
Stimulus history invariance
n = 27 locusts
4 s bza
4 s hex
n = 27 locusts
4 s cit
4 s hex
D
Background invariance
n = 21 locusts
Trained odor (iaa)
Untrained odor (bza)
4 s
or
4 s
n = 21 locusts
4 s
10 s
n = 21 locusts
4 s
10 s
E
Ambient conditions invariance
n = 21 locusts
Dry background (train)
Humid background
4 s
n = 20 locusts
Dry background
Humid background (train)
4 s

Figure 5.3: Invariant odor recognition in an appetitive conditioning assay.

(a) Schematic showing the training and testing protocols followed for the palp-opening response assays. Briefly, starved locusts were presented six trials of the training odorant (conditioned stimulus) followed by a food reward (unconditioned stimulus). The odorant pulse was 10 s in duration and the food reward was presented 5 s following the onset of the conditioning stimulus. Locusts that accepted food rewards in 4/6 training trials were regarded as successfully 'trained locusts,' and their palp-opening responses (PORs) were evaluated in an unrewarded testing phase. Selective opening of their maxillary palps (sensory appendage close to the mouth) upon onset of the conditioning stimulus was regarded as successful recognition of the training odorant. The PORs were quantified by painting and tracking the distal ends of the palps (see **Methods**). A sample POR trajectory is shown on the right where the training odor presentation (color bar) led to increased palp separation, indicating a palp-opening response.

(b) Locusts were trained using hexanol as a conditioning stimulus and were tested using hexanol pulses that varied in their duration. The mean palp opening responses (± s.e.m.) of all trained locusts are shown for test pulses of 0.75 s (n = 30 locusts), and 10 s (n = 30 locusts) durations, and a sequence of two pulses that was 2 s ON–2 s gap–2 s ON (n = 27 locusts). The color bar indicates when the odor was presented.

(c) Locusts were trained using hexanol as the conditioning stimulus and tested by presenting hexanol pulses in a non-overlapping sequence following the termination of a distractor odorant (i.e., introducing variations in stimulus history). Trained locusts first encountered a distractor odor pulse for 4 s, followed by a 0.5 s gap, which was then followed by a 4 s pulse of hexanol during the testing phase. The mean responses (± s.e.m.) of locusts (n = 27) tested with hexanol presentations following two distractor odors (bza and cit) are shown. The color bars indicate when odors were presented. Blue bars indicate the time periods when the distractor was presented, and the red bars indicate the duration of exposure to the trained odorant.

(d) Locusts were trained using iaa as a conditioned stimulus and tested by presenting iaa atop a background odorant (bza). Left panel, the mean palp opening responses to solitary presentations of iaa and bza are shown. Note that only the conditioned stimulus evokes POR responses, whereas the bza introductions did not elicit any detectable POR responses. Middle and Right panels, PORs (mean ± s.e.m; n = 21 locusts) are shown during presentations of iaa that was introduced 2 s and 4 s after the onset of a sustained bza pulse (i.e., the background odorant). The color bars indicate when odors were presented and how they overlapped.

(e) Left: Locusts trained with hexanol in a dry background (0% RH) were tested for hexanol responses in dry (red) and humid (100% RH, blue) conditions (see **Methods**). The mean PORs of trained locusts (n = 21) are shown. The color bar at the bottom indicates when the odor was presented. The shaded regions indicate the s.e.m. **Right:** Similar plots as the left panel, but for locusts trained for hexanol in humid (100% RH) conditions are shown (n = 20 locusts).

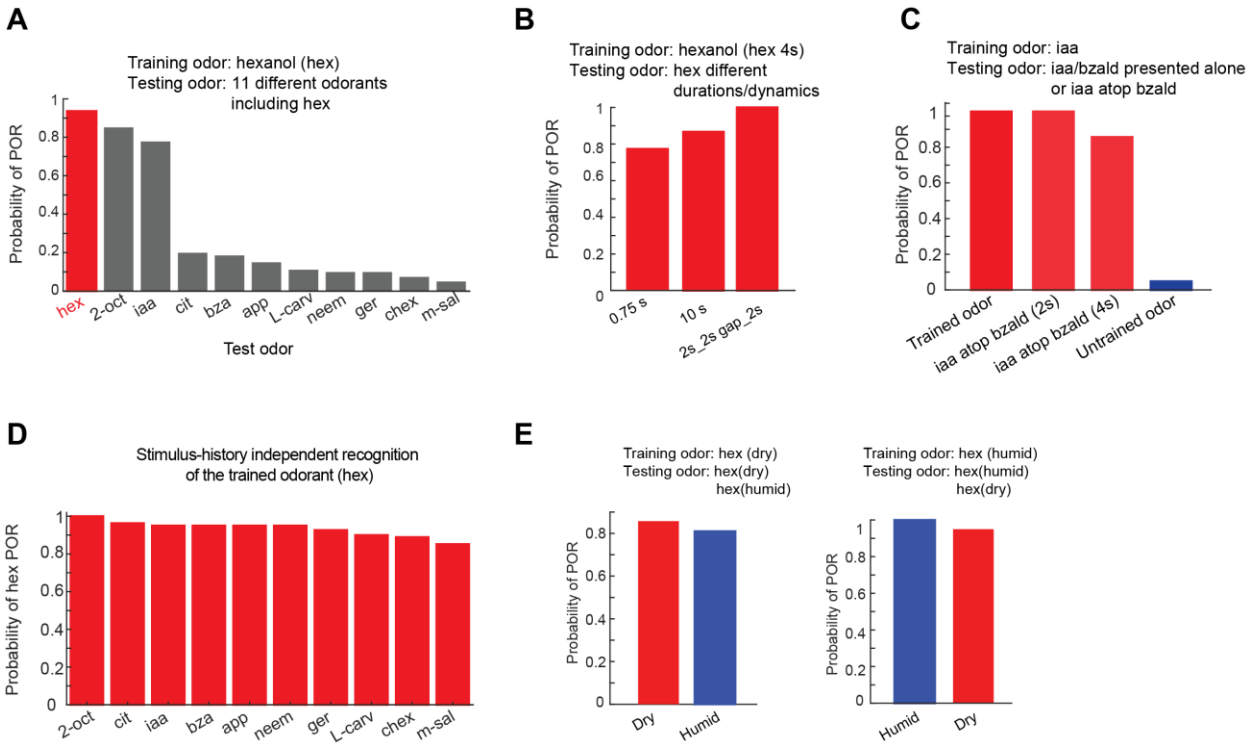

Figure 5.4: Summary of odor recognition performance in the behavioral assay.
(a) The probability of PORs for locusts trained using hexanol (hex) as conditioning stimulus is shown as a bar plot. PORs to the trained odorant (shown in red) and to a diverse odor panel (non-trained odors shown in gray) are shown to allow comparison (see **Methods**). A higher probability indicates a larger proportion of trained locusts performed significant PORs during the testing phase when presented with that corresponding odorant (identified along x axis). As can be seen, locusts had the highest POR probability to the trained odorant. Interestingly, locusts trained with hexanol also had significant PORs to 2-octanol (2-oct) and isoamyl acetate (iaa). Other odorants: citral (cit), benzaldehyde (bza), apple (app), L-carvone (L-carv), neem, geraniol (ger), cyclohexanone (chex), and methyl salicylate (m-sal) did not evoke strong PORs in hex-trained locusts. These results were obtained by combining two datasets to yield n = 47 locusts for hex, n = 27 locusts tested with random presentations of hex, 2-oct, iaa, cit, bza, app, and n = 20 locusts tested with random presentations of hex, L-carv, neem, ger, chex, m-sal.
(b) POR response probability for locusts trained and tested with the same conditioning stimulus (hexanol) but presented for different durations (0.75 s or 10 s), or in a pulsatile fashion (2s ON – 2s gap – 2s ON). Refer **Figure 1B** for representative POR traces**.** As can be noted, locusts have a high probability of response for all test pulses indicating robust recognition invariant of the stimulus duration or dynamics.
(c) POR response probability following iaa introductions either solitarily or atop a background odorant (bza). Note that iaa was presented with two different latencies (2s and 4s) following the onset of the sustained bza pulse. Representative POR traces for this stimulation protocol are shown in **Figure 1D**. Iaa-trained locusts showed a very low probability of response to the untrained distractor odor (bza). All introductions of iaa, either solitarily or atop bza background, evoked

strong POR responses with a high probability of response across locusts. These results indicate that locusts could recognize a trained odorant in a background-invariant fashion.
(d) POR probabilities during hex introductions following ten different non-overlapping distractor pulses are shown. Hexanol was used as the conditioning odorant. Representative PORs are shown in **Figure 1C**. As mentioned earlier, n = 27 locusts were tested with 2-oct, cit, iaa, bza, app as distractor stimuli, and a different set (n = 20 locusts) were tested neem, ger, L-carv, chex, m-sal as distractors. Distractor odorants, the first pulse used in the sequence, are identified along the x-axis. These results indicate that hex-trained locusts have a high probability of response to the trained odor irrespective of which distractor odorant was encountered prior to their onset (i.e., invariance with respect to stimulus history).
(e) The POR probability for locusts trained with hexanol in a dry background (left) and for locusts trained with hexanol in a humid background (right) are shown. As can be seen, for both training paradigms, locusts have a high probability of response to hex under both dry and humid testing conditions. The results indicate that a trained stimulus could be recognized independent of changes in ambient humidity conditions. The difference in POR responses, though they appear to be slightly stronger in training conditions, are not statistically significant ($p = 0.405$ for dry training, $p = 0.054$ for humid training; t-test).

5.2.3 Stimulus dynamics, history and competing cues induce variations in PN responses

How were odor-evoked responses of individual projection neurons (PNs) in the locust antennal lobe perturbed? To understand this, we designed a stimulation protocol that presented two 'target odorants', hexanol (hex) and isoamyl acetate (iaa), in a pulsatile fashion (**Figure 5.5a, b**). Note that the two target odorants (hex and iaa) were also used as CST in the behavioral experiments. These target odor introductions were of different durations with varying inter-stimulus intervals, or presented atop a background cue (benzaldehyde; bzald), or following a distractor odorant (citral; cit).

We recorded responses of eighty-nine PNs in the locust antennal lobe ($n = 25$ locusts). First, we examined the ability of individual PNs to robustly encode the identity of two 'target' odorants. In general, we found that most individual PNs had robust and reliable responses during certain exposures of the target odorant but not all. In the entire ensemble of PNs that was recorded (n = 89 in total), we found that four PNs had a detectable response to all encounters of the target

odorants (**Figure 5.5a, b**; PN6). Since these 'reliable' PNs were activated by both the target odorants (hex and iaa), and their response intensity and spiking patterns varied considerably across pulses (**Figure 5.5c**), we note that these PNs individually did not provide discrimination between these two odorants.

To quantify the response variability observed at the level of individual PNs, we computed

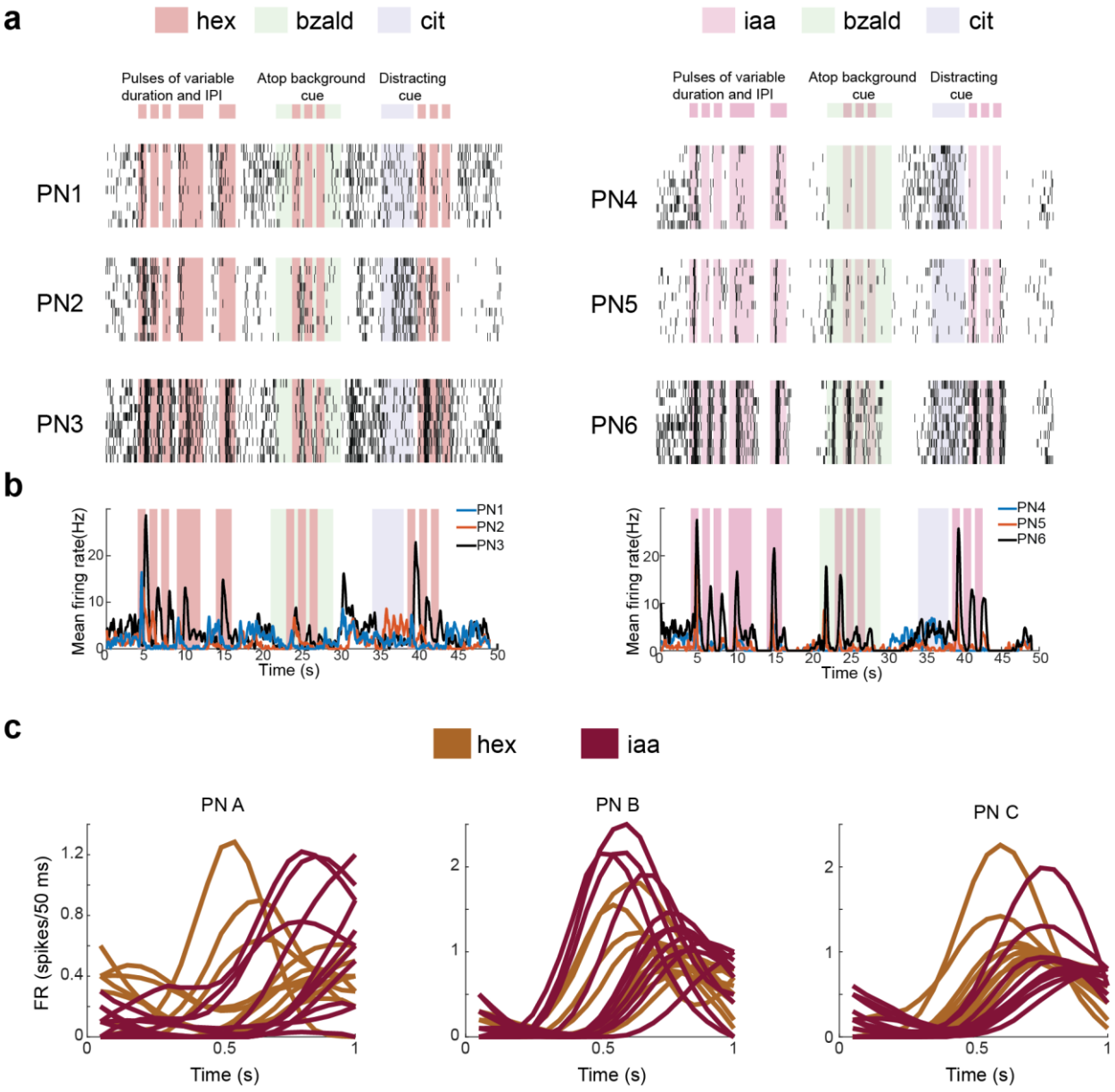

Figure 5.5: Individual projection neuron responses are highly variable.

(a) Left plots, raster plots showing PN responses (PN1 and PN2) during a pulsatile presentation of a target stimulus (hexanol; hex) in back-to-back sequences of variable duration and inter-pulse intervals, atop a background cue (benzaldehyde; bzald), following a distracting stimulus (citral; cit). Each black tick represents an action potential fired by the PN. PN responses are shown for 10 consecutive trials (10 rows). Right plots, similar plots as in the left, but the target stimulus was isoamyl acetate (iaa). Notice the responses evoked by the target odorant in these six PNs were highly variable.
(b) Firing rates of the two PNs (50 ms time bins; trial averaged) shown in panel **a** are now plotted as a function of time. While both the PNs responded strongly to the first pulse of the target odorant, the response diminished during later encounters of the same stimuli.
(c) Firing rates of three PNs that reliably responded across all the encounters of hex/iaa are plotted. Each panel shows trial-averaged first 1 s response to 11 encounters of hex (orange) or iaa (red). When compared across all the 11 encounters of the same stimulus, response features such as the peak firing rate, response latency, and firing rate changes over time all seem variable and did not vary consistently with odor identity.

correlations between the PN response to the first pulse of the target odorant and all the other introductions of the same chemical (**Figure 5.6a**;). A high correlation value would indicate that PN firing rate patterns remained consistent across different pulses. However, the computed distribution of the PN response correlations in our dataset revealed that spiking activities during different encounters of the target odorant had only a weak pattern match with the responses elicited during the very first encounter of an odorant (**Figure 5.6b, c**). Note that even for those PNs that had detectable responses across different pulses (PN6 in **Figure 5.5a**), the mean correlations were low as the spike patterns across the different target odor pulses were not consistent.

Furthermore, we computed the ratio of mean spike counts across the eleven pulses of the same odorant (and across the ten trials) with variance in spike counts (i.e., Fano factor; **Figure 5.6d, e**). A Fano-factor of one indicates Poisson variability. As can be noted, most PNs had a supra-Poisson variability. Taken together, these results suggest that individual projection neuron responses vary considerably and may not provide a reliable read-out of odor identity across diverse conditions.

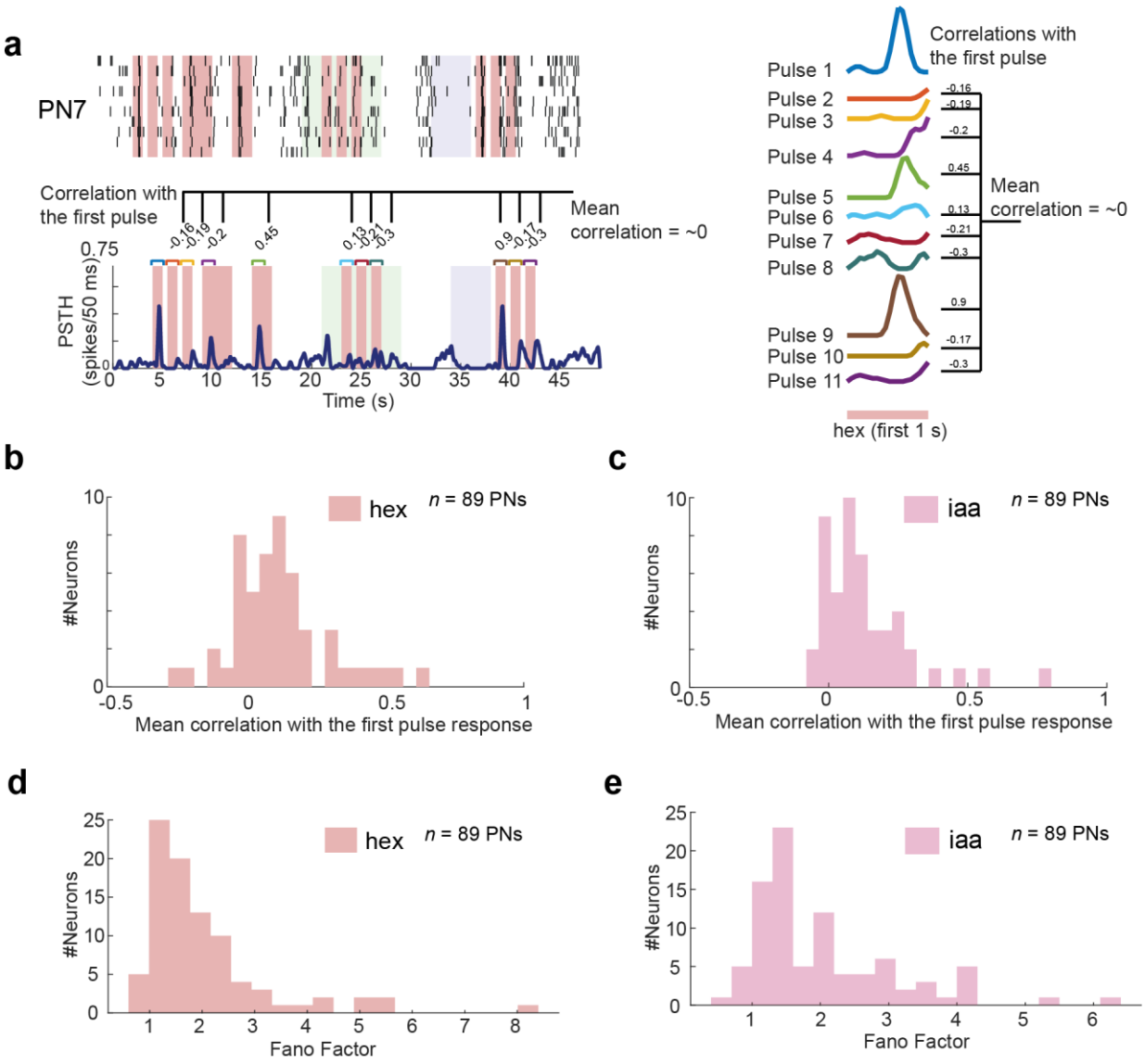

Figure 5.6: Projection neuron responses are highly variable under different encounters of stimuli.

(a) Left, Raster plot and PSTH of a PN are shown. Average spike rates across ten trials are plotted as a function of time. The color line shown on the top of each hex presentation indicates the first 1 s response that was used to compute correlations. Right, a schematic showing how the correlations were computed. Neural response to the first pulse was used as the response template to be pattern matched. Pairwise correlations with the first stimulus pulse were computed and averaged to obtain a mean correlation value for each PN. Note that a higher mean correlation value indicates a consistent response across all odor pulses.

(b, c) Similarities between PN responses evoked during the first pulse of hex (target odorant) with all other encounters were computed. For this quantification, PN response was first binned into 50 ms time bins and averaged across 10 trials. The first 1 s response following the onset of each target odorant pulse was used to compare response similarity between different target odor encounters

(i.e., 20-dimensional response vectors). For each PN, the mean similarity across odor pulses was determined, and the response similarity across PNs was then plotted as a distribution. **(c)** Similar distribution as plotted in **panel b** but for iaa.
(d, e) Distributions of the Fano factor are shown across 89 PNs for *hex* and *iaa*. **Panel d**, distributions are shown for *hex* pulses. Mean of the first 1 s neural response across 11 presentations of *hex* and 10 repeated trials was used to compute Fano factor (σ^2/μ) for each PN. **Panel e**, the similar plot as in left but Fano factors were computed for *iaa* trials.

5.2.4 Variations due to changes in ambient conditions

Next, we examined whether changes in humidity conditions would further exacerbate the problem of robustly encoding odorant identity. For this purpose, we used the same stimulus delivery protocol but using either dry air (0% relative humidity (RH)) or humid air (100% RH) as the carrier stream. We found that again most PNs in our dataset had responses that were variable in both dry and humid conditions (**Figure 5.7a, b**). The overall distribution of response correlation between the first pulse and the subsequent encounters of the same odorant was low but comparable between dry and humid conditions (**Figure 5.7c**).

Next, we sought to examine whether the ensemble neural responses across all PNs could reliably represent information about the identity of the target stimulus. To understand this, we visualized data after a principal component analysis dimensionality reduction. Briefly, spikes were binned in non-overlapping 50 ms time bins, and the average spike counts (across ten trials) of all eighty-nine neurons became a high-dimensional snapshot of odor-evoked neural response in a particular time bin. The high dimensional vectors were projected onto the three eigenvectors of the data covariance matrix (corresponding to the largest eigenvalues) for the purpose of visualization. The three-dimensional representations of the ensemble PN activity were color-coded to differentiate among the eleven target odor pulses (**Figure 5.7d; left panel**). As can be noted, the ensemble responses were variable and did not form a single well-defined cluster (i.e., not a unimodal distribution). More importantly, the PN response vectors in dry and humid conditions

clearly formed distinct response clusters (**Figure 5.7d**; **right panel**), indicating that changes in humidity might also pose an additional challenge for achieving invariant odor recognition.

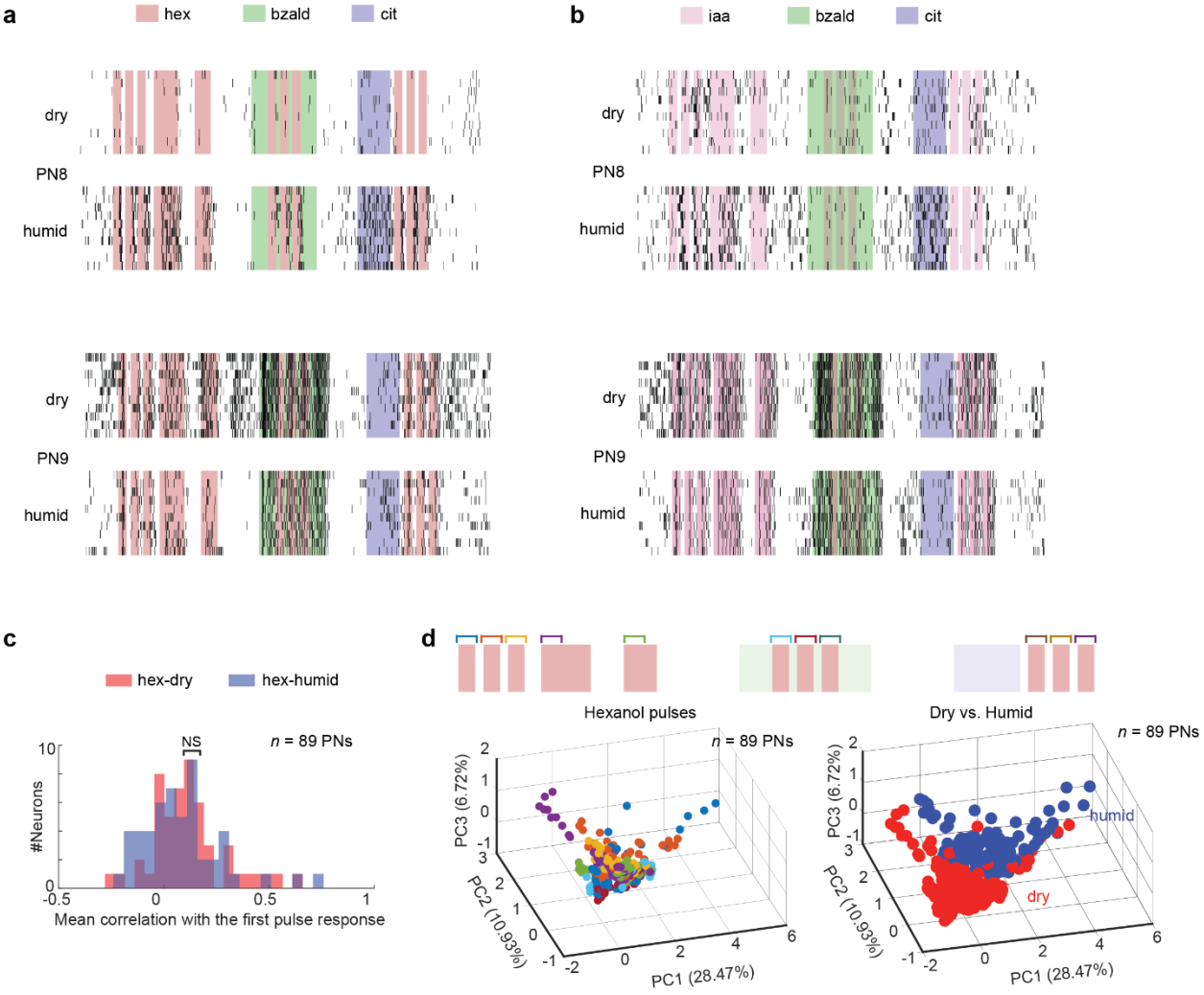

Figure 5.7: Changing humidity conditions alters both individual and ensemble level PN activity.
(a) Similar raster plot showing PN responses to the stimulation protocol used in Figure 1. For each PN shown, the top and bottom plots reveal the spiking activity of the same PN between dry (carrier stream – 0% RH) and humid (carrier stream – 100% RH) conditions are shown. Note that changes in humidity levels of the carrier stream resulted in an increase or decrease in spiking activity in individual PNs. **(b)** Similar plots as in panel **a** but showing PN responses to a different target stimulus (iaa). Note that the same set of PNs is shown. **(c)** Similar plot as in **Figure 5.6b** but comparing response similarity between PN responses observed in dry and humid conditions. 'NS'

indicates that the two distributions are not significantly different (Two-sample Kolmogorov-Smirnov test; $p = 0.05$). **(d)** Left, spiking activities of all 89 PNs during different pulses of the target odorant are shown after PCA dimensionality reduction. Spikes in individual PNs were binned in 50 ms non overlapping windows and treated as vector components. Each colored sphere represents an 89-dimensional PN spike count vector along with the first three principal components. Different time segments are indicated by different color codes. The right panel shows a similar plot but comparing odor-evoked responses in dry and humid conditions. Red and blue colored spheres are used to indicate the differences observed in the ensemble PN spiking activity in dry and humid conditions, respectively.

5.2.5 A decoding scheme for robust odor recognition

Our results indicate that the behavioral recognition (i.e., the POR) remained invariant with respect to stimulus dynamics, history, the presence of competing cues, and changes in ambient conditions (**Figure 5.4**; also refer to prior results on background[67] and history invariance[80]). However, odor-evoked neural responses at single-cell and ensemble-level vary with most of these perturbations (**Figure 5.5, 5.6 and 5.7**). Given this discrepancy between variability in neural encoding and robustness in behavioral output, we sought to determine whether a neural decoder could be designed for achieving robust odor recognition.

To investigate this issue, we again regarded the ensemble activity across the 89 PNs recorded in a 50 ms time bin as a high-dimensional neural activity (i.e., 89-dimensional firing rate vector). To detect the presence of the target odorant and selectively recognize the identity of the target odorant, we trained a linear support vector machine classifier (SVM). Note that the SVM classifier was trained using a separate set of training trials where only a solitary four-second pulse of the target odorant was presented. Two different classifiers, one for recognizing hexanol (hex-SVM; **Figure 5.8**) and another for recognizing isoamyl acetate (iaa-SVM; **Figure 5.9**) were trained. The probability that hexanol is present in any particular 50 ms time segment, as predicted using the hex-SVM, is plotted as a function of time (**Figure 5.8a-c;** similar plots for iaa-SVM

shown in **Figure 5.9a-c**). As can be noted, all introductions of the target odorant are detected and selectively recognized by both hex-SVM and iaa-SVM classifiers.

How did the linear classification approach manage to robustly recognize the target odorant from highly variable neural responses? To understand this, we examined what weights were assigned to different PNs in the dataset (**Figure 5.8d, Figure 5.9d**). We sorted the PNs based on the weights they were assigned by the SVM classifier, and plotted their average spike counts to the solitary target odor pulse (i.e., training data that was used). Note that PNs with strong ON responses are at the top and PNs with stronger OFF responses are at the bottom. The weights assigned to each PN by the hex-SVM classifier are shown next to the firing rate plots to allow comparison. Our results indicate that ON responsive PNs received mostly positive weights and the OFF responsive PNs were assigned negative weights (**Figure 5.8d, e**). A similar weighting scheme was also used by the iaa-SVM classifier (**Figure 5.9d, e**). This result suggests that although individual and population neuron responses vary, both detection and recognition of the odor identity can still be achieved using a linear coding scheme and the weight assignment to individual neurons had a simple structure, i.e., positive weights to ON neurons and negative weights to OFF neurons.

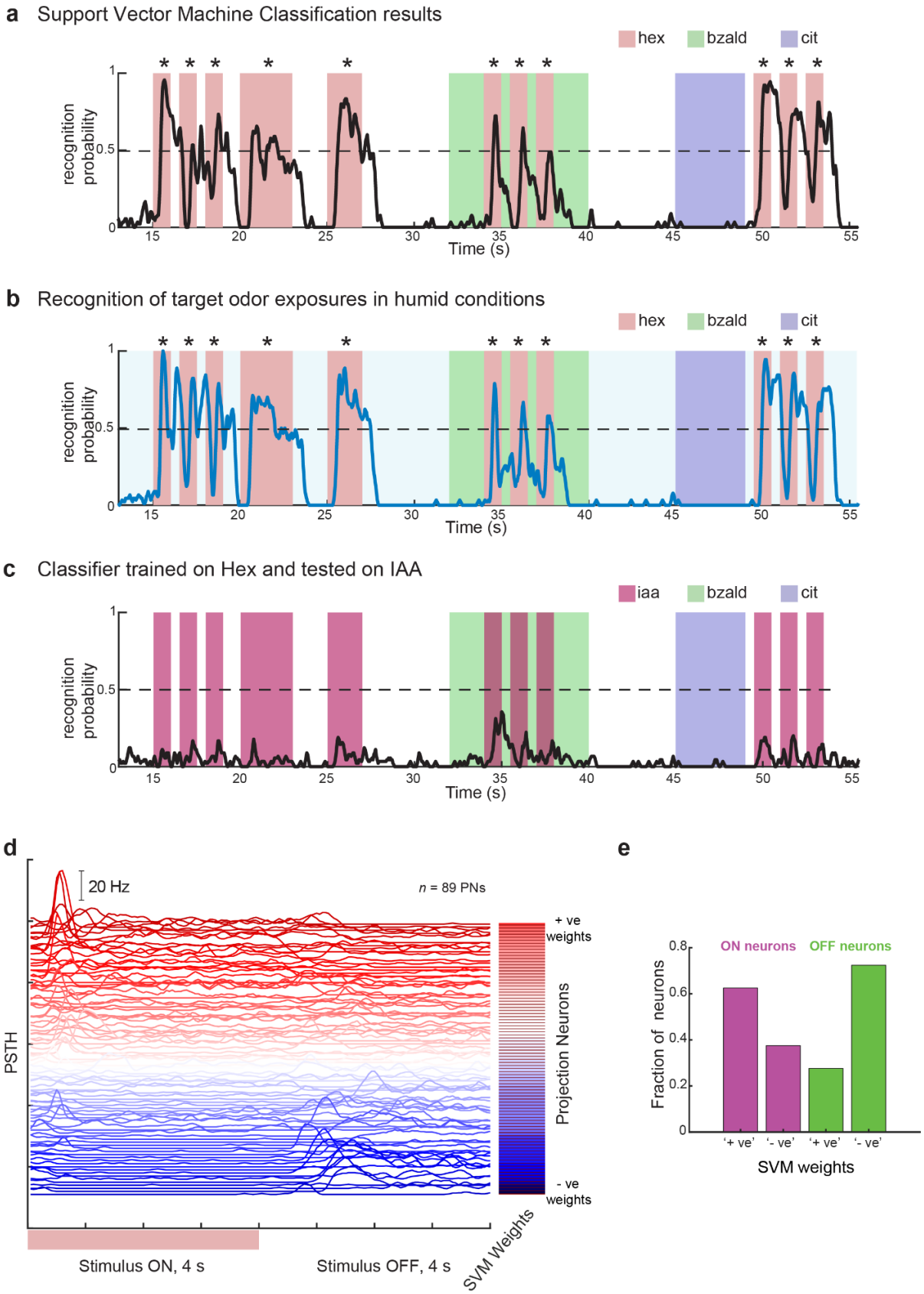
a
Support Vector Machine Classification results
hex
bzald
cit
recognition probability
Time (s)
b
Recognition of target odor exposures in humid conditions
hex
bzald
cit
recognition probability
Time (s)
c
Classifier trained on Hex and tested on IAA
iaa
bzald
cit
recognition probability
Time (s)
d
20 Hz
n = 89 PNs
PSTH
+ ve weights
Projection Neurons
- ve weights
Stimulus ON, 4 s
Stimulus OFF, 4 s
SVM Weights
e
ON neurons
OFF neurons
Fraction of neurons
'+ ve'
'- ve'
'+ ve'
'- ve'
SVM weights

Figure 5.8: Support Vector Machine classification for robust hexanol recognition.
(a) Classification probabilities for the target stimulus, hexanol (hex), under different conditions using a support vector machine (SVM) classifier are shown. The classifier was trained using ten trials where only a solitary pulse of hexanol was presented. For each time bin, the probability was obtained by averaging classification results across ten trials. Time segments when a stimulus was presented, and the identity of the stimulus that was presented are indicated using colored bars. The dotted line indicates the classification probability of 0.5 (an arbitrary threshold) that was used to detect the presence of hexanol. The segments when the trial-averaged classification probability exceeded this threshold are indicated using an asterisk.
(b) Performance of the hexanol classifier but tested during those trials in the humid condition. Note that humidity did not perturb target order classification.
(c) Performance of the hexanol classifier but tested during those trials when isoamyl acetate (iaa) was used as the target odorant. Note that none of the iaa presentations were classified as the target stimulus being present.
(d) The PSTHs of each PN during 4 s solitary hex presentation and 4 s after stimulus termination are shown. Each trace shows PSTH of one PN. The PSTHs are sorted and color-coded based on the hex SVM classifier weights assigned to each PN. The neurons that were assigned the most positive weights are at the top and the most negatively weighted neurons are near the bottom. SVM classifier weights that were assigned to each PN are also schematically shown as a heatmap to the right.
(e) The fraction of ON and OFF neurons that received a '+ve' or '-ve' weights are shown as a bar plot for comparison.

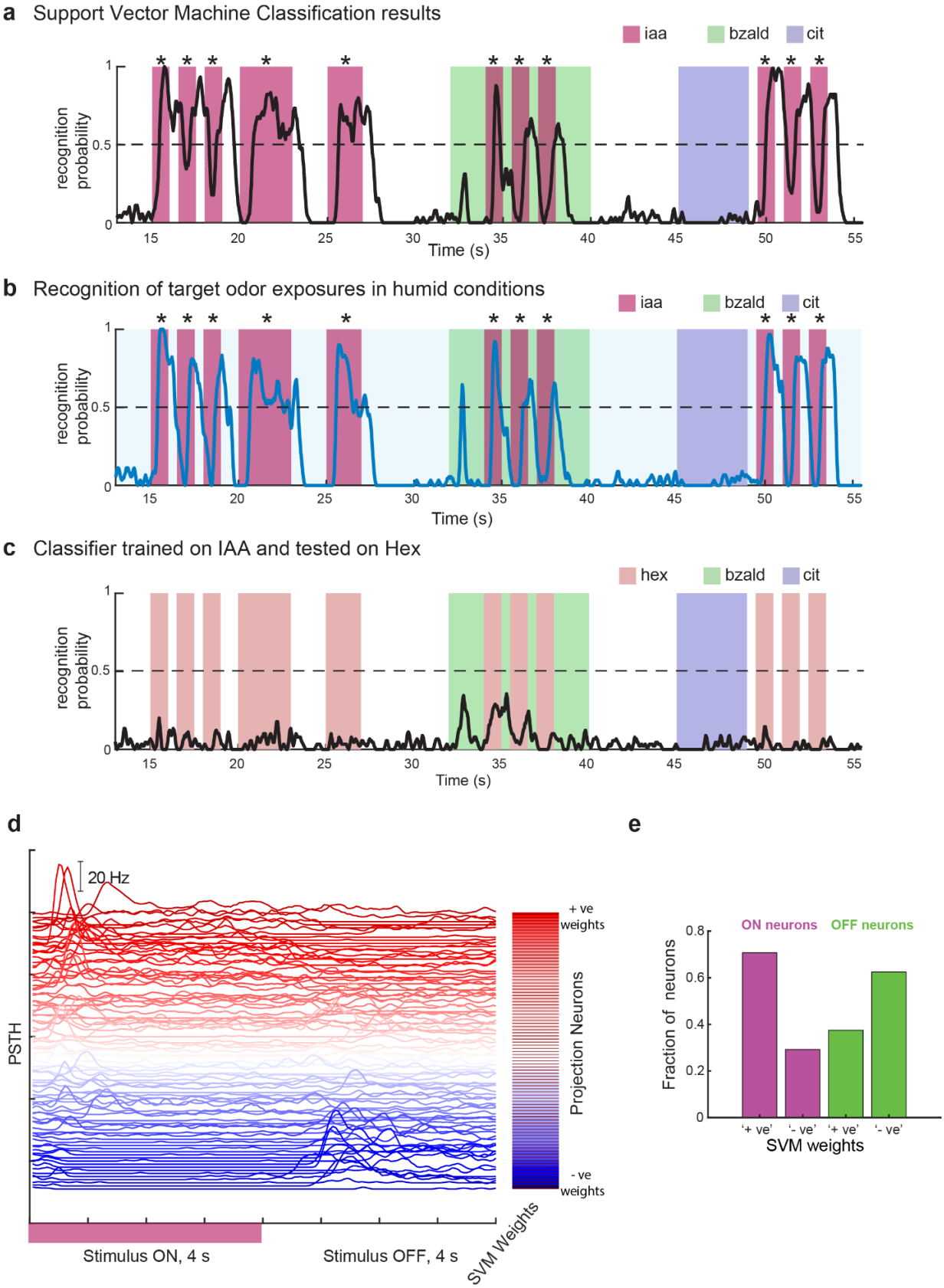
a Support Vector Machine Classification results
iaa
bzald
cit
recognition probability
Time (s)
b Recognition of target odor exposures in humid conditions
iaa
bzald
cit
recognition probability
Time (s)
c Classifier trained on IAA and tested on Hex
hex
bzald
cit
recognition probability
Time (s)
d
20 Hz
PSTH
+ ve weights
Projection Neurons
- ve weights
Stimulus ON, 4 s
Stimulus OFF, 4 s
SVM Weights
e
ON neurons
OFF neurons
Fraction of neurons
'+ ve'
'- ve'
'+ ve'
'- ve'
SVM weights

Figure 5.9: SVM classification for robust isoamyl acetate recognition.
A similar set of plots as in **Figure 5.6** shows the results for an SVM classifier trained to recognize isoamyl acetate (iaa). Note that all iaa introductions were correctly detected and recognized. Like the hex-SVM classifier, most ON neurons received '+ve' weights and most OFF neurons were assigned '-ve' weights.

5.2.6 Discrete classifier with ternary weights allows robust recognition

Finally, we wondered how stable this classification approach was. The variations we examined here are but only a few of the many intrinsic or extrinsic perturbations feasible. Therefore, we particularly wondered how important the analog weights assigned to each neuron were. The PNs that had the strongest ON and OFF responses to solitary pulses of the target odorant might not necessarily have similarly intense responses during other encounters of the same stimulus. However, the set of PNs that get excited or inhibited can be expected to be maintained across different encounters of the same odorant. Therefore, we wondered if the classification approach could be simplified by replacing the analog weights assigned to each neuron with a simpler scheme.

The first simplification we examined was converting the analog SVM weights into just three values: {-1, 0, +1}. This discretization was done by comparing the analog SVM weights with two arbitrarily chosen thresholds. We found that this simpler approach was still able to allow robust detection as well as discrimination of both the target odorants (**Figure 5.10a and Figure 5.11a**).

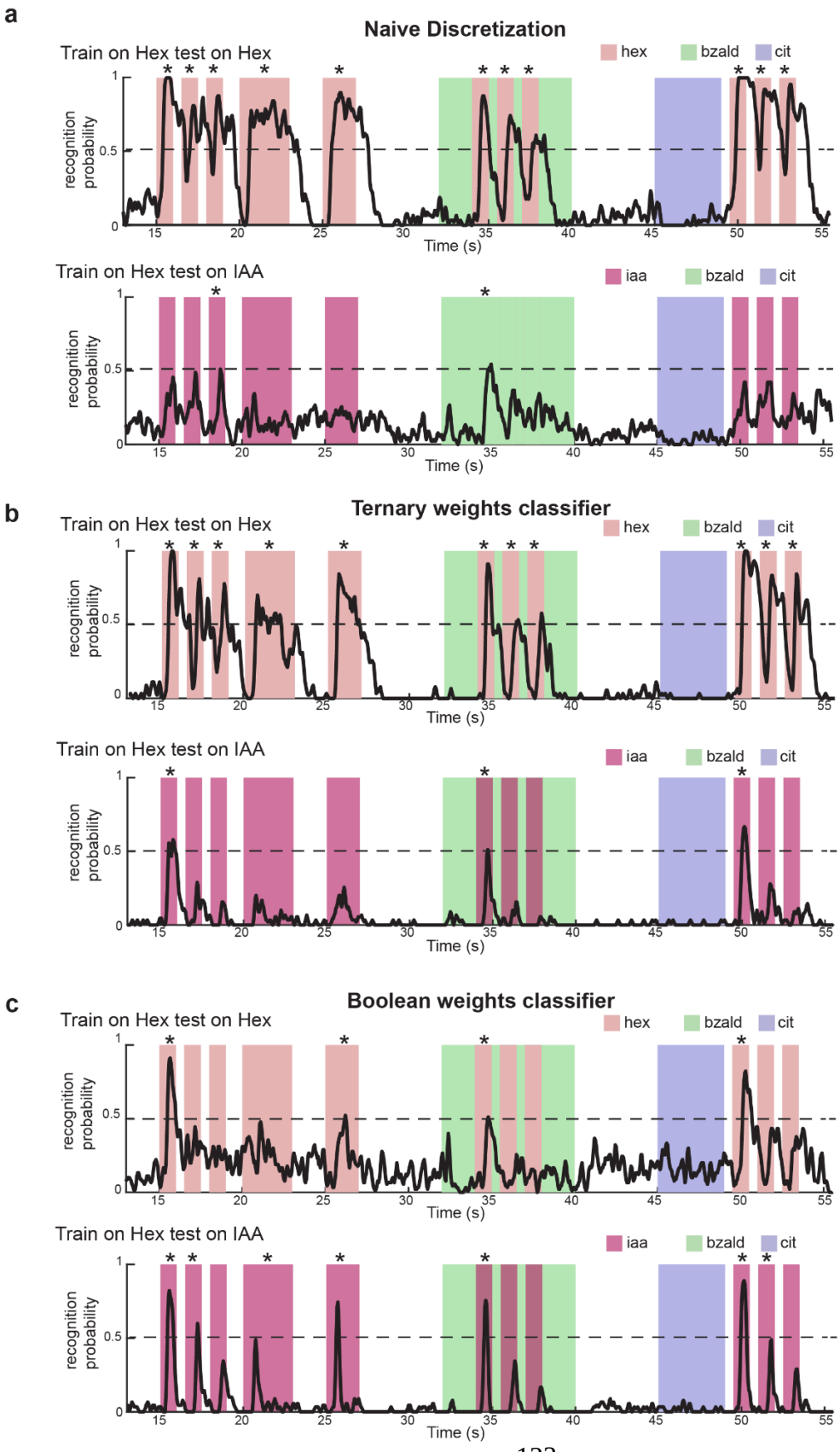
a
Naive Discretization
Train on Hex test on Hex
hex
bzald
cit
recognition probability
Time (s)
Train on Hex test on IAA
iaa
bzald
cit
recognition probability
Time (s)
b
Ternary weights classifier
Train on Hex test on Hex
hex
bzald
cit
recognition probability
Time (s)
Train on Hex test on IAA
iaa
bzald
cit
recognition probability
Time (s)
c
Boolean weights classifier
Train on Hex test on Hex
hex
bzald
cit
recognition probability
Time (s)
Train on Hex test on IAA
iaa
bzald
cit
recognition probability
Time (s)

Figure 5.10: Performance comparison between discrete SVM vs. ternary vs. Boolean classifiers.
(a) Classification probabilities for an SVM classifier that used discrete set of weights: {-1, 0, 1} are shown. The ternary weights were obtained from the SVM classifier by discretizing SVM weights using two preset thresholds. Other conventions are the same as Figures 3 and 4 (bottom row). Performance of the Hex-SVM classifier with discrete weights on recognizing isoamyl acetate introductions.
(b) Similar plots as earlier but showing performance of a Bayesian logistic regression approach where each neuron was directly assigned a ternary weight ('-1' or '0' or '1'; see **Methods** for details). Ten trials of solitary exposures to hexanol were used to train the classifier.
(c) Similar plots as earlier but showing performance of a Bayesian logistic regression approach where each neuron was directly assigned a Boolean weight {'1' or '0'}. Ten trials of solitary exposures to hexanol were used to train the classifier.

Since the thresholding of analog SVM weights might not provide an optimal approach to derive a ternary classifier, we sought to directly determine the optimal ternary weights (see **Methods**). We found that the ternary weights learned using this constrained approach also provided robust recognition of the target odorants (**Figure 5.10b** and **Figure 5.11b**). Further simplification of this approach by just using Boolean weights {1 or 0}, allowed detection of the target odorant, but discrimination between the two target odorants was compromised **(Figure 5.10c** and **Figure 5.11a)**. Furthermore, as a control, random assignment of ternary weights to individual PNs failed to provide decent recognition performance (**Figure 5.12**). A comparison of the weights assigned by the different classifiers is shown in **Figure 5.13**. These results indicate that the ternary classifier provides a sort of lower bound on the recognition performance that could be achieved. In other words, it strikes a fine balance between decoding scheme complexity and recognition performance.

In sum, our results indicate that a very simple classification scheme using just ternary weights could provide robust odor recognition.

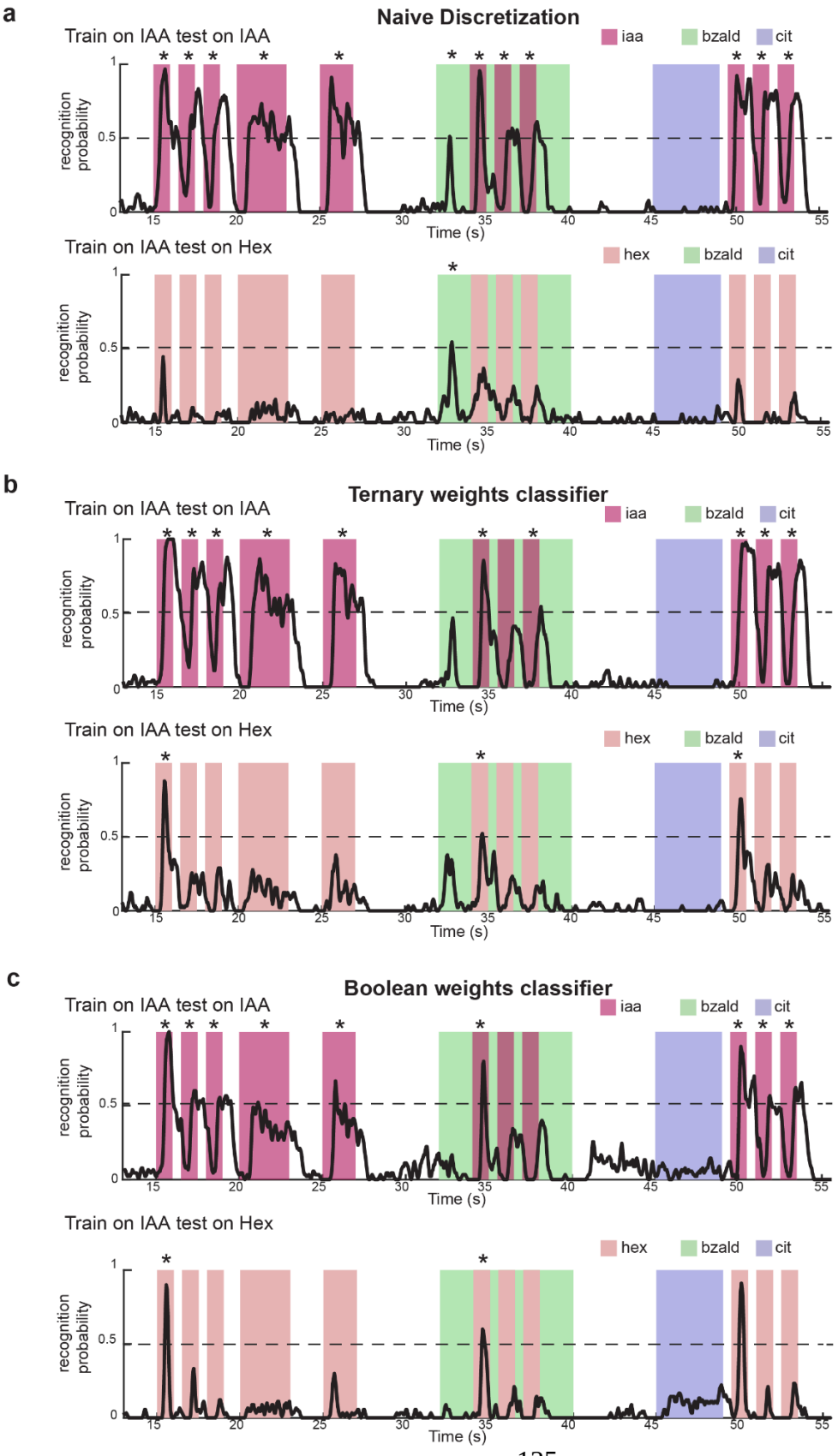
a
Naive Discretization
Train on IAA test on IAA
iaa
bzald
cit
recognition probability
Time (s)
Train on IAA test on Hex
hex
bzald
cit
b
Ternary weights classifier
c
Boolean weights classifier

Figure 5.11: Performance comparison for isoamyl acetate recognition.
Similar results as in **Figure 5.8** but showing performance of discrete weights classifiers that were trained to recognize isoamyl acetate. All color conventions are the same as in **Figure 5.8**.

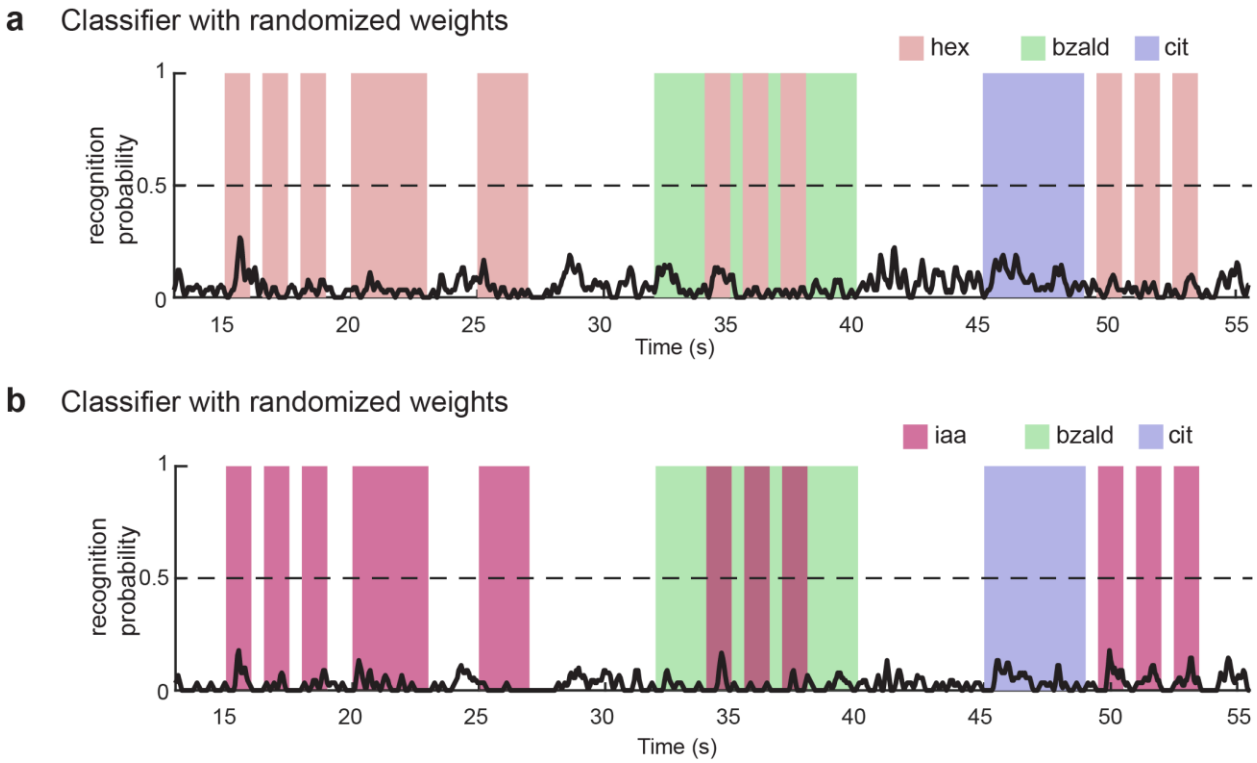

Figure 5.12: Performance of a classifier with randomized weight assignment.
(a, b) A classifier with randomized ternary weights was used to test the presence of the target odor (panel **a**, Hex; panel **b**, Iaa). Note that none of the target odor introductions were picked up by the classifier with randomized weights.

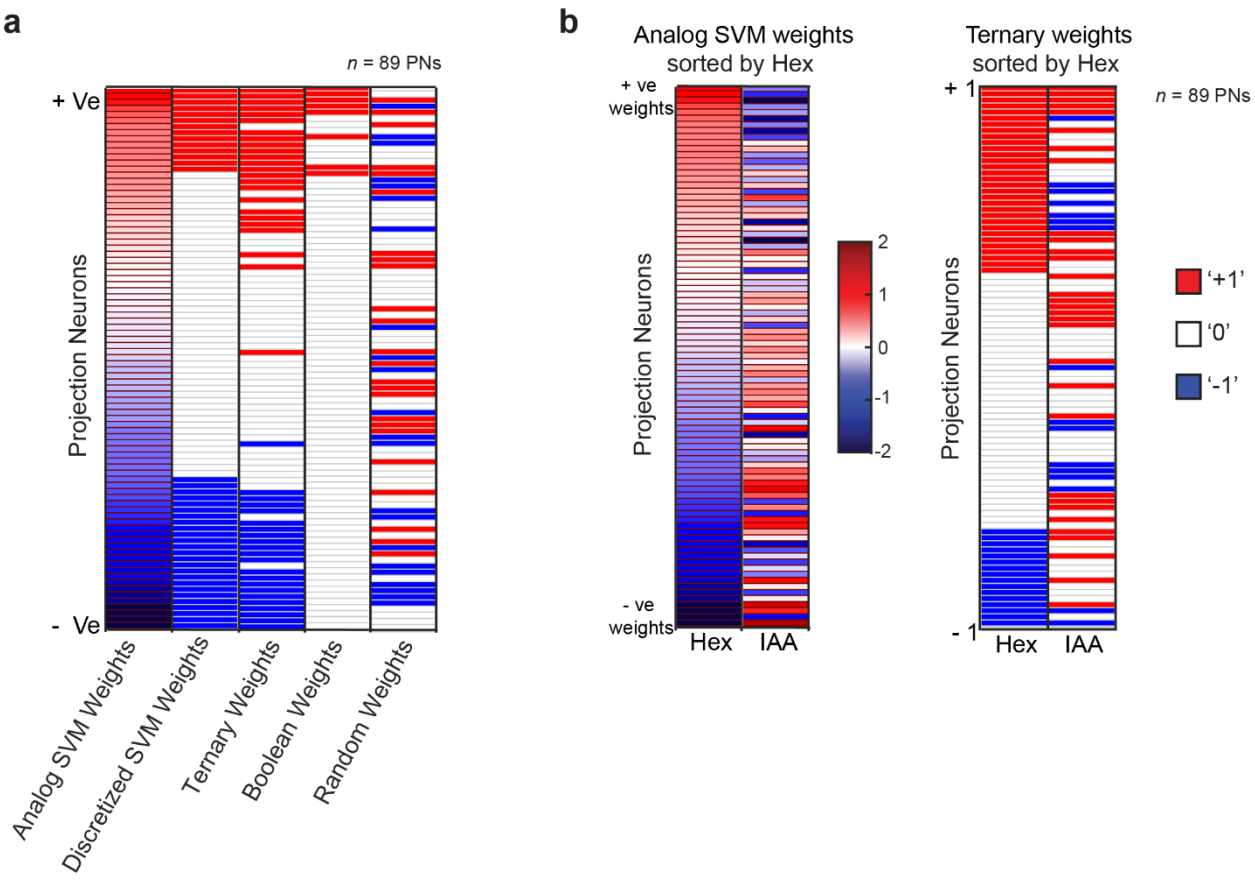

Figure 5.13: Weights assigned to each PN in different classification schemes are shown. **(a)** The neurons are sorted such that the most positive weights are at the top and the most negatively weighted neurons are near the bottom. The first column shows analog SVM weights learned. The ternary weights after discretization that were assigned to each PN are shown in the second column: red indicates a weight of '+1', white indicates a weight of '0,' and blue indicates a weight of '-1'. The third column shows the ternary weights learned using the Bayesian framework as a heatmap. The fourth column shows the Boolean weights learned and the last column shows random weights generated. All columns use the same index as column one. **(b)** The weight vector learned by the analog SVM trained with hexanol exposures (i.e., hex-SVM) and its ternarized version are shown along with analog and ternary weights learned by the SVM classifier trained with iaa exposures (i.e., iaa-SVM). Note that each weight vector has the same number of components as the number of neurons in the dataset. The weights are sorted based on the values assigned by the analog Hex-SVM classifier.

5.2.7 A generic binary neural network inspired by the insect olfactory system

We wondered whether the simple approach for achieving invariance in the locust olfactory system could be extended to create a general-purpose pattern recognition neural network. Note

that the goal is to develop an artificial neural network (ANN) that has a similar architecture to the insect olfactory system and uses binary values ({-1 and 1} or {0 and 1}) as learned parameters/weights for connections between individual nodes (**Figure 5.14A**). Most ANNs use real-valued parameters that are unconstrained and routinely learned through a back-propagation algorithm. However, with a Boolean or ternary weights constraint, backpropagation with regular gradient descent would not be feasible. To overcome this issue, we reformulated this problem as one of fitting a Bayesian model and choosing a Boolean distribution as a prior distribution for ANN weights. As direct inference of weights using the posterior distribution would be intractable, we used a variational inference approach to approximate the posterior with a lower bound. An unbiased estimator of the derivative of the lower bound can be found by relaxing and reparametrizing the weights using Gumbel-Softmax variables (**Figure 2.2; see Methods**).

An advantage of this Bayesian neural network architecture is that it can be simply scaled to multiple layers in a neural network. Additionally, we can train the neural network with different layers that take different combinations of weights (for example, binary or ternary), but are still limited to a set of discrete weights. This is particularly advantageous when the desired outcome can be obtained from an interpretable neural network model.

To examine how well a neural network with only binary weights can perform, we trained a fully connected neural network with one hidden layer on the MNIST dataset (**Figure 5.14**). We constrained the first layer with weights {1, -1} and the second layer with weights {1, 0}. After training to classify the ten digits, we found that the loss function had converged within a similar window of iterations compared to a regular neural network with real-valued weights (**Figure 5.14a**). Next, we wondered how this simple neural network compares with state-of-the-art deep neural networks when it comes to image classification. The performance of the trained binary

weights neural network on a held-out dataset revealed an error rate of 2.68%, only modestly poorer than the benchmark performance of 1.8% for an ANN with similar architecture but with real-valued weights [185]. This result indicates that constraining the weights in a layer of neural network with just two values only results in a minimal drop in performance.

As mentioned earlier, the binary-valued ANN allowed us to understand what features were extracted and how they were used to improve classification performance. We found that the hidden-layer neurons performed two types of feature extraction (**Figure 5.14c**): a subset that weighted 'ON pixels' for a digit with a weight of '1' and 'OFF pixels' with a weight of '-1,' and another subset that weighted the pixels in the opposite fashion (i.e., '-1' for ON pixels and '1' for OFF pixels). It is worth noting that this approach is strikingly similar to the one we used for robust recognition of the odorant in this study. In sum, these results indicate that a binary neural network, inspired based on results from the insect olfactory system, performed relatively well as a general-purpose pattern recognition algorithm.

5.3 DISCUSSION

We examined how invariant recognition of odorants can be achieved in a relatively simple locust olfactory system. Our results indicate that individual PN responses can vary with one or several of the perturbations we studied, including stimulus dynamics, repetition, stimulus history, presence of background odorants, and changes in humidity conditions. Nevertheless, a simple linear classification scheme was sufficient to extract the relevant information. The classifier essentially boiled down to adding the contribution of PNs that were strongly activated when the odorant was presented (ON neurons) and subtracting the contribution of PNs that were activated after the termination of the odorant (OFF neurons). Notably, such a classifier was not only able to

robustly detect all introductions of a target stimulus (i.e., solve the detection problem), but also provided sufficient discrimination between the two target odorants (i.e., solve the recognition problem as well).

We found that not all neurons were perturbed and only a small subset (4/89 PNs) of them responded reliably to all introductions of both the target odorants. While these neurons allowed robust detection of the target odorants, they were not specific and responded to both the target odorants examined in this study. Furthermore, various response features such as spike counts, response latency, etc. varied across different encounters of the same stimulus thereby making discrimination between target odorants based on just these reliable PNs not feasible (**Figure 5.3c**). Therefore, an approach based on a single or on a small subset of neurons encoding for a stimulus under all conditions cannot be expected to be fault tolerant.

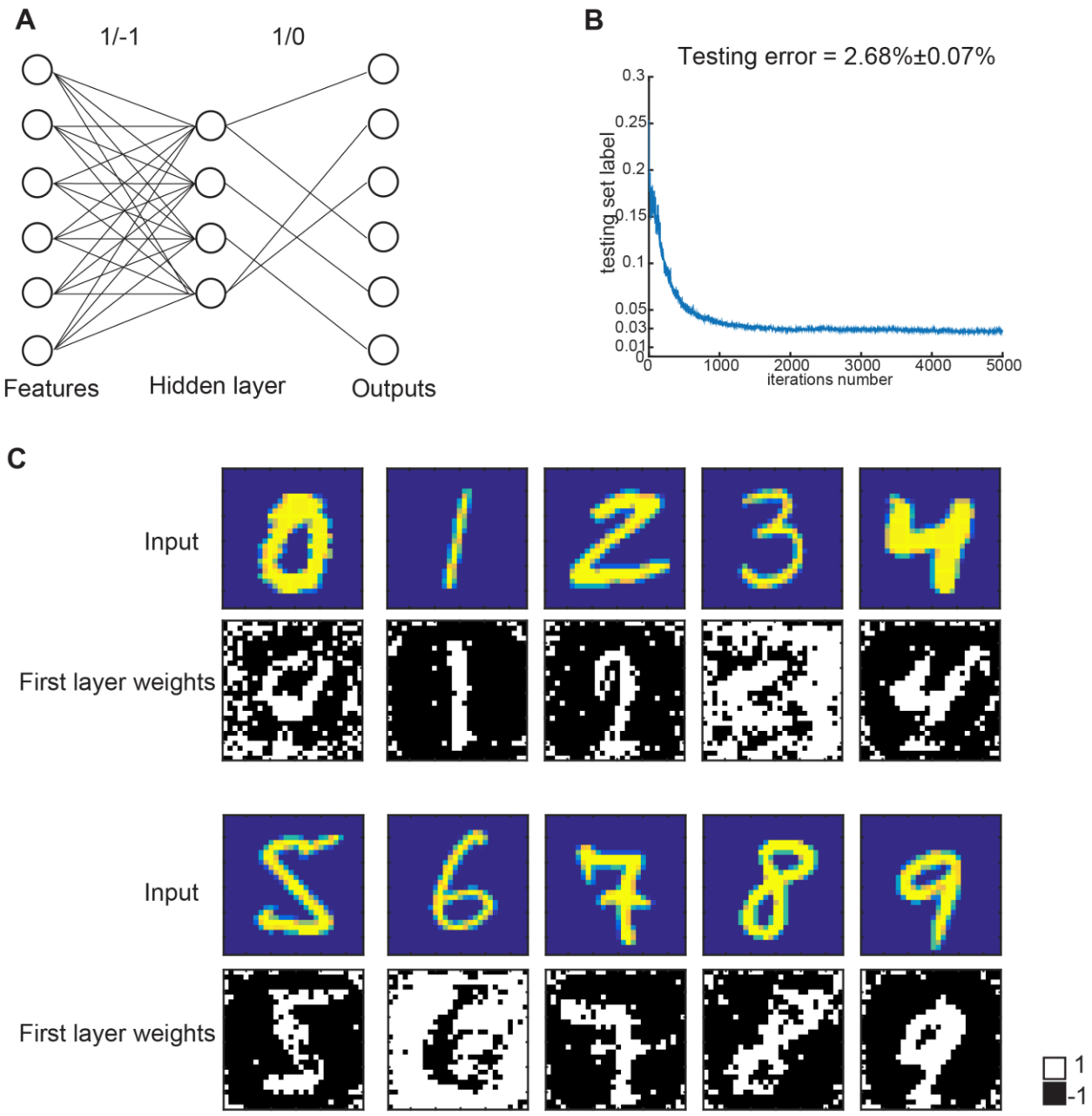

Figure 5.14: Boolean neural network for non-olfactory pattern recognition.
(a) Schematic of a feed-forward neural network model. Note that all the weights were constrained to be discrete. The weights from the first layer to the hidden layer were constrained to be either 1 or -1. The weights from the hidden layer to the output layer are constrained to 1 or 0.
(b) The learning curve of the network is shown in panel (**a**).
(c) Representative learned weights connecting the input layer with the hidden layer neurons are shown. To compare with the input patterns, the weights were reshaped to match the size of the input image. In each sub-panel, the top image shows a 'close' input digit and the bottom image shows the representative weights. Note that weight assignment mimicked ON pixels to +1 (digits 0, 1, 2, 4, 5, 7, 8, 9) and OFF pixels to -1 or vice versa (digits 3, 6).

Prior publications[67, 77, 80, 122, 184] have also found individual neurons to be unreliable but found that robustness emerged at an ensemble level. However, our prior results indicated that odorants delivered atop different background cues generated ensemble responses that only partially overlap across conditions[67]. When additional perturbations were introduced, our results indicate that the ensemble response features also tend to vary unreliably. In other words, even at the ensemble level, there was not a single feature that could remain consistent when the odor-evoked responses were minimally perturbed. How then could sensory invariance be achieved?

Given the complexity of individual PN response changes, we did not expect that a linear classifier could provide robust recognition. Nevertheless, both a linear support vector machine and logistic regression classifier were able to decode target odor identity independent of the perturbations made. Surprisingly, simplification of this approach by constraining weights to assume ternary values {-1 or 0 or 1} also provided robust recognition. The goal for constraining the decoding scheme in this fashion was two-fold: interpretability of the approach taken and determining the simplest possible approach i.e., a sort of a lower-bound in recognition performance. Our results indicate that not only did such a scheme exist, but it exploited a simple stratagem. We found that successful decoding schemes (discrete SVM or a logistic regression approach) assigned '+1' weights to ON neurons, '0' weight to non-responders, and '-1' weight to OFF neurons (i.e., an 'ON minus OFF' classifier). Notably, robust recognition was achieved using this simple approach in both dry (**Figure 5.10**) and humid conditions (**Figure 5.15a, b**).

If ensemble response features varied across conditions, how did this 'ON minus OFF' classification approach achieve invariance? It is worth breaking this classification scheme into its two components: the ON component and the OFF component. Assigning '+1' to the most strongly responding ON neurons and setting a recognition threshold that is less than this sum allows the

classification scheme to be flexible. Interpreted differently, this indicates that an odor can be recognized as long as a subset of strongly responding ON neurons are activated so that their sum reaches the threshold. The composition of this subset can change across conditions thereby allowing this approach to be more flexible.

What then is the contribution of the OFF component of the classifier? In an earlier study[179], we found that OFF responses were better at predicting when the behavioral response to a conditioned odorant terminated. In this study, we found that the OFF component increased separability between activation patterns of different odorants. This effect was particularly noticeable when the ternary weights were further simplified to a Boolean classifier with binary weights. While the Boolean classifier allowed detection of the target odor pulses, there was a significant increase in the false positive rates. Therefore, we conclude that assigning a negative weight to the OFF neurons enhanced discrimination between odorants and thereby reduced false positives.

There were other considerations that went behind considering this simpler classification scheme. As we have noted, the response evoked by an odorant in each neuron (i.e., changes in firing rates) can vary with most of the perturbations we introduced. In addition, repeated presentation of a stimulus will also lead to adaptation that can further attenuate the neural responses. Therefore, weighing individual neurons based on their response to solitary exposures of the target odorant might make the classification scheme unstable when recognition under other conditions/perturbations are required. Could the combination of neurons activated alone be a more robust indicator than the firing rate distribution across the same set of neurons: i.e., vector direction being more important than the length of the vector in any direction? If this is the case, a ternary weight vector should allow robust decoding of odor identity. Our results confirm this expectation.

Furthermore, it can be shown that a ternary version of a high-dimensional weight vector in a classifier is highly aligned with the analog version of the same weight vector (i.e., angular distance is low compared to pairs of random vectors; see **Figure 5.16**).

Earlier studies have argued that the antennal lobe neural network can be viewed as a non-linear dynamical system [65, 186, 187]. Under this perspective, both the initial conditions and odor-evoked response dynamics become important for recognizing the identity of the encountered stimulus. Our data indicate both the odor-evoked responses, and the spontaneous activity can vary across conditions. Yet at direct odds with our neural data, we find the behavioral recognition is robust even during these drastic changes. No detectable differences in response latency, intensity or duration were found. Hence, our results indicate that the rules for translating neural responses and their dynamics to generate appropriate behavioral output need further investigation.

The behavioral data also indicates that locusts trained with one odorant as CST generalized their responses to a few other odorants (**Figure 5.4a**). Both analog SVM and the ternary classification schemes were able to generate prediction results from neural data that matched with the observed trends in behavioral data (**Figure 5.17)**. These results further support the proposed scheme for translating the variable neural responses to robust behavioral outcomes.

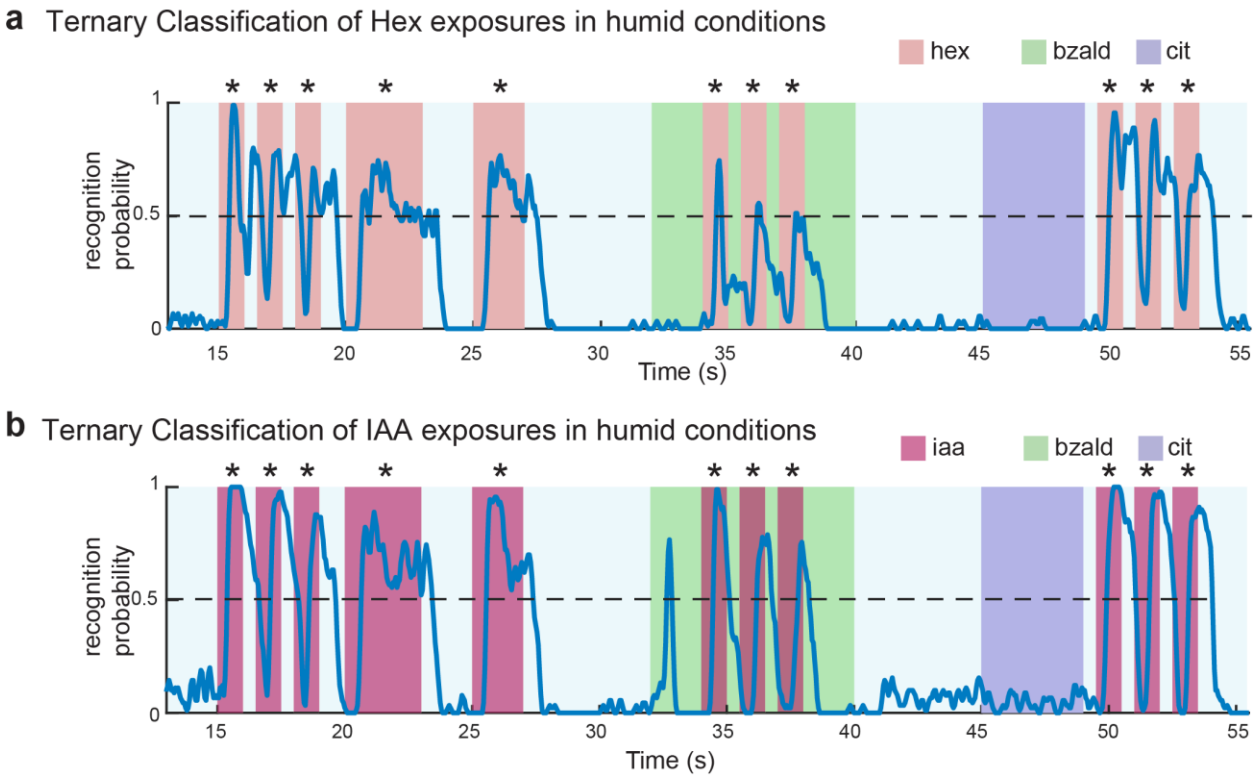

Figure 5.15: Performance of ternary classifiers in humid condition.
(a) Hex-classifier showing robust recognition of hexanol introductions in 100% RH ambient conditions.
(b) Similar plot but showing performance of iaa ternary classifier.

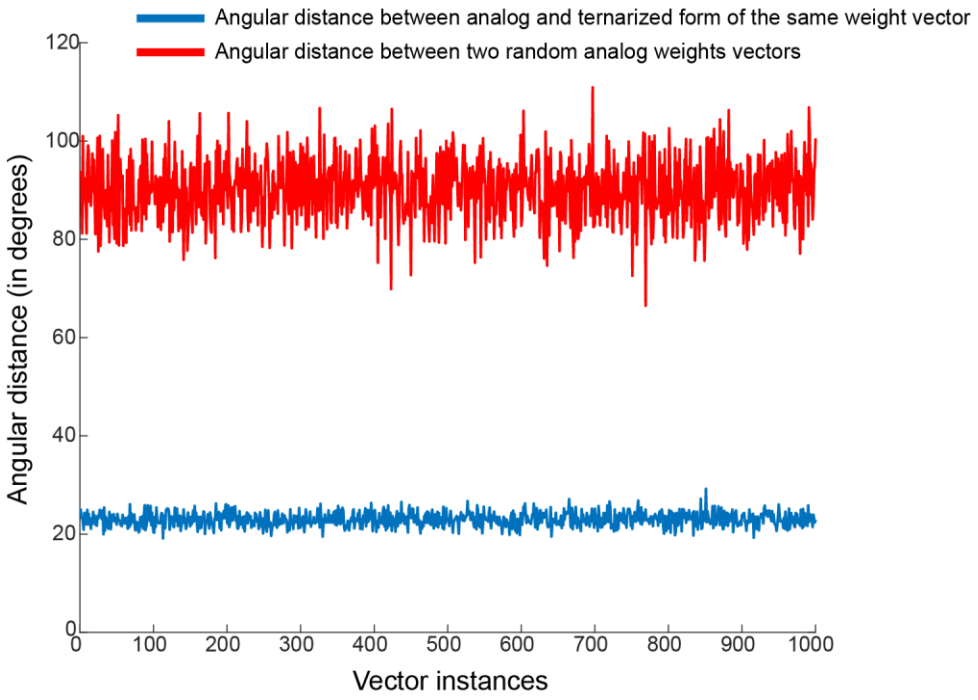

Figure 5.16: Similarity analysis between analog and discrete high-dimensional weight vectors.
The angular distance between high-dimensional vectors is analyzed and shown. The red curve shows the distribution of angles between pairs of randomly generated analog weight vectors. The blue curve shows angles between analog and ternarized forms of the same weights vector. Like the approach used to threshold SVM weights, random vectors were thresholded and assigned {+1, 0, -1} values.

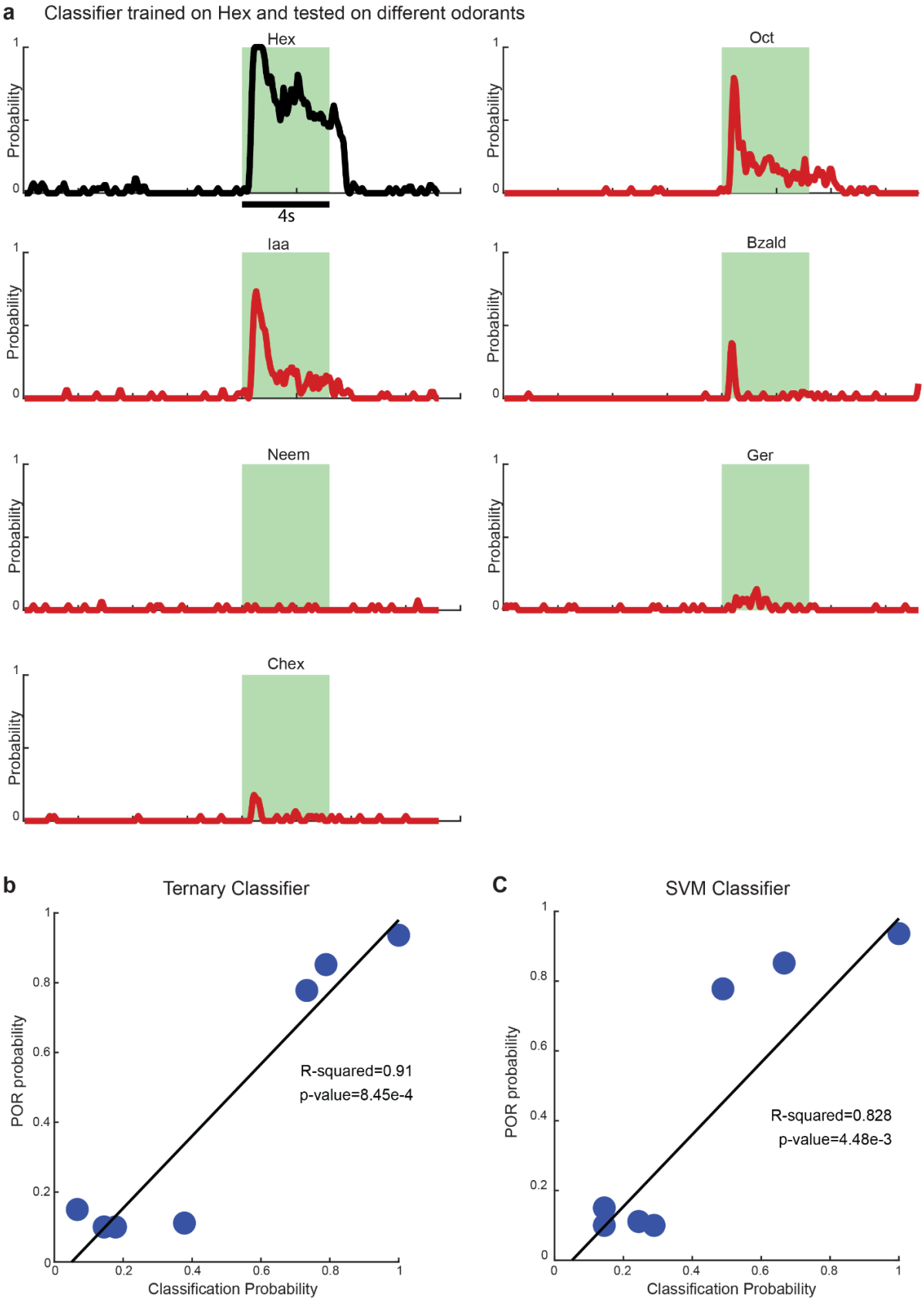
a
Classifier trained on Hex and tested on different odorants
Hex
Oct
Iaa
Bzald
Neem
Ger
Chex
Probability
4s
b
Ternary Classifier
POR probability
Classification Probability
R-squared=0.91
p-value=8.45e-4
c
SVM Classifier
POR probability
Classification Probability
R-squared=0.828
p-value=4.48e-3

Figure 5.17: Generalization performance of the Hex-trained classifier.
(a) The output of a ternary Bayesian logistic regression classifier is shown for a panel of odorants. The classifier was trained using ten trials where only a solitary pulse of hexanol was presented. The pre-, and post-stimulus periods, and 1 trial of all other odorants were included as a negative class to train the classifier. The odors used during the testing phase are identified in each panel.
(b) The peak classification probabilities (ternary classifier) during odor presentation (x-axis) are plotted against the POR probabilities from behavior experiments (y-axis, **Figure. 5.2A**). A regression analysis (solid line) revealed that the correlation between the peak classification probabilities and POR is significant (R^2 = 0.91, p = 8.45e-4; n=7 odors).
(c) The peak classification probabilities (analog SVM) during odor presentation (x-axis) are plotted against the POR probabilities from behavior experiments (y-axis). A regression analysis (solid line) revealed that the correlation between the peak classification probabilities and POR is significant (R^2 = 0.828, p = 4.48e-3; n=7 odors).

Finally, we wondered if the internal state of an organism such as its hunger level and whether it was trained to associate a particular target odorant with a reward would alter the stability of neural responses. To examine this issue, we compared the neural responses in locusts with different hunger levels (unstarved vs. starved) and/or training states (untrained vs. trained). Our results indicate that irrespective of the internal state, the neural responses to target odorants were highly variable (supra-Poisson Fano factors), and the odor-evoked responses were just as inconsistent across different encounters of the same target odorant **Figure 5.18-20**). While hunger level and odor-reward pairing have been suggested to alter certain odor-evoked response features in this neural circuit[188-190], our data indicate that such state-dependent changes may still not compensate for variations induced by the battery of extrinsic perturbations such as those explored in this study. Moreover, we applied our SVM classifier on the neural responses from PNs pooled across unstarved locusts, starved locusts and starved then trained locusts. We were noted that, with this dataset, the lack of solitary presentation resulting in slightly less recognition performance. However, the decoder can still pick up the majority of stimulus presentations with various

perturbations **(Figure 5.21)**. Therefore, we conclude that the decoding scheme proposed by our results would still be relevant and necessary for robust odor recognition.

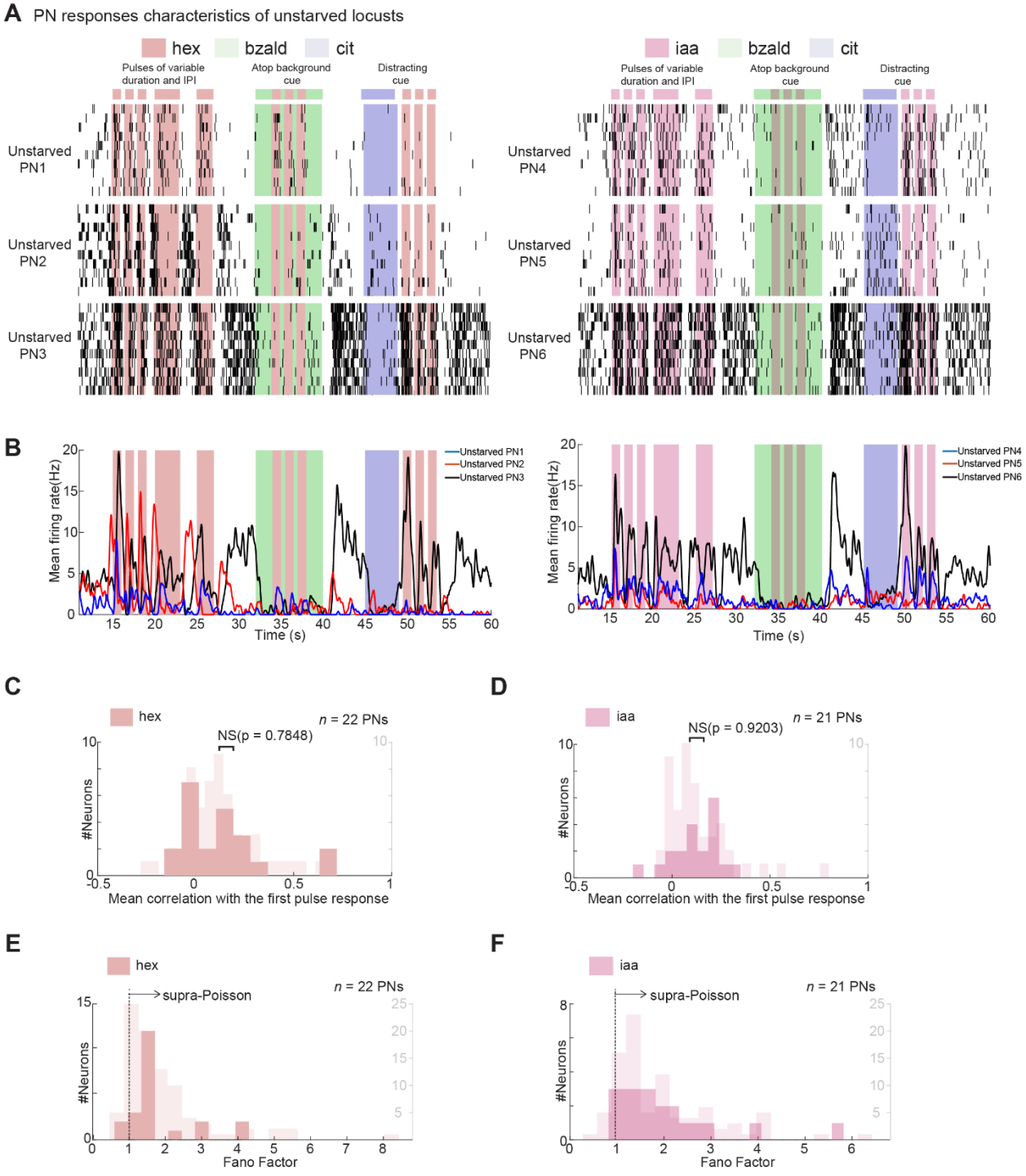

Figure 5.18: **Characterization of PN responses recorded from unstarved locusts.**

(a) Similar raster plots as **Figure 3** but showing PN responses recorded in unstarved locusts. Left panel, PN responses to a pulsatile presentation of a target stimulus (hexanol; hex) in back-to-back sequences of variable durations and inter-pulse intervals, atop a background cue (benzaldehyde; bza), and following a distracting stimulus (citral; cit). Each black tick mark represents an action potential fired by the PN. PN responses are shown for 10 consecutive trials (10 rows). Right panel, similar plots as in the left, but the target stimulus was isoamyl acetate (iaa). Notice the responses evoked by the target odorant in these six PNs were highly variable.
(b) Firing rates of the three PNs (50 ms time bins; 10 trials averaged) shown in panel A are now plotted as a function of time. While all the PNs responded strongly to the first pulse of the target odorant, the response diminished during later encounters of the same stimuli.
(c) Similar plot as in **Figure 3d, e**. Similarities between PN responses evoked during the first pulse of hex (target odorant) with all other encounters were computed and shown. PN responses were first binned into 50 ms time bins and averaged across 10 trials. The first 1 s response following the onset of each target odorant pulse was used to compare response similarity between different target odor encounters (i.e., 20-dimensional response vectors). For each PN, the mean similarity across odor pulses was determined, and the response similarity across PNs was then plotted as a distribution. The correlation distribution for PNs recorded from unstarved locusts and the distribution of PN response correlation observed in the original dataset shown in **Figure 3** are overlaid to allow comparison. No significant difference in the mean of the two distributions was found (two-sample t test; p value = 0.7848). **(d)** Similar comparison as in **panel c** but showing response correlations for the second target odorant (iaa).
(e, f) Distributions of the Fano factor are shown across PNs for both target odorants hex and iaa. **Panel e**, distributions are shown for hex pulses. Mean of the first 1 s neural response across 11 presentations of hex and 10 repeated trials were used to compute Fano factor (σ^2/μ) for each PN. **Panel f**, the similar plot as in left but Fano factors were computed for iaa trials. The original distribution of Fano factors (from **Figure 3**) is shown in the background to allow comparison.

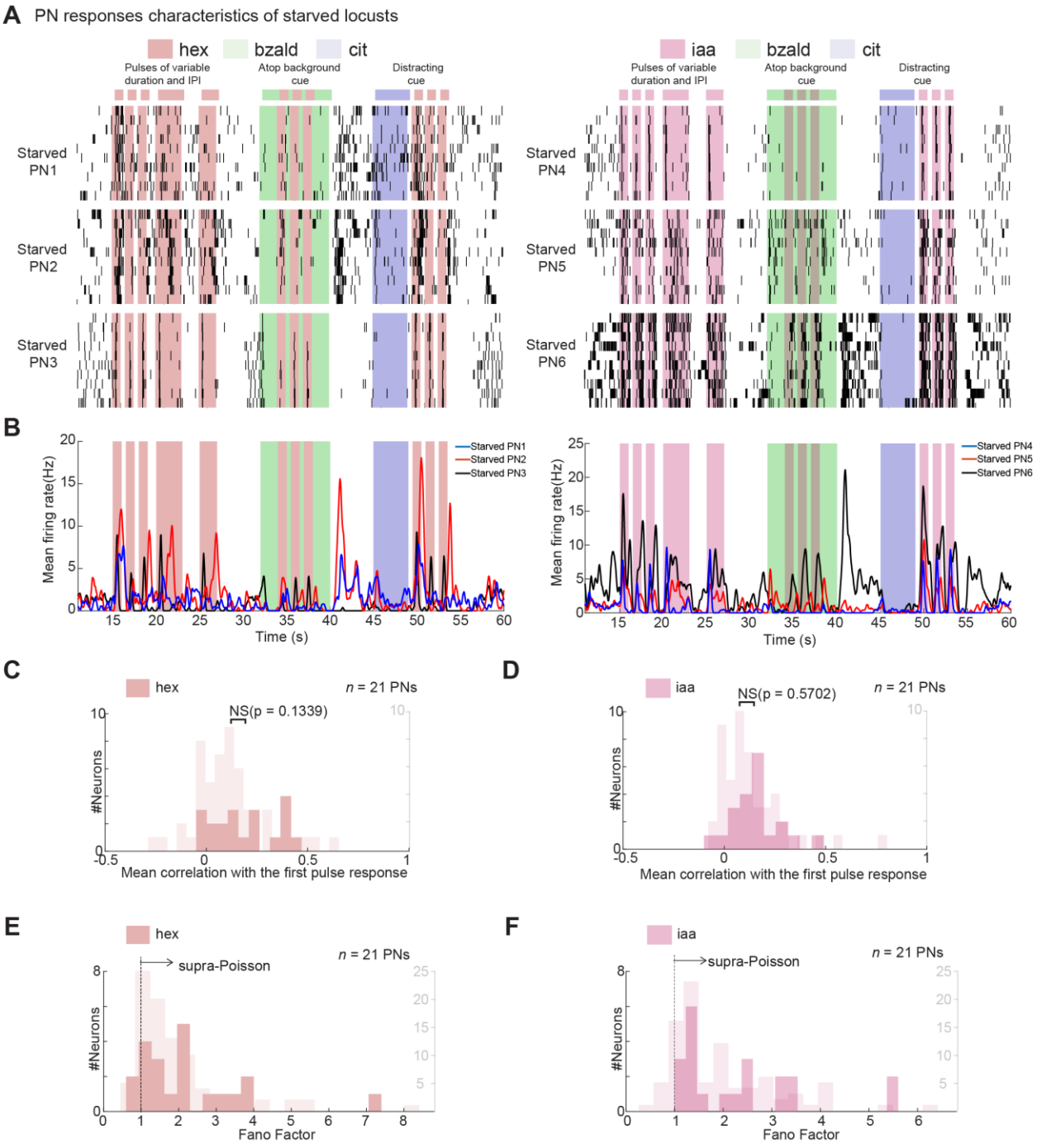

Figure 5.19: Characterization of PN responses recorded from starved locusts.
Similar plots as **Figure 5.15**, but for PNs recorded from starved locusts. Note that locusts were starved for 24 hours prior to surgery.

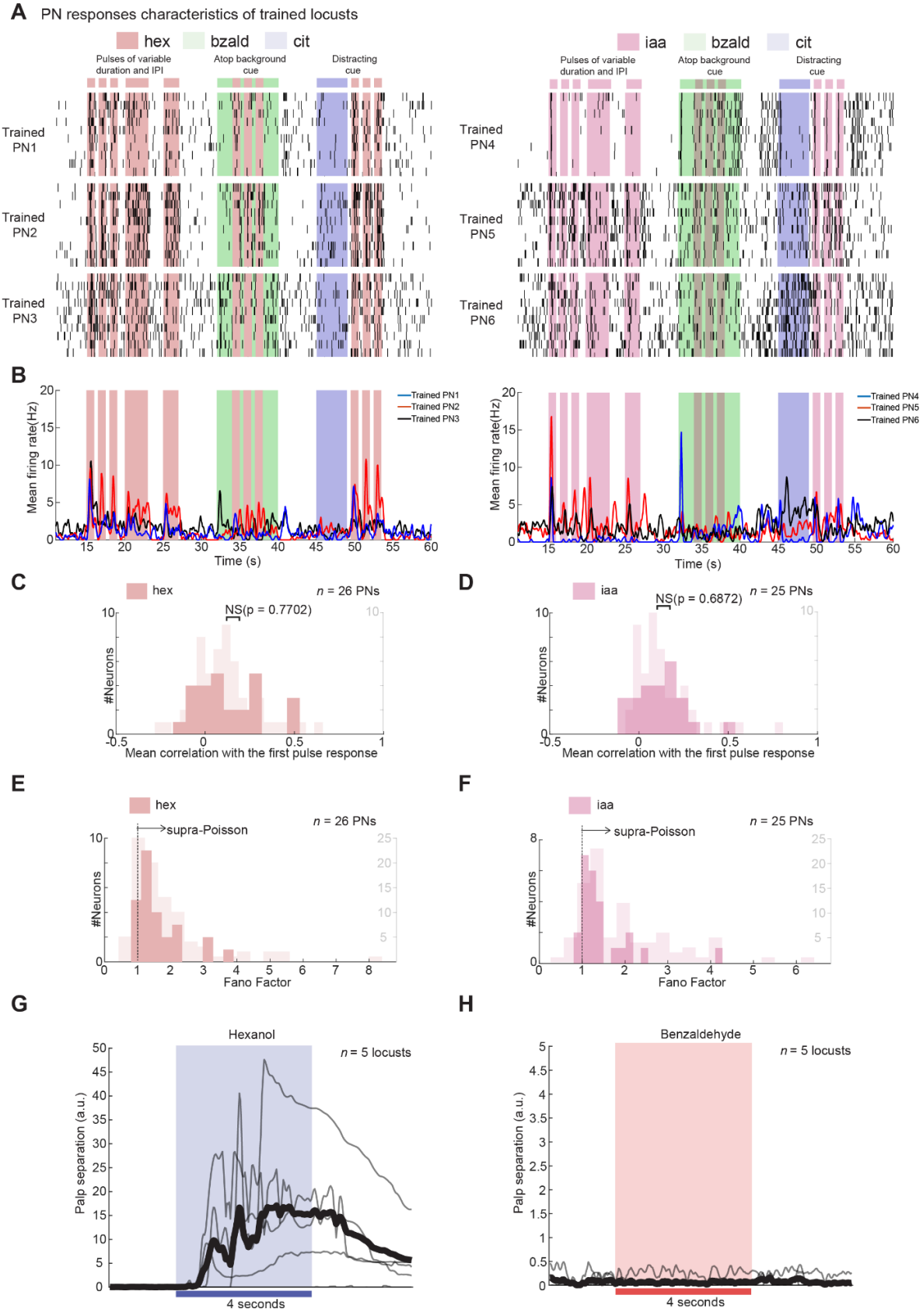
A
PN responses characteristics of trained locusts
hex
bzald
cit
Pulses of variable duration and IPI
Atop background cue
Distracting cue
Trained PN1
Trained PN2
Trained PN3
iaa
Trained PN4
Trained PN5
Trained PN6
B
Mean firing rate(Hz)
Time (s)
C
NS(p = 0.7702)
n = 26 PNs
#Neurons
Mean correlation with the first pulse response
D
NS(p = 0.6872)
n = 25 PNs
E
supra-Poisson
Fano Factor
F
G
Hexanol
n = 5 locusts
Palp separation (a.u.)
4 seconds
H
Benzaldehyde

Figure 5.20: Characterization of PN responses recorded from starved and then trained locusts.
Locusts were starved for 24 hours. Following this starvation period, locusts were trained using the same appetitive-conditioning paradigm used in **Figures 1, 2**. This was followed by a testing phase when the behavioral POR responses to the conditioned stimulus (hex) and an untrained stimulus (bza) were evaluated. Subsequently, the locusts were surgically implanted with electrode arrays and the response of PNs to the same stimulation protocol was evaluated.
(a-f) Similar plots as **Figure 5.15**, but PNs are recorded from trained locusts.
(g) Palp-opening responses of the five locusts that were trained with hexanol as the conditioning stimulus are shown. Note that the PN responses shown above were recorded from these five locusts.
(h) Palp-opening responses of the trained five locusts to benzaldehyde, an untrained odorant, are shown. As can be noted, none of the locusts responded with a POR upon introduction of the untrained odorant.

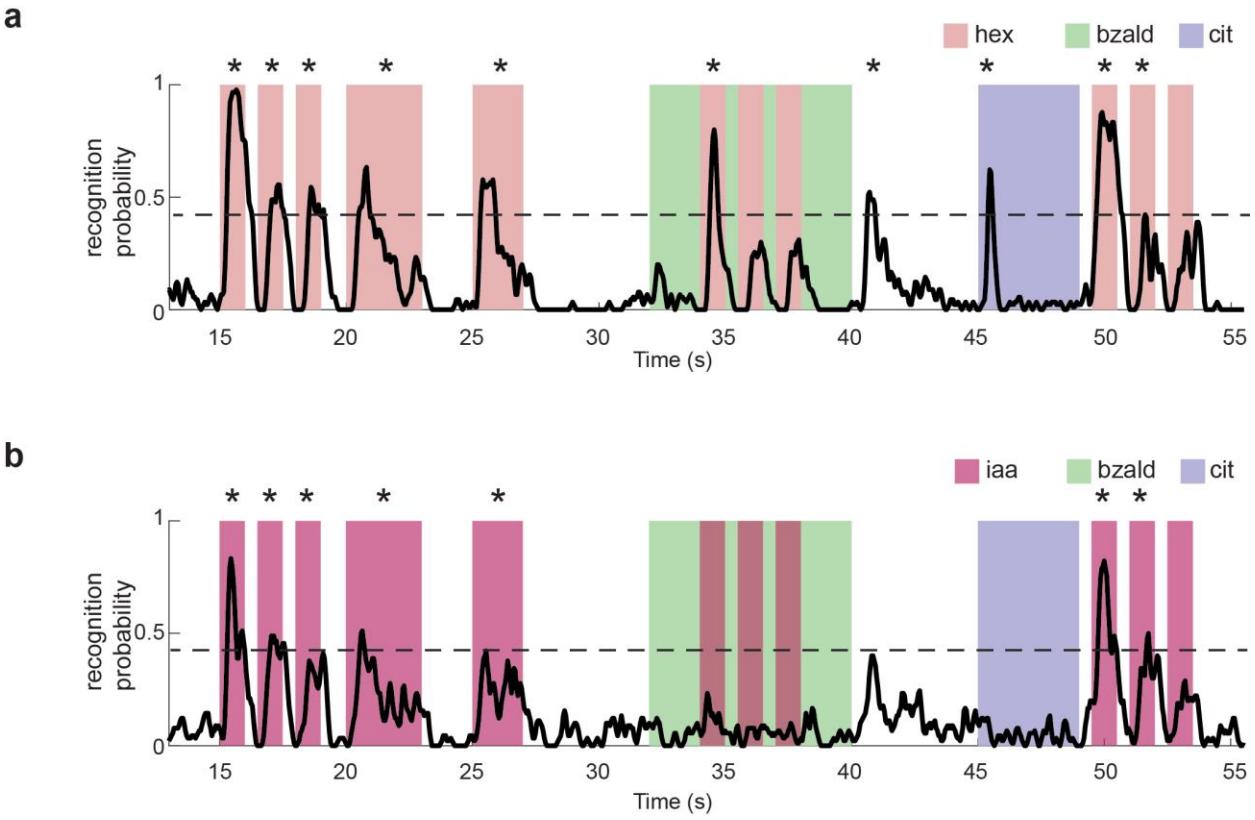

Figure 5.21: Performance of SVM classifiers for PNs pooled across from unstarved locusts, starved locusts and starved then trained locusts.
(a) Hex-classifier showing recognition of hexanol from PNs pooled across from unstarved locusts, starved locusts and starved then trained locusts.
(b) Similar plot but showing performance of iaa SVM classifier.

5.4 Author contributions

Srinath Nizampatnam, Lijun Zhang and Barani Raman conceived the study and designed the experiments/analyses. Srinath Nizampatnam, Rishabh Chandak performed all the electrophysiology experiments and collected the data. Rishabh Chandak collected the behavioral data. Lijun Zhang developed the Bayesian logistic regression approach. James Li collected experimental data to compare odor-evoked responses in unstarved vs. starved vs. trained animals. Srinath Nizampatnam, Lijun Zhang and Barani Raman wrote the paper taking inputs from all the authors. Barani Raman supervised all aspects of the work.

This research was supported by NSF CAREER Award (Grant #1453022), NSF CRCNS (Grant#1724218), NSF BII (Grant #2021795) and ONR grant (#N000141912049) to B.R.

Chapter 6: Conclusion

The main objective of this work is to study how sensory memory impacts olfactory information processing. To achieve this goal, we used both locust and fruit fly olfactory systems as our models. In the locust olfactory system, we examined how spontaneous neural activity in the antennal lobe network was altered upon repetition of a stimulus and how short-term memory impacted processing novel cues. Using the genetic and imaging tools available in the fruit fly olfactory system, we examined how temporal patterning of odor-evoked responses changed due to short-term memory in different sub-types of neurons within the antennal lobe. Overall, this dissertation work provides several key insights on the role of short-term memory in olfaction.

6.1 Short-term memory in locust antennal lobe

First, we started by examining how PNs responses in the locust antennal lobe changed upon repeated presentation of the same stimulus. The response elicited by a sensory stimulus often reduces when the same stimulus is repeatedly encountered [138, 139, 143]. In this study, we examined whether the spontaneous activity in the neural network also gets altered in an odor-specific manner indicating persistence of odor-specific memory. After the first exposure to an odorant, our results indicated that the spontaneous spiking responses became negatively correlated with the odor-evoked PN ensemble responses (**Fig. 3.1**). The spontaneous activities changed depending on the identity of the odorant that was repeatedly presented (**Fig. 3.2b**). Repeated presentations of two different odorants presented during two non-overlapping epochs resulted in distinct ensemble-level PN spontaneous activity clusters (**Fig. 3.2c**). Note that the spontaneous ensemble PN activities in the very first trial were random. However, subsequent evolution after

the first encounter with a repetitive stimulus reduced the correlation between neural activities observed in these two epochs (**Fig. 3.2d, Fig. 3.11, Fig. 3.12**).

Exposure to a stimulus reduced sensitivity to subsequent exposures of the same stimulus [138, 139, 143]. Consistent with previous findings[72], our data also indicated that odor-evoked PN responses reduced, and response changes were most significant in the first few trials. However, we found that most PN spiking responses continued to change, albeit modestly, even after twenty repetitions of the same stimulus (**Fig. 3.4**). Could diminishing the neural response to the recurring stimulus potentially confound pertinent information about the same adapting stimulus, such as its intensity? Our results indicate that adaptation does not lead to a loss of stimulus-specific information. The ensemble response profiles remained relatively consistent across trials (**Fig. 3.5**). The combination of PNs activated robustly encoded both the stimulus identity and intensity (**Figs. 3.6**). Information about odorant identity and intensity was encoded more efficiently with fewer spikes. This result also suggests that percept about odor intensity won't change with adaptation, but this remains to be behaviorally tested. Intuitively, such an encoding scheme does make sense as no matter how many times one is exposed to high-intensity vapors of skatole, it is expected to still not smell floral!

Could the short-term memory induced by the recurring stimulus also alter how information regarding other stimuli gets encoded? Previous results showed exposure to a stimulus also reduces sensitivity to subsequent exposures of other cues but to a lesser degree [138, 139, 143]. This carry-over cross adaptation effect happens when two odorants are chemically similar (same functional groups; e.g., hexanol to octanol) [72]. In this study, we tested the cross adaptation by using two pairs of odors (hexanol and isoamyl acetate; hexanol and apple). we repeatedly presented an odorant (hex) for twenty-five trials, but in the twenty-sixth trial (a 'catch trial'), we switched and

presented a different stimulus (i.e. a 'deviant' stimulus). Our results reveal that although responses to the repeating odorant reduced in many PNs, the response features unique to the deviant stimulus were unaltered (**Fig. 3.7b, c; unique responders**). Responses of PNs that were commonly activated by both repetitive and deviant stimuli were diminished during the catch trial. As a result, during the catch trial, the neural response trajectory became more distinct from the repetitive stimuli at the ensemble level, indicating a population-level contrast enhancement of neural representation.

In sum, our results present unique insights about how repeated stimuli alter the post-odor spontaneous activities and how stimulus intensity information remains unchanged under sensory adaptation. Further, it provides insights regarding how adapting to one stimulus altered how the neural circuit processed other stimuli. Lastly, we proposed a simple linear model that considers both the pre-adapted response and the ongoing activity to explain the changes in stimulus-evoked responses observed for a recurring or a novel stimulus.

6.2 Short-term memory in fruit fly olfactory system

What is the loci of short-term memory in the antennal lobe? Do different sub-types of neurons that are part of the same network, and different compartments of same neural subtype adapt differently? To answer these questions, we used a light-sheet, volumetric, calcium-imaging technique and simultaneously monitored the odor-evoked activities at the ORN axons entering the antennal lobe (input), ePNs dendrites located within the antennal lobe, and ePN and iPNs axons (output) entering mushroom body calyx and lateral horn in fruit fly olfactory system.

Our results indicate that during the first stimulus presentation, the initial responses immediately after the stimulus onset (during the first 500 ms of stimulation) were strong but did

not have much discriminatory information (**Figure 4.4, 4.5**). Neural activity patterns evoked by different stimuli became more distinct, e.g., stimulus-specific, over the time course of the stimulus. This decorrelation of odor-evoked responses over time was observed in all three neural populations examined: ORNs, ePNs and iPNs.

When the same set of stimuli were repeated for a second block of trials, our results indicated that the odor-evoked responses elicited by the odor panel again decorrelated over time. The pairwise correlation between odorants were strikingly similar across two trials of recordings made from a single fly (**Figure 4.11a** or **4.11b**; left vs. right column). However, the overall speed at which decorrelation between odorants occurred was accelerated (**Figure 4.12**) during the second block of trials. Such acceleration was observed in ePNs from antennal lobe dendritic inputs to lateral horn and calyx outputs. This result suggests that a role of short-term memory was to expedite the speed of discrimination between odorants.

We also found neural responses across all sub-populations decreased in strength. However, similar to results from locust studies, overall responses patterns across different trials still clustered in an odor-identity dependent manner (**Figure 4.10**). Notably, ensemble iPNs responses exhibited a more significant reduction in overall response strength than other sub-group of neurons (**Figure 4.10**).

Although the decorrelation over time was ubiquitous and observed in all flies, both the pairwise odor decorrelation patterns (**Figure 7A**) and decorrelation rates (**Figure 6D**) varied from one fly to another. Across all regions recorded, the standard deviation between flies were relatively low at the level of ePN axons compared to their dendritic activity, whereas the multiglomerular iPNs had the higher levels of variability (**Figure 7B**). These results indicate that while odor-evoked

response patterns decorrelated to become more distinct over time in all flies, this computation was performed in an idiosyncratic fashion.

Lastly, we examined the responses after stimulus termination. In flies, less attention has been paid to the ensemble dynamics after the stimulus termination. At the level of the sensory neurons, activities observed during the odor presentation period persisted after odor termination. However, in the ePN and iPN dendrites and axons, nearly orthogonal stimulus ON and OFF responses were observed in all flies (**Figure 4.13**). These nearly orthogonal, sometimes anti-correlated patterns are consistent with those reported in other sensory systems, particularly the locust olfactory system[179].

6.3 Robust odor recognition with 'ON' and 'OFF' features

Can odorants still be robustly recognized independent of variations induced by short-term memory? In the locust antennal lobe, we found combinatorial PN activity profiles can retain information about odor identity and intensity and is robust to changes that occur due to adaptation (**Figure 3.5, 3.6**); In the fruit fly olfactory system, decorrelation of neural responses between pairs of odors persisted and became faster upon repetition. We wondered if there exists a classification scheme that can robustly recognize stimulus independent of any interference from adaptation/short-term memory induced by the same of a different odorant. Surprisingly, a simple linear support vector machine classifier could decode target odor identity in a robust fashion (**Figure 5.1**). Moreover, we found that this simple approach was sufficient to deal with more complex extrinsic perturbations such as those induced by varying recurring stimulus, background cues, distractor odorants and humid ambient conditions. Additionally, we found that this linear

decoding scheme assigned ON responsive neurons with mostly positive weights and OFF responsive neurons with mostly negative weights (**Figure 5.2**).

If ensemble response features varied across conditions, how did this 'ON minus OFF' classification approach achieve invariance? Essentially, this classification scheme can be segregated into the ON and OFF components. Assigning '+1' to the most strongly responding ON neurons and setting a recognition threshold that is less than this sum allows the classification scheme to be flexible. The composition of this subset can change across conditions, thereby allowing this approach to be more flexible. What then is the contribution of the OFF component of the classifier? In an earlier study[179], we found that OFF responses were better at predicting when the behavioral response to a conditioned odorant terminated. In this study, we found that the OFF component increased separability between activation patterns of different odorants. This effect was particularly noticeable when the ternary weights were further simplified to a Boolean classifier with binary weights. While the Boolean classifier allowed detection of the target odor pulses, there was a significant increase in the false positive rates (**Figure 5.10, 5.11**). Therefore, we conclude that assigning a negative weight to the OFF neurons enhanced discrimination between odorants and reduced false positives.

Lastly, we wondered whether the simple approach for achieving invariance in the locust olfactory system can be extended to create a general-purpose pattern recognition neural network. We developed an artificial neural network (ANN) using layers with binary values ({-1 and 1} or {0 and 1}) (**Figure 5.14a**). We trained the network with the Bayesian variational inference method and achieved performance close to the benchmark performance of an ANN with similar architecture but with real-valued weights (**Figure 5.14b**) in the well-studied MNIST digits dataset[191]. In addition, the binary weights made the features extracted by each hidden unit highly

interpretable (**Figure 5.14c**). Taken together, these results indicate that the neural circuits in the insect olfactory system delicately balance discrimination between odorants with the flexibility necessary for robustness and fault tolerance to achieve sensory invariance.

6.4 Future work

What's the potential mechanism for short-term memory? One possible mechanism that could underlie these results is that the synapses between the olfactory sensory neurons and the antennal lobe PNs could depress to mediate adaptation [146]. However, our results have shown some PN responses to the deviant/unexpected stimulus during the catch trial were stronger than the unadapted responses evoked by the same stimulus immediately after a 15 min no-odor reset window (**Fig. 3.7c**), which cannot be explained by the depression of ORN-PN synapses and indicate that some aspects of this short-term memory may also reside within the antennal lobe neural network. The feedback inhibition from local neurons may play a role in adaptation. Prior studies found strengthening of inhibitory synapses from LNs to a subset of PNs [149]. This synapse-specific enhancement of recurrent inhibition was hypothesized to cause odorant-selective response adaptation in the PNs [192, 193]. Further systematic studies of the contribution made cell-intrinsic adaptation mechanisms and network-level adaptation due to LNs would be needed to dissect the precise contribution to the phenomenological results we reported in this dissertation.

We sought to take functional mapping one step further. Nine ROIs have been registered across flies and assigned to corresponding glomeruli in the reference fly brain. However, the current methods are still preliminary and require human expert knowledge for ROI labeling across flies. Computational approaches to register all ROIs and map to glomeruli maps automatically still

need to be developed. A more quantitative investigation into conservative/variable features across organisms can also be realized with such a method.

We developed a discrete weights neural network inspired by the architecture and results from the locust olfactory system and tested it in the standard MNIST dataset. Current states of deep learning technologies have gone beyond digits recognition[194]. It could be interesting to try different neural network structures with discrete weights on other tasks, such as speech recognition, machine translation, language modeling, etc. The binary weights can also utilize to help reduce network model size and accelerate neural network computation.

Reference

1. Kipke, D.R., et al., *Advanced neurotechnologies for chronic neural interfaces: new horizons and clinical opportunities.* J Neurosci, 2008. **28**(46): p. 11830-8.
2. Kerr, J.N. and W. Denk, *Imaging in vivo: watching the brain in action.* Nat Rev Neurosci, 2008. **9**(3): p. 195-205.
3. Saha, D., et al., *Multi-unit recording methods to characterize neural activity in the locust (Schistocerca americana) olfactory circuits.* J Vis Exp, 2013(71).
4. Ahrens, M.B., et al., *Whole-brain functional imaging at cellular resolution using light-sheet microscopy.* Nat Methods, 2013. **10**(5): p. 413-20.
5. Brown, E.N., R.E. Kass, and P.P. Mitra, *Multiple neural spike train data analysis: state-of-the-art and future challenges.* Nat Neurosci, 2004. **7**(5): p. 456-61.
6. Cunningham, J.P. and B.M. Yu, *Dimensionality reduction for large-scale neural recordings.* Nature Neuroscience, 2014. **17**(11): p. 1500-1509.
7. Kobak, D., et al., *Demixed principal component analysis of neural population data.* Elife, 2016. **5**.
8. Saha, D., et al., *Behavioural correlates of combinatorial versus temporal features of odour codes.* Nat Commun, 2015. **6**: p. 6953.
9. Wilt, B.A., et al., *Advances in light microscopy for neuroscience.* Annu Rev Neurosci, 2009. **32**: p. 435-506.
10. Keller, P.J., M.B. Ahrens, and J. Freeman, *Light-sheet imaging for systems neuroscience.* Nat Methods, 2015. **12**(1): p. 27-9.
11. Rekwot, P.I., et al., *The role of pheromones and biostimulation in animal reproduction.* Anim Reprod Sci, 2001. **65**(3-4): p. 157-70.
12. Masante-Roca, I., C. Gadenne, and S. Anton, *Plant odour processing in the antennal lobe of male and female grapevine moths, Lobesia botrana (Lepidoptera: Tortricidae).* J Insect Physiol, 2002. **48**(12): p. 1111-1121.
13. De Boer, J.G., T.A.L. Snoeren, and M. Dicke, *Predatory mites learn to discriminate between plant volatiles induced by prey and nonprey herbivores.* Animal Behaviour, 2005. **69**: p. 869-879.
14. Nguyen, D.M.T., et al., *Flow-mediated olfactory communication in honeybee swarms.* Proc Natl Acad Sci U S A, 2021. **118**(13).
15. Guo, X.J., et al., *4-Vinylanisole is an aggregation pheromone in locusts.* Nature, 2020. **584**(7822): p. 584-+.
16. Sullivan, R.M., et al., *Olfactory memory networks: from emotional learning to social behaviors.* Front Behav Neurosci, 2015. **9**: p. 36.
17. Kay, L.M. and M. Stopfer, *Information processing in the olfactory systems of insects and vertebrates.* Seminars in Cell & Developmental Biology, 2006. **17**(4): p. 433-442.
18. Keller, A., et al., *Predicting human olfactory perception from chemical features of odor molecules.* Science, 2017. **355**(6327): p. 820-826.
19. Araneda, R.C., A.D. Kini, and S. Firestein, *The molecular receptive range of an odorant receptor.* Nat Neurosci, 2000. **3**(12): p. 1248-55.

20. Cunningham, A.M., et al., *Olfactory receptor neurons exist as distinct subclasses of immature and mature cells in primary culture.* Neuroscience, 1999. **93**(4): p. 1301-12.
21. Serizawa, S., et al., *Mutually exclusive expression of odorant receptor transgenes.* Nat Neurosci, 2000. **3**(7): p. 687-93.
22. Buck, L.B., *Information coding in the vertebrate olfactory system.* Annu Rev Neurosci, 1996. **19**: p. 517-44.
23. Shipley, M.T. and M. Ennis, *Functional organization of olfactory system.* J Neurobiol, 1996. **30**(1): p. 123-76.
24. Liu, S., et al., *Olfactory bulb short axon cell release of GABA and dopamine produces a temporally biphasic inhibition-excitation response in external tufted cells.* J Neurosci, 2013. **33**(7): p. 2916-26.
25. Haberly, L.B., *Parallel-distributed processing in olfactory cortex: new insights from morphological and physiological analysis of neuronal circuitry.* Chem Senses, 2001. **26**(5): p. 551-76.
26. Chapuis, J. and D.A. Wilson, *Bidirectional plasticity of cortical pattern recognition and behavioral sensory acuity.* Nat Neurosci, 2011. **15**(1): p. 155-61.
27. McGuire, S.E., P.T. Le, and R.L. Davis, *The role of Drosophila mushroom body signaling in olfactory memory.* Science, 2001. **293**(5533): p. 1330-1333.
28. Menzel, R. and U. Muller, *Learning and memory in honeybees: from behavior to neural substrates.* Annu Rev Neurosci, 1996. **19**: p. 379-404.
29. Mizunami, M., J.M. Weibrecht, and N.J. Strausfeld, *Mushroom bodies of the cockroach: Their participation in place memory.* Journal of Comparative Neurology, 1998. **402**(4): p. 520-537.
30. Gupta, N. and M. Stopfer, *Functional analysis of a higher olfactory center, the lateral horn.* J Neurosci, 2012. **32**(24): p. 8138-48.
31. Schultzhaus, J.N., et al., *The role of the Drosophila lateral horn in olfactory information processing and behavioral response.* J Insect Physiol, 2017. **98**: p. 29-37.
32. Ochieng, S.A., E. Hallberg, and B.S. Hansson, *Fine structure and distribution of antennal sensilla of the desert locust, Schistocerca gregaria (Orthoptera: Acrididae).* Cell Tissue Res, 1998. **291**(3): p. 525-36.
33. Raman, B., et al., *Temporally diverse firing patterns in olfactory receptor neurons underlie spatiotemporal neural codes for odors.* J Neurosci, 2010. **30**(6): p. 1994-2006.
34. Larsson, M.C., et al., *Or83b encodes a broadly expressed odorant receptor essential for Drosophila olfaction.* Neuron, 2004. **43**(5): p. 703-14.
35. Clyne, P.J., et al., *A novel family of divergent seven-transmembrane proteins: candidate odorant receptors in Drosophila.* Neuron, 1999. **22**(2): p. 327-38.
36. Leitch, B. and G. Laurent, *GABAergic synapses in the antennal lobe and mushroom body of the locust olfactory system.* J Comp Neurol, 1996. **372**(4): p. 487-514.
37. Ernst, K.D., J. Boeckh, and V. Boeckh, *A neuroanatomical study on the organization of the central antennal pathways in insects.* Cell Tissue Res, 1977. **176**(3): p. 285-306.
38. Hansson, B.S. and S. Anton, *Function and morphology of the antennal lobe: new developments.* Annu Rev Entomol, 2000. **45**: p. 203-31.
39. Davis, R.L., *Traces of Drosophila memory.* Neuron, 2011. **70**(1): p. 8-19.
40. de Belle, J.S. and M. Heisenberg, *Associative odor learning in Drosophila abolished by chemical ablation of mushroom bodies.* Science, 1994. **263**(5147): p. 692-5.

41. Laurent, G., *Dynamical representation of odors by oscillating and evolving neural assemblies.* Trends Neurosci, 1996. **19**(11): p. 489-96.
42. Laurent, G., *Olfactory network dynamics and the coding of multidimensional signals.* Nat Rev Neurosci, 2002. **3**(11): p. 884-95.
43. Jortner, R.A., S.S. Farivar, and G. Laurent, *A simple connectivity scheme for sparse coding in an olfactory system.* Journal of Neuroscience, 2007. **27**(7): p. 1659-1669.
44. de Bruyne, M., P.J. Clyne, and J.R. Carlson, *Odor coding in a model olfactory organ: the Drosophila maxillary palp.* J Neurosci, 1999. **19**(11): p. 4520-32.
45. Dobritsa, A.A., et al., *Integrating the molecular and cellular basis of odor coding in the Drosophila antenna.* Neuron, 2003. **37**(5): p. 827-41.
46. Hallem, E.A. and J.R. Carlson, *The odor coding system of Drosophila.* Trends Genet, 2004. **20**(9): p. 453-9.
47. Bates, A.S., et al., *Complete Connectomic Reconstruction of Olfactory Projection Neurons in the Fly Brain.* Curr Biol, 2020. **30**(16): p. 3183-3199 e6.
48. Shimizu, K. and M. Stopfer, *A Population of Projection Neurons that Inhibits the Lateral Horn but Excites the Antennal Lobe through Chemical Synapses in Drosophila.* Frontiers in Neural Circuits, 2017. **11**.
49. Yaksi, E. and R.I. Wilson, *Electrical Coupling between Olfactory Glomeruli.* Neuron, 2010. **67**(6): p. 1034-1047.
50. Honegger, K.S., R.A. Campbell, and G.C. Turner, *Cellular-resolution population imaging reveals robust sparse coding in the Drosophila mushroom body.* J Neurosci, 2011. **31**(33): p. 11772-85.
51. Sayin, S., et al., *Internal State Dependent Odor Processing and Perception-The Role of Neuromodulation in the Fly Olfactory System.* Front Cell Neurosci, 2018. **12**: p. 11.
52. Johnson, K.O., *Neural coding.* Neuron, 2000. **26**(3): p. 563-6.
53. Gerstner, W., et al., *Neural codes: firing rates and beyond.* Proc Natl Acad Sci U S A, 1997. **94**(24): p. 12740-1.
54. Wilson, R.I. and Z.F. Mainen, *Early events in olfactory processing.* Annu Rev Neurosci, 2006. **29**: p. 163-201.
55. Knaden, M., et al., *Spatial representation of odorant valence in an insect brain.* Cell Rep, 2012. **1**(4): p. 392-9.
56. Laurent, G., et al., *Odor encoding as an active, dynamical process: Experiments, computation, and theory.* Annual Review of Neuroscience, 2001. **24**: p. 263-297.
57. Kurtovic, A., A. Widmer, and B.J. Dickson, *A single class of olfactory neurons mediates behavioural responses to a Drosophila sex pheromone.* Nature, 2007. **446**(7135): p. 542-6.
58. Sakurai, T., et al., *Identification and functional characterization of a sex pheromone receptor in the silkmoth Bombyx mori.* Proc Natl Acad Sci U S A, 2004. **101**(47): p. 16653-8.
59. Gollisch, T. and M. Meister, *Rapid neural coding in the retina with relative spike latencies.* Science, 2008. **319**(5866): p. 1108-11.
60. Hopfield, J.J., *Pattern-Recognition Computation Using Action-Potential Timing for Stimulus Representation.* Nature, 1995. **376**(6535): p. 33-36.
61. Spors, H., et al., *Temporal dynamics and latency patterns of receptor neuron input to the olfactory bulb.* J Neurosci, 2006. **26**(4): p. 1247-59.

62. Wilson, C.D., et al., *A primacy code for odor identity.* Nat Commun, 2017. **8**(1): p. 1477.
63. Friedrich, R.W. and G. Laurent, *Dynamic optimization of odor representations by slow temporal patterning of mitral cell activity.* Science, 2001. **291**(5505): p. 889-94.
64. Giraudet, P., F. Berthommier, and M. Chaput, *Mitral cell temporal response patterns evoked by odor mixtures in the rat olfactory bulb.* J Neurophysiol, 2002. **88**(2): p. 829-38.
65. Mazor, O. and G. Laurent, *Transient dynamics versus fixed points in odor representations by locust antennal lobe projection neurons.* Neuron, 2005. **48**(4): p. 661-73.
66. Fdez Galan, R., et al., *Odor-driven attractor dynamics in the antennal lobe allow for simple and rapid olfactory pattern classification.* Neural Comput, 2004. **16**(5): p. 999-1012.
67. Saha, D., et al., *A spatiotemporal coding mechanism for backgroundinvariant odor recognition.* Nature Neuroscience, 2013. **16**(12): p. 1830-1839.
68. Ito, I., et al., *Frequency transitions in odor-evoked neural oscillations.* Neuron, 2009. **64**(5): p. 692-706.
69. Stopfer, M., et al., *Impaired odour discrimination on desynchronization of odour-encoding neural assemblies.* Nature, 1997. **390**(6655): p. 70-74.
70. Zibrowski, E.M. and C.H. Vanderwolf, *Oscillatory fast wave activity in the rat pyriform cortex: relations to olfaction and behavior.* Brain Res, 1997. **766**(1-2): p. 39-49.
71. Friedrich, R.W., C.J. Habermann, and G. Laurent, *Multiplexing using synchrony in the zebrafish olfactory bulb.* Nature Neuroscience, 2004. **7**(8): p. 862-871.
72. Stopfer, M. and G. Laurent, *Short-term memory in olfactory network dynamics.* Nature, 1999. **402**(6762): p. 664-668.
73. Denker, M., et al., *Neural correlates of odor learning in the honeybee antennal lobe.* Eur J Neurosci, 2010. **31**(1): p. 119-33.
74. Laurent, G. and M. Naraghi, *Odorant-induced oscillations in the mushroom bodies of the locust.* J Neurosci, 1994. **14**(5 Pt 2): p. 2993-3004.
75. Laurent, G. and H. Davidowitz, *Encoding of Olfactory Information with Oscillating Neural Assemblies.* Science, 1994. **265**(5180): p. 1872-1875.
76. Stopfer, M., V. Jayaraman, and G. Laurent, *Intensity versus identity coding in an olfactory system.* Neuron, 2003. **39**(6): p. 991-1004.
77. Broome, B.M., V. Jayaraman, and G. Laurent, *Encoding and decoding of overlapping odor sequences.* Neuron, 2006. **51**(4): p. 467-482.
78. Vickers, N.J., et al., *Odour-plume dynamics influence the brain's olfactory code.* Nature, 2001. **410**(6827): p. 466-70.
79. Brown, S.L., J. Joseph, and M. Stopfer, *Encoding a temporally structured stimulus with a temporally structured neural representation.* Nature Neuroscience, 2005. **8**(11): p. 1568-1576.
80. Nizampatnam, S., et al., *Dynamic contrast enhancement and flexible odor codes.* Nature Communications, 2018. **9**.
81. Blakemore, C. and F.W. Campbell, *On the existence of neurones in the human visual system selectively sensitive to the orientation and size of retinal images.* J Physiol, 1969. **203**(1): p. 237-60.
82. Fang, F., et al., *Orientation-tuned FMRI adaptation in human visual cortex.* J Neurophysiol, 2005. **94**(6): p. 4188-95.

83. Perez-Gonzalez, D. and M.S. Malmierca, *Adaptation in the auditory system: an overview.* Front Integr Neurosci, 2014. **8**: p. 19.
84. Wilson, D.A., A.R. Best, and R.M. Sullivan, *Plasticity in the olfactory system: lessons for the neurobiology of memory.* Neuroscientist, 2004. **10**(6): p. 513-24.
85. Wilson, R.I., *Early olfactory processing in Drosophila: mechanisms and principles.* Annu Rev Neurosci, 2013. **36**: p. 217-41.
86. Leinders-Zufall, T., et al., *Imaging odor-induced calcium transients in single olfactory cilia: specificity of activation and role in transduction.* J Neurosci, 1998. **18**(15): p. 5630-9.
87. Leinders-Zufall, T., M. Ma, and F. Zufall, *Impaired odor adaptation in olfactory receptor neurons after inhibition of Ca2+/calmodulin kinase II.* J Neurosci, 1999. **19**(14): p. RC19.
88. Ma, M., *Encoding olfactory signals via multiple chemosensory systems.* Crit Rev Biochem Mol Biol, 2007. **42**(6): p. 463-80.
89. Zufall, F. and T. Leinders-Zufall, *The cellular and molecular basis of odor adaptation.* Chemical Senses, 2000. **25**(4): p. 473-481.
90. Stortkuhl, K.F., B.T. Hovemann, and J.R. Carlson, *Olfactory adaptation depends on the Trp Ca2+ channel in Drosophila.* J Neurosci, 1999. **19**(12): p. 4839-46.
91. Deshpande, M., et al., *The inositol 1,4,5-trisphosphate receptor is required for maintenance of olfactory adaptation in Drosophila antennae.* Journal of Neurobiology, 2000. **43**(3): p. 282-288.
92. Burns, M.E. and D.A. Baylor, *Activation, deactivation, and adaptation in vertebrate photoreceptor cells.* Annu Rev Neurosci, 2001. **24**: p. 779-805.
93. Hardie, R.C. and P. Raghu, *Visual transduction in Drosophila.* Nature, 2001. **413**(6852): p. 186-93.
94. Hudspeth, A.J. and P.G. Gillespie, *Pulling springs to tune transduction: adaptation by hair cells.* Neuron, 1994. **12**(1): p. 1-9.
95. Ricci, A.J., Y.C. Wu, and R. Fettiplace, *The endogenous calcium buffer and the time course of transducer adaptation in auditory hair cells.* J Neurosci, 1998. **18**(20): p. 8261-77.
96. Locatelli, F.F., et al., *Nonassociative plasticity alters competitive interactions among mixture components in early olfactory processing.* European Journal of Neuroscience, 2013. **37**(1): p. 63-79.
97. Das, S., et al., *Plasticity of local GABAergic interneurons drives olfactory habituation.* Proc Natl Acad Sci U S A, 2011. **108**(36): p. E646-54.
98. Bazhenov, M., et al., *Fast odor learning improves reliability of odor responses in the locust antennal lobe.* Neuron, 2005. **46**(3): p. 483-92.
99. Ramaswami, M., *Network Plasticity in Adaptive Filtering and Behavioral Habituation.* Neuron, 2014. **82**(6): p. 1216-1229.
100. Cho, W., U. Heberlein, and F.W. Wolf, *Habituation of an odorant-induced startle response in Drosophila.* Genes Brain Behav, 2004. **3**(3): p. 127-37.
101. Shea, S.D., L.C. Katz, and R. Mooney, *Noradrenergic induction of odor-specific neural habituation and olfactory memories.* J Neurosci, 2008. **28**(42): p. 10711-9.
102. Wilson, D.A., *Comparison of odor receptive field plasticity in the rat olfactory bulb and anterior piriform cortex.* J Neurophysiol, 2000. **84**(6): p. 3036-42.

103. Zhao, F.Q., et al., *fMRI study of olfaction in the olfactory bulb and high olfactory structures of rats: Insight into their roles in habituation.* Neuroimage, 2016. **127**: p. 445-455.
104. Best, A.R. and D.A. Wilson, *Coordinate synaptic mechanisms contributing to olfactory cortical adaptation.* J Neurosci, 2004. **24**(3): p. 652-60.
105. Wilson, D.A., *Synaptic correlates of odor habituation in the rat anterior piriform cortex.* J Neurophysiol, 1998. **80**(2): p. 998-1001.
106. Linster, C., et al., *Synaptic adaptation and odor-background segmentation.* Neurobiol Learn Mem, 2007. **87**(3): p. 352-60.
107. Bro, R., *PARAFAC. Tutorial and applications.* Chemometrics and Intelligent Laboratory Systems, 1997. **38**(2): p. 149-171.
108. Bro, R. and H.A.L. Kiers, *A new efficient method for determining the number of components in PARAFAC models.* Journal of Chemometrics, 2003. **17**(5): p. 274-286.
109. Pnevmatikakis, E.A., et al., *Simultaneous Denoising, Deconvolution, and Demixing of Calcium Imaging Data.* Neuron, 2016. **89**(2): p. 285-299.
110. Maddison, C.J., A. Mnih, and Y.W. Teh, *The concrete distribution: A continuous relexation of discrete random variables*, in *International Conference on Learning Representations*. 2017.
111. Jang, E., S. Gu, and B. Poole, *Categorical Reparameterization by Gumbel-Softmax*, in *International Conference on Learning Representations*. 2017.
112. Kingma, D.P. and J. Ba, *Adam: A method for stochastic optimization*, in *International Conference on Learning Representations*. 2015.
113. Rong, H., et al., *Early warning signals regarding environmental suitability in the Drosophila antenna.* bioRxiv, 2017.
114. Yoshida, K., et al., *Odour concentration-dependent olfactory preference change in C. elegans.* Nat Commun, 2012. **3**: p. 739.
115. Stensmyr, M.C., et al., *Novel natural ligands for Drosophila olfactory receptor neurones.* J Exp Biol, 2003. **206**(Pt 4): p. 715-24.
116. Getchell, T.V. and G.M. Shepherd, *Responses of olfactory receptor cells to step pulses of odour at different concentrations in the salamander.* The Journal of Physiology, 1978. **282**(1): p. 521-540.
117. Kurahashi, T. and A. Menini, *Mechanism of odorant adaptation in the olfactory receptor cell.* Nature, 1997. **385**(6618): p. 725-9.
118. Kaupp, U.B., *Olfactory signalling in vertebrates and insects: differences and commonalities.* Nat Rev Neurosci, 2010. **11**(3): p. 188-200.
119. De Palo, G., et al., *Common dynamical features of sensory adaptation in photoreceptors and olfactory sensory neurons.* Sci Rep, 2013. **3**: p. 1251.
120. Christensen, T.A., T. Heinbockel, and J.G. Hildebrand, *Olfactory information processing in the brain: encoding chemical and temporal features of odors.* J Neurobiol, 1996. **30**(1): p. 82-91.
121. Jacobson, G.A., P. Rupprecht, and R.W. Friedrich, *Experience-Dependent Plasticity of Odor Representations in the Telencephalon of Zebrafish.* Curr Biol, 2018. **28**(1): p. 1-14 e3.
122. Brown, S.L., J. Joseph, and M. Stopfer, *Encoding a temporally structured stimulus with a temporally structured neural representation.* Nat Neurosci, 2005. **8**(11): p. 1568-76.

123. Hattori, D., et al., *Representations of Novelty and Familiarity in a Mushroom Body Compartment.* Cell, 2017. **169**(5): p. 956-969 e17.
124. Friedrich, R.W. and S.I. Korsching, *Combinatorial and chemotopic odorant coding in the zebrafish olfactory bulb visualized by optical imaging.* Neuron, 1997. **18**(5): p. 737-52.
125. Bathellier, B., et al., *Dynamic ensemble odor coding in the mammalian olfactory bulb: sensory information at different timescales.* Neuron, 2008. **57**(4): p. 586-98.
126. Laurent, G., M. Wehr, and H. Davidowitz, *Temporal representations of odors in an olfactory network.* Journal of Neuroscience, 1996. **16**(12): p. 3837-3847.
127. Laurent, G., *Olfactory network dynamics and the coding of multidimensional signals.* Nature Reviews Neuroscience, 2002. **3**(11): p. 884-895.
128. Broome, B.M., V. Jayaraman, and G. Laurent, *Encoding and Decoding of Overlapping Odor Sequences.* Neuron. **51**(4): p. 467-482.
129. Friedrich, R.W. and G. Laurent, *Dynamic optimization of odor representations by slow temporal patterning of mitral cell activity.* Science, 2001. **291**(5505): p. 889-894.
130. Kreher, S.A., et al., *Translation of sensory input into behavioral output via an olfactory system.* Neuron, 2008. **59**(1): p. 110-124.
131. Saha, D., et al., *A spatiotemporal coding mechanism for background-invariant odor recognition.* Nat Neurosci, 2013. **16**(12): p. 1830-9.
132. Laurent, G., *A systems perspective on early olfactory coding.* Science, 1999. **286**(5440): p. 723-728.
133. Li, C., *Relating neural dynamics to olfactory coding and behavior.* Ph.D. dissertation, Washington University in St. Louis, 2015.
134. Ringo, J.L., *Stimulus specific adaptation in inferior temporal and medial temporal cortex of the monkey.* Behavioural Brain Research, 1996. **76**(1-2): p. 191-197.
135. Anderson, L.A., G.B. Christianson, and J.F. Linden, *Stimulus-Specific Adaptation Occurs in the Auditory Thalamus.* Journal of Neuroscience, 2009. **29**(22): p. 7359-7363.
136. Lampl, I. and Y. Katz, *Neuroscience Forefront Review Neuronal Adaptation in the Somatosensory System of Rodents.* Neuroscience, 2017. **343**: p. 66-76.
137. Maffei, L., A. Fiorentini, and S. Bisti, *Neural Correlate of Perceptual Adaptation to Gratings.* Science, 1973. **182**(4116): p. 1036-1038.
138. Moncrieff, R.W., *Olfactory Adaptation and Odour Likeness.* Journal of Physiology-London, 1956. **133**(2): p. 301-316.
139. Adrian, E.D., *The Electrical Activity of the Mammalian Olfactory Bulb.* Electroencephalography and Clinical Neurophysiology, 1950. **2**(4): p. 377-388.
140. Gutfreund, Y., *Stimulus-specific adaptation, habituation and change detection in the gaze control system.* Biol Cybern, 2012. **106**(11-12): p. 657-68.
141. Postle, B.R., *Delay-period activity in the prefrontal cortex: One function is sensory gating.* Journal of Cognitive Neuroscience, 2005. **17**(11): p. 1679-1690.
142. Miller, D.J., et al., *Relationships between Early Habituation and Later Cognitive Performance in Infancy.* Child Development, 1977. **48**(2): p. 658-661.
143. Cain, W.S., *Odor Intensity after Self-Adaptation and Cross-Adaptation.* Perception & Psychophysics, 1970. **7**(5): p. 271-&.
144. Hallem, E.A. and J.R. Carlson, *Coding of odors by a receptor repertoire.* Cell, 2006. **125**(1): p. 143-160.

145. Tichy, H. and M. Hellwig, *Independent processing of increments and decrements in odorant concentration by ON and OFF olfactory receptor neurons.* Journal of Comparative Physiology a-Neuroethology Sensory Neural and Behavioral Physiology, 2018. **204**(11): p. 873-891.
146. Nagel, K.I., E.J. Hong, and R.I. Wilson, *Synaptic and circuit mechanisms promoting broadband transmission of olfactory stimulus dynamics.* Nature Neuroscience, 2015. **18**(1): p. 56-+.
147. Galan, R.F., et al., *Sensory memory for odors is encoded in spontaneous correlated activity between olfactory glomeruli.* Neural Computation, 2006. **18**(1): p. 10-25.
148. Das, S., et al., *Plasticity of local GABAergic interneurons drives olfactory habituation.* Proceedings of the National Academy of Sciences of the United States of America, 2011. **108**(36): p. E646-E654.
149. Sudhakaran, I.P., et al., *Plasticity of Recurrent Inhibition in the Drosophila Antennal Lobe.* Journal of Neuroscience, 2012. **32**(21): p. 7225-7231.
150. Nelson, A.B., et al., *Long-lasting increases in intrinsic excitability triggered by inhibition.* Neuron, 2003. **40**(3): p. 609-20.
151. McElvain, L.E., et al., *Bidirectional Plasticity Gated by Hyperpolarization Controls the Gain of Postsynaptic Firing Responses at Central Vestibular Nerve Synapses.* Neuron, 2010. **68**(4): p. 763-775.
152. Fishilevich, E. and L.B. Vosshall, *Genetic and Functional Subdivision of the Drosophila Antennal Lobe.* Current Biology, 2005. **15**(17): p. 1548-1553.
153. Couto, A., M. Alenius, and B.J. Dickson, *Molecular, anatomical, and functional organization of the Drosophila olfactory system.* Current Biology, 2005. **15**(17): p. 1535-1547.
154. Chou, Y.H., et al., *Diversity and wiring variability of olfactory local interneurons in the Drosophila antennal lobe.* Nat Neurosci, 2010. **13**(4): p. 439-49.
155. Olsen, S.R. and R.I. Wilson, *Lateral presynaptic inhibition mediates gain control in an olfactory circuit.* Nature, 2008. **452**(7190): p. 956-60.
156. Yaksi, E. and R.I. Wilson, *Electrical Coupling between Olfactory Glomeruli (vol 67, pg 1034, 2010).* Neuron, 2010. **68**(4): p. 801-801.
157. Debelle, J.S. and M. Heisenberg, *Associative Odor Learning in Drosophila Abolished by Chemical Ablation of Mushroom Bodies.* Science, 1994. **263**(5147): p. 692-695.
158. Heisenberg, M., et al., *Drosophila mushroom body mutants are deficient in olfactory learning.* J Neurogenet, 1985. **2**(1): p. 1-30.
159. Gupta, N. and M. Stopfer, *Functional Analysis of a Higher Olfactory Center, the Lateral Horn.* Journal of Neuroscience, 2012. **32**(24): p. 8138-8148.
160. Heimbeck, G., et al., *A central neural circuit for experience-independent olfactory and courtship behavior in Drosophila melanogaster.* Proc Natl Acad Sci U S A, 2001. **98**(26): p. 15336-41.
161. Shimizu, K. and M. Stopfer, *A Population of Projection Neurons that Inhibits the Lateral Horn but Excites the Antennal Lobe through Chemical Synapses in Drosophila.* Frontiers in Neural Circuits, 2017. **11**(30).
162. Ahsan, J., et al., *Spatial representation of odorant valence in an insect brain.* Mechanisms of Development, 2017. **145**: p. S115-S115.

163. Strutz, A., et al., *Decoding odor quality and intensity in the Drosophila brain.* Elife, 2014. **3**.
164. Parnas, M., et al., *Odor discrimination in Drosophila: from neural population codes to behavior.* Neuron, 2013. **79**(5): p. 932-44.
165. Greer, C.J. and T.E. Holy, *Fast objective coupled planar illumination microscopy.* Nature Communications, 2019. **10**.
166. de Bruyne, M., K. Foster, and J.R. Carlson, *Odor coding in the Drosophila antenna.* Neuron, 2001. **30**(2): p. 537-552.
167. Bhandawat, V., et al., *Sensory processing in the Drosophila antennal lobe increases reliability and separability of ensemble odor representations.* Nature Neuroscience, 2007. **10**(11): p. 1474-1482.
168. Raman, B., et al., *Temporally Diverse Firing Patterns in Olfactory Receptor Neurons Underlie Spatiotemporal Neural Codes for Odors.* Journal of Neuroscience, 2010. **30**(6): p. 1994-2006.
169. Gschwend, O., et al., *Neuronal pattern separation in the olfactory bulb improves odor discrimination learning.* Nature Neuroscience, 2015. **18**(10): p. 1474-+.
170. Vosshall, L.B., A.M. Wong, and R. Axel, *An olfactory sensory map in the fly brain.* Cell, 2000. **102**(2): p. 147-159.
171. Jefferis, G.S., et al., *Comprehensive maps of Drosophila higher olfactory centers: spatially segregated fruit and pheromone representation.* Cell, 2007. **128**(6): p. 1187-203.
172. Vosshall, P.P.L.L.B., *The Olfactory Sensory Map in Drosophila*, in *Brain Development in Drosophila melanogaster*, G.M. Technau, Editor. 2008, Springer-Verlag New York.
173. Wang, K.Y., et al., *Parallel pathways convey olfactory information with opposite polarities in Drosophila.* Proceedings of the National Academy of Sciences of the United States of America, 2014. **111**(8): p. 3164-3169.
174. Wilson, C.D., et al., *A primacy code for odor identity.* Nature Communications, 2017. **8**(1477).
175. Bekesy, G.V., *Sensory Inhibition.* 2017.
176. Honegger, K.S., et al., *Idiosyncratic neural coding and neuromodulation of olfactory individuality in Drosophila.* PNAS, 2020. **117**: p. 23292-23297.
177. Nizampatnam, S., et al., *Dynamic contrast enhancement and flexible odor codes.* Nat Commun, 2018. **9**(1): p. 3062.
178. Burgstaller, M. and H. Tichy, *Functional asymmetries in cockroach ON and OFF olfactory receptor neurons.* J Neurophysiol, 2011. **105**(2): p. 834-45.
179. Saha, D., et al., *Engaging and disengaging recurrent inhibition coincides with sensing and unsensing of a sensory stimulus.* Nat Commun, 2017. **8**: p. 15413.
180. Ito, I., et al., *Sparse odor representation and olfactory learning.* Nature Neuroscience, 2008. **11**(10): p. 1177-1184.
181. Galan, R.F., et al., *Odor-driven attractor dynamics in the antennal lobe allow for simple and rapid olfactory pattern classification.* Neural Computation, 2004. **16**(5): p. 999-1012.
182. Riffell, J.A., H. Lei, and J.G. Hildebrand, *Neural correlates of behavior in the moth Manduca sexta in response to complex odors.* Proc Natl Acad Sci U S A, 2009. **106**(46): p. 19219-26.

183. Geffen, M.N., et al., *Neural encoding of rapidly fluctuating odors.* Neuron, 2009. **61**(4): p. 570-86.
184. Aldworth, Z.N. and M.A. Stopfer, *Trade-Off between Information Format and Capacity in the Olfactory System.* Journal of Neuroscience, 2015. **35**(4): p. 1521-1529.
185. Simard, P.Y., D. Steinkraus, and J.C. Platt. *Best practices for convolutional neural networks applied to visual document analysis*. in *Icdar*. 2003.
186. Rabinovich, M., et al., *Dynamical encoding by networks of competing neuron groups: winnerless competition.* Phys Rev Lett, 2001. **87**(6): p. 068102.
187. Laurent, G., et al., *Odor encoding as an active, dynamical process: experiments, computation, and theory.* Annu Rev Neurosci, 2001. **24**: p. 263-97.
188. Beshel, J. and Y. Zhong, *Graded Encoding of Food Odor Value in the Drosophila Brain.* The Journal of Neuroscience, 2013. **33**(40): p. 15693-15704.
189. Martelli, C., et al., *IFamide Translates Hunger Signals into Appetitive and Feeding Behavior in Drosophila.* Cell Reports, 2017. **20**(2): p. 464-478.
190. Faber, T., J. Joerges, and R. Menzel, *Associative learning modifies neural representations of odors in the insect brain.* Nature Neuroscience, 1999. **2**(1): p. 74-78.
191. Lecun, Y., et al., *Gradient-based learning applied to document recognition.* Proceedings of the Ieee, 1998. **86**(11): p. 2278-2324.
192. MacLeod, K. and G. Laurent, *Distinct mechanisms for synchronization and temporal patterning of odor-encoding neural assemblies.* Science, 1996. **274**(5289): p. 976-9.
193. Twick, I., J.A. Lee, and M. Ramaswami, *Olfactory habituation in Drosophila-odor encoding and its plasticity in the antennal lobe.* Prog Brain Res, 2014. **208**: p. 3-38.
194. LeCun, Y., Y. Bengio, and G. Hinton, *Deep learning.* Nature, 2015. **521**(7553): p. 436-444.